University Tokyo
Graduate School of Science
Department of Astronomy
2016, Summer
High Energy Astronomy Advanced Course (III)

Ken EBISAWA (JAXA/ISAS)

December 28, 2018

Contents

[1]See `ftp://ftp.cis.upenn.edu/pub/graphics/shoemake/quatut.ps.Z`
[2]See, "Classical Mechanics" by H. Goldstein.

Chapter 1

Introduction: Extent of the Universe

1.1 The Three Most Important Natural Constants

The most fundamental physical constants are Gravitational constant, velocity of light, and Planck constant:

$$G = 6.67428(67) \times 10^{-11} \text{ N·m}^2/\text{kg}^2 \ (\text{m}^3/\text{kg/s}^2)$$
$$c = 2.99792458 \times 10^8 \text{ m/s}$$
$$h = 6.62606896(33) \times 10^{-34} \text{ J·s} \quad (\text{kg·m}^2/\text{s})$$

$\hbar \equiv h/2\pi$ is often used:

$$\hbar = 1.054571628(53) \times 10^{-34} \text{ J·s} \quad (\text{kg·m}^2/\text{s})$$

In the Newtonian mechanics, the equation of motion includes the gravitational constant, G, but not the light speed, c. This is because the Newtonian mechanics handle motion of the objects only when their velocities are much less than c.

When the velocities get closer to c, we need *special relativity*, where the equations include c. However, the equations of special relativity do not include G, that is because special relativity is valid only when the gravity is negligible.

Equations of *general relativity* include both c and G, so that they can handle the cases when velocities of the motions caused by the gravity get closer to the light velocity (i.e., strong gravity).

Still, equations of general relativity do not include the Planck constant h, that is because general relativity can handle only macroscopic phenomena, where quantum effects are negligible.

The Planck constant h appears in the Schrödinger equation of *quantum mechanics*, which describes microscopic world. However, c does not appear in the Schrödinger equation, since particles are assumed to move much slower than c. This is not correct, and we need *relativistic quantum mechanics*, where the Dirac equation includes h and c.

Today, we know that there are four fundamental forces in the Universe; electro-magnetic force, weak interaction, strong interaction, and gravity. All the forces but the gravity are described by the *standard theory*, whose equations include h and c. Goal of the standard theory is to unify the three fundamental forces, electro-magnetic force, weak interaction and strong interaction. This goal has not been achieved yet, but hopefully, is not too far.

What about the "final" theory which takes into account the gravity between elementary particles, whose equations have h, c and G? We do not know such theory of *quantum gravity* yet, at least the one which is generally accepted.

In any case, our universe is described by physical laws using c, G and h.

1.2 Planck Time, Planck Length, Planck Mass

From these three natural constants, we may derive time, length and mass, which are called *Planck time*, *Planck length* and *Plank mass*. Also, *Planck density* is defined as the *Plank mass* divided by the cube of *Planck length*.

Roughly speaking, the current physical laws can describe evolution from the initial universe, of which age, size and density are Planck time, Planck length and Planck density, respectively. How such an initial universe is created is beyond the scope of physics.

Look at the units (dimensions) of $G, c, \hbar$, and create quantities having the units (dimensions) of time, length, mass and density to give Planck time, Planck length, Planck mass and Planck density.

$$Planck\ Time = t_P \equiv \sqrt{\frac{\hbar G}{c^5}} = 5.39 \times 10^{-44}\ \ [\mathrm{sec}] \tag{1.1}$$

$$Planck\ Length = l_P \equiv \sqrt{\frac{\hbar G}{c^3}} = 1.61 \times 10^{-35}\ \ [\mathrm{m}] \tag{1.2}$$

$$Planck\ Mass = m_P \equiv \sqrt{\frac{\hbar c}{G}} = 2.18 \times 10^{-8}\ \ [\mathrm{kg}] \tag{1.3}$$

$$Planck\ Density = \rho_P \equiv \frac{c^5}{\hbar G^2} = 5.16 \times 10^{96}\ \ [\mathrm{kg/m^3}] = 5.16 \times 10^{93}\ \ [\mathrm{g/cm^3}] \tag{1.4}$$

1.3 Age and Size of the Universe

Age of the size is estimated as 13.8 billion year (4.3×10^{17} sec) from precise measurement of the Cosmic Microwave Background. Thus, size of the universe is estimated as 13.8 billion light-year (1.3×10^{26} m). If we compare these values with Planck Time and Planck Length, we can see that the difference is 61 orders of magnitudes. In other words, the universe, the one which we may study physically, has the spatial and temporal extent having 61 orders of magnitudes.

1.4 Black Hole and Planck Particle

Schwarzschild radius of an object having mass M is given as R_S is $2GM/c^2$. This gives an estimate of the black hole size of a object having the mass M[1].

Relationship between Planck mass and Planck length is given as $l_P = Gm_P/c^2$. Namely, if we ignore the factor 2, a virtual particle having the Planck mass and Planck length (radius) is considered as a black hole. This may be called as Planck particle.

[1] Let's remember that Schwarzschild of the Sun and the earth are approximately 3km and 9mm, respectively.

Meanwhile, the *Compton wave-length*, λ_C, for a particle with mass m is defined such that

$$E = mc^2 = h\nu = hc/\lambda_C. \tag{1.5}$$

Namely,

$$\lambda_C = \frac{h}{m\,c}. \tag{1.6}$$

Relationship between the Planck length and Planck mass is

$$l_P = \frac{\hbar}{m_P\,c}. \tag{1.7}$$

Thus, if we ignore 2π, the Schwarzschild radius and the Compton wave-length of the Planck particle coincide. In other words, the Planck particle is the quantum black hole, and the Planck mass gives the mass of the minimum black hole in the universe.

Let's compare these values with those of a realistic elementary particle, e.g., proton. Proton mass is 1.67×10^{-27} kg, and its Compton wave-length is[2] 1.3214×10^{-15}m. Namely, the virtual Planck particle is much more massive and tinier than a realistic elementary particle.

[2]Let's remember the proton mass (energy) as $m_p c^2 \approx 1$ GeV. It is also useful to remember $\hbar c \approx 2000$ eV·A. Thus, Compton wave-length of proton is $h/mc = 2\pi\hbar c/mc^2 \approx 2\pi \times 2000[\text{eV}\cdot\text{A}]/10^9[\text{eV}] \approx 10^{-15}$ m. In addition, using 1 eV $\approx 1.6\times10^{-12}$ erg (you should remember this relation too). $m_p \approx 1[\text{GeV}]/\text{c}^2 \approx 10^9 \times 1.6\times10^{-12}[\text{erg}]/(3\times10^{10}[\text{cm/s}])^2 \approx 2\times10^{-24}$ g.

Chapter 2

How to Interpret the X-ray data

2.1 Basics

2.1.1 Basic of Basics

It is useful to remember these basic numbers and formulae.

1 pc $\approx 3 \times 10^{18}$ **cm**

light-velocity $c \approx 3 \times 10^{10}$ cm/s

1 year $= 3.15 \times 10^7 \approx \pi \times 10^7$**sec**

Distance between Sun and Earth $\equiv$ 1Astronomical Unit (AU) ≈ 500 **light-seconds**

In X-ray astronomy, arrival (detection) time is usually recorded for each photon. The "barycentric correction", up to ~500 sec, is applied to each photon to assign the photon arrival time at the solar-system barycenter (that is located inside the Sun), taking account of orbital motions of the earth and the satellite.

Conversion between the X-ray wavelength and energy

$$E\ [\mathrm{keV}] \approx \frac{12.4}{\lambda\ [\text{Å}]}$$

Remember, an X-ray photon at 12.4 keV has the wave-length 1 Å.

Conversion between X-ray energy and temperature

$$1\ \mathrm{eV} = 11604\ \mathrm{K} \approx 10^4\ \mathrm{K}$$

Very crudely, an object shining with a spectrum of ~1 keV has an temperature of $\sim 10^7$ K.

Energy unit conversion

$$1\ \mathrm{eV} \approx 1.6 \times 10^{-12}\ \mathrm{erg}$$

Boltzmann constant

$$k = 1.38 \times 10^{-16} \ \text{erg/K}$$

Stephan-Boltzmann constant

$$\sigma \approx 1.0 \times 10^{24} \ \text{erg/s/cm}^2/\text{keV}^4$$

For the derivation of the Stephan-Boltzmann constant, see section 5.3.3. It is practical to remember with this unit. For instance, a 10 km radius neutron star shining with 2 keV blackbody has the luminosity,

$$L = 4\,\pi\,(10 \text{ km})^2\,\sigma\,(2\text{keV})^4 \approx 2 \times 10^{38} \text{ erg/s}.$$

A white-dwarf shining at the Eddington-luminosity (2.17) has the surface temperature,

$$T = \left(\frac{L}{4\pi\sigma R^2}\right)^{1/4} \approx 80 \text{ eV} \left(\frac{M}{M_\odot}\right)^{1/4} \left(\frac{R}{5000\text{km}}\right)^{-1/2}.$$

The ROSAT satellite discovered many "Super-soft Sources", which typically have temperatures of $50 \sim 100$ eV. These are actually considered to be blackbody emission from white dwarf surfaces shining at nearly Eddington luminosities.

2.1.2 Units in electromagnetic theory

In electromagnetic theory, different unit systems are commonly used. Coulomb's law for electricity and magnetism may be written as,

$$F = \frac{1}{h_1 \epsilon}\frac{qq'}{r^2}, \tag{2.1}$$

$$F = \frac{1}{h_2 \mu}\frac{mm'}{r^2}. \tag{2.2}$$

where h_1 and h_2 are proportional constants (no dimension), ϵ and μ are constants with dimension. The left-hand side is the "force" with the dimension of [mass·length· time^{-2}]; depending the dimensions of electrical and magnetic charges, q and m, dimensions of ϵ and μ are determined.

The MKSA unit system

Using [m], [kg], and [s] for length, mass and time, and introduce [A] for electrical current. Unit of electrical charge will be [C], where 1 [C] = 1 [A·s]. Coulomb's laws are written as follows;

$$F = \frac{1}{4\pi\epsilon_0}\frac{qq'}{r^2}, \tag{2.3}$$

$$F = \frac{1}{4\pi\mu_0}\frac{mm'}{r^2}.. \tag{2.4}$$

Here, from (2.3), ϵ_0 has the dimension [$\mathrm{A}^2 \cdot \mathrm{time}^4 \cdot \mathrm{length}^{-3} \cdot \mathrm{mass}^{-1}$] . The light-velocity c is written as

$$c = \frac{1}{\sqrt{\epsilon_0\ \mu_0}}, \tag{2.5}$$

from which dimension of μ_0 is determined. Using (2.4), dimension of magnetic charge is determined.

MKSA unit system is often used in engineering and laboratory experiments, since it is useful to handle electric circuits. Most undergraduate text books adopt MKSA units

The Gauss unit system

Coulomb's law may be simply written as

$$F = \frac{qq'}{r^2}, \tag{2.6}$$

$$F = \frac{mm'}{r^2}. \tag{2.7}$$

In this case, both electric and magnetic charges have dimensions of [$\mathrm{mass}^{1/2} \cdot \mathrm{length}^{3/2} \cdot \mathrm{time}^{-1}$]. Gauss unit is useful to describe natural phenomena, so often adopted in atomic physics and astrophysics. In fact, most papers and graduate level text books are written using Gauss unit.

In my lecture, I adopt the Gauss unit system.

Basic equations in electromagnetic theory

Expression of Maxwell's equations and other basic equations are dependent on the unit-system:

	MKSA unit-system	Gauss unit-system
$\mathrm{div}\boldsymbol{D} =$	ρ	$4\pi\rho$
$\mathrm{div}\boldsymbol{B} =$	0	0
$\mathrm{rot}\boldsymbol{H} =$	$\boldsymbol{j} + \frac{\partial \boldsymbol{D}}{\partial t}$	$\frac{4\pi}{c}\boldsymbol{j} + \frac{1}{c}\frac{\partial \boldsymbol{D}}{\partial t}$
$\mathrm{rot}\boldsymbol{E} =$	$-\frac{\partial \boldsymbol{B}}{\partial t}$	$-\frac{1}{c}\frac{\partial \boldsymbol{B}}{\partial t}$
$\boldsymbol{D} =$	$\epsilon\boldsymbol{E}$	$\frac{\epsilon}{\epsilon_0}\boldsymbol{E}$
$\boldsymbol{B} =$	$\mu\boldsymbol{H}$	$\frac{\mu}{\mu_0}\boldsymbol{H}$

Magnetic flux density and energy density

Magnetic energy density is written as

$$\epsilon\ [\mathrm{erg/cm^3}] = \frac{1}{8\pi}\,(B\,[\mathrm{gauss}])^2 \quad \text{(Gauss unit)} \tag{2.8}$$

or

$$\epsilon'\ [\mathrm{J/m^3}] = \frac{1}{2\mu_0}\left(B'\,[\mathrm{T}]\right)^2 \quad \text{(MKSA unit)}, \tag{2.9}$$

where $\mu_0 = 4\pi \times 10^{-7}$ [N/A^2] is the magnetic permeability in vacuum. Here, in order to clarify difference of the same physical quantities expressed by two different units, we put $'$ for ϵ and B in the second equation.

Note that [gauss] has the dimension of [cm$^{-1/2}$ g$^{1/2}$ s^{-1}], so that [gauss^2] corresponds to [erg/cm^3]. Also, [T] has the dimension of [N/(A·m)], so that [T^2]/μ_0 corresponds to [J/m^3]. Magnetic flux density strength of 1 [T] is equal to 10^4 [gauss], thus $B' = 10^{-4}\ B$. However, **be careful that dimensions of [T] and [gauss] are different**[1] :

$$1\ \mathrm{T}\ (\mathrm{MKSA\ unit}) \Longleftrightarrow 10,000\ \mathrm{gauss}\ (\mathrm{cgs\ unit}).$$

Note,

$$[\mathrm{J/m^3}] = [10^7 \mathrm{erg}/(100\mathrm{cm})^3] = 10\ [\mathrm{erg/cm^3}],$$

thus,

$$\epsilon' = 1/10\ \epsilon.$$

Similarly,

$$\epsilon' = \frac{1}{2\mu_0} B'^2 = \frac{1}{2 \times 4\pi \times 10^{-7}} (10^{-4}\ B)^2$$
$$= \frac{1}{10} \frac{B^2}{8\pi} = \frac{1}{10} \epsilon.$$

Now, we see that equations (2.8) and (**??**) agree.

2.2 Review of Atomic Physics

2.2.1 Things useful to remember

Electron/Positron mass

$$m_e c^2 \approx 511\ \ \mathrm{keV}$$

The pair-production of e^+-e^- creates two gamma-ray photons at 511 keV (annihilation line), which are typically observed from the Galactic center (an example below, by the INTEGRAL satellite).

Compton wavelength

The Compton wavelength, λ_c, is defined as the wavelength of the electro-magnetic wave corresponding to the electron mass energy, 511 keV, so that

$$m_e\ c^2 = h\nu = hc/\lambda_c,$$

and $\lambda_c = hc/m_e\ c^2 \approx 12.4\ [\mathrm{keV} \cdot \text{Å}]/511\ \mathrm{keV} \approx 0.024\text{Å}_\circ$

Mass of the nucleons (proton or neutron)

$$m_p c^2 \approx m_n c^2 \approx 940\ \mathrm{MeV} \approx 1\ \mathrm{GeV}$$

[1] In this relation, often the left-hand side and the righ-hand side are connected by equal sign, as "1 T = 10^4 gauss" which, I belive, is mis-leading and should be avoided.

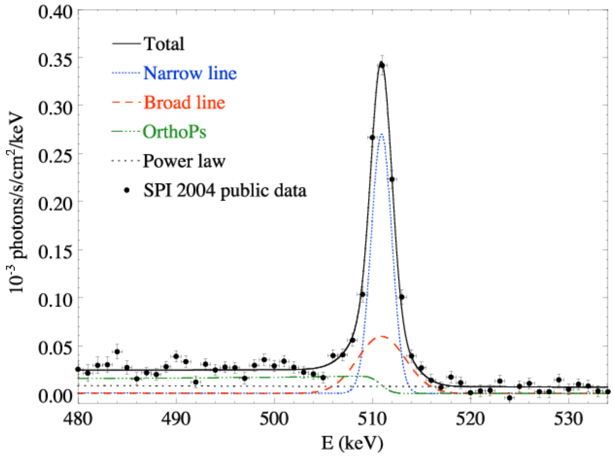

Figure 2.1: Annihilation line from the Galactic center, observed by the INTEGRAL satellite (Knödlseder et al. 2006, A&A, 445, 579).

Fine structure constant

$$\frac{e^2}{\hbar c} \approx \frac{1}{137}$$

How to remember the Planck constant

$$\hbar c = 1973 \text{ eV Å} \approx 2000 \text{ eV Å}$$

You may derive several important atomic parameters as below, by remembering these formulae.

Classical electron radius

Classically, an electron is regarded as a sphere having the *classical photon radius*, r_0, which is defined as the radius where the electric potential and the mass energy are equal, so that

$$\frac{e^2}{r_0} = m_e c^2,$$

$$r_0 = \frac{e^2}{m_e c^2} = \frac{e^2}{\hbar c}\frac{\hbar c}{m_e c^2} \approx \frac{1}{137}\frac{2000 \text{ eV Å}}{511 \text{ keV}} \approx 3 \times 10^{-5} \text{ Å}.$$

More precisely, $r_0 = 2.818 \times 10^{-5}$ Å.

Thomson scattering cross-section σ_T

Approximately, geometrical cross-section of the sphere having the classical electron radius (πr_0^2), but precisely,

$$\sigma_T = \frac{8}{3}\pi r_0^2 = 6.65 \times 10^{-25}\text{cm}^2. \tag{2.10}$$

The inverse is $\sim 1.5 \times 10^{24}$ cm^{-2}. If hydrogen column density of the matter, N_H, exceeds this value, the matter is considered *Thomson thick* or *Compton thick*, since the scattering optical depth $\tau_{scat} = N_H \sigma_T$ exceeds unity.

Thomson Scattering Opacity

In radiation transfer, cross-section of matter [cm^2] per 1 [g] in the line-of-sight, namely, *mass-absorption coefficient*, is often used as a measure of the *opacity*, expressed as κ [cm^2/g]。In X-ray regime, Thomson scattering opacity is not negligible. To calculate Thomson scattering opacity of the matter precisely, it is necessary to take into account the element abundance. However, approximately, only assuming hydrogen,

$$\kappa_T \approx \frac{\sigma_T}{m_p} \approx \frac{\sigma_T\, c^2}{1\mathrm{GeV}} \approx \frac{6.65 \times 10^{-25}\mathrm{cm}^2 \times (3 \times 10^{10}\mathrm{cm/s})^2}{10^9 \times 1.6 \times 10^{-12}\mathrm{erg}} \approx 0.4\ [\mathrm{cm}^2/\mathrm{g}]. \tag{2.11}$$

Bohr radius

Assuming a classical circular motion of electron around proton with the radius r_B. The angular momentum is quantized.

$$m_e \frac{v^2}{r_B} = \frac{e^2}{r_B^2}$$

$$m_e\, v\, r_B = \hbar$$

Eliminating v,

$$r_B = \frac{\hbar^2}{m_e\, e^2}.$$

You should remember that $r_B \approx 0.5\mathring{A}$. You may also easily derive as follows (need to remember fine structure constant and $\hbar c$);

$$\frac{\hbar^2}{m_e\, e^2} \approx \frac{\hbar c}{m_e c^2} \frac{\hbar c}{e^2} \approx \frac{2000\ \mathrm{eV\mathring{A}}}{511\ \mathrm{keV}}\ 137 \approx 0.5\ \mathrm{\mathring{A}}.$$

The same discussion holds for ions having only a single electron (hydrogenic-ion). For atoms with the atomic number Z, the positive electric charge of the nucleus is Ze. Replacing one of the e to Ze, the radius will be $1/Zr_B$. The electron is more strongly bound to the nucleus due to the stronger electric force.

Lyman edge energy

Hydrogen binding energy is,

$$E = \frac{1}{2} m_e v^2 - \frac{e^2}{r_B} = -\frac{1}{2}\frac{e^2}{r_B} = -\frac{m_e e^4}{2\hbar^2}.$$

If you add this energy to the bound electron, the hydrogen is ionized. This energy corresponds to the Lyman edge energy, 13.6 eV. You may derive as follows;

$$\frac{m_e e^4}{2\hbar^2} = \frac{m_e\, c^2}{2} \left(\frac{e^2}{\hbar c}\right)^2 = \frac{511\ \mathrm{keV}}{2} \left(\frac{1}{137}\right)^2 = 13.6\ [\mathrm{eV}].$$

Remember the corresponding wave-length, as

$$12.4\ [\mathrm{keV\AA}]/13.6\mathrm{eV} = 911\mathring{A}.$$

Lyman edge of hydrogenic-ions

Binding energy of hydrogen atom is

$$E = -\frac{1}{2}\frac{e^2}{r_B}.$$

In the case of hydrogenic-ions with the atomic number Z (hydrogenic-ion), the radius will be r_B/Z, and one of the e should be replace by Ze. Thus, the binding energy of hydrogenic-ions with the atomic number Z is 13.6 Z^2 eV。

In X-ray astronomy, iron ($Z = 26$) K-feature is often important. K-edge energy of the hydrogenic iron ion (Fe 26) is 13.6 [eV] $\times\ 26 \times 26 \approx 9.2$ keV。

Cyclotron frequency

Consider electrons in the magnetic field, B, where electrons make circular motion around the magnetic field lines with the radius r and velocity v;

$$m_e\frac{v^2}{r} = \frac{e\,v\,B}{c}. \tag{2.12}$$

The angular frequency is $\omega = v/r = eB/mc$, and *cyclotron emission* is made with the same frequency. Consequently, the cyclotron energy, E_c, is

$$E_c = \frac{\hbar eB}{m_e c} = \frac{\hbar e}{2m_e c}\ \ 2B. \tag{2.13}$$

Here, $\hbar e/(2m_e c)$ is the *Bohr magneton*, 9.3×10^{-21} [erg/gauss].

In X-ray astronomy, it is useful to remember the following relation;

$$E_c = 12\ \ \mathrm{keV}\ \ \frac{B}{10^{12}\ [\mathrm{Gauss}]} \tag{2.14}$$

In fact, cyclotron absorption lines are observed from X-ray binary pulsars, in which neutron stars have strong magnetic fields over 10^{12} Gauss.

2.2.2 Cross-section due to photoelectric absorption

X-ray from 0.1 − 10 keV are mainly absorbed photoelectric absorptions due to M-, L- or K-shells of C, N, O, Ne, Si, S, and Fe. Absorptions by H and He are almost negligible in this energy band. Absorptions by other rare elements are not significant either. The photoelectric absorption cross sections suddenly increases at the edges, then degrees with energy as $\sigma(E) \propto E^{-3}$.

In the case of neutral Fe, X-rays below $\mathrm{L_{II}}$ edge (0.708 keV) are absorbed by M-shell electrons. X-rays between this energy and K-edge (7.11 keV) are absorbed by L-electrons. X-rays slightly above K-edge are absorbed by K-electrons, but soon iron will be transparent as the cross section decreases with $\propto E^{-3}$.

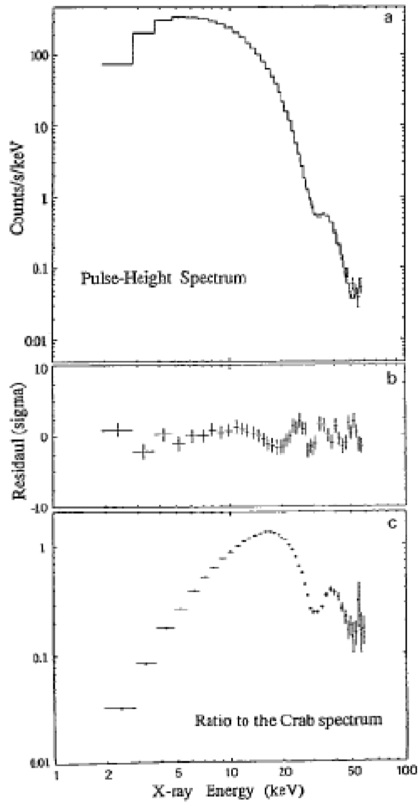

Figure 2.2: The cyclotron absorption line at $\sim$ 28.5 keV observed from X0331+35 with the Ginga satellite (Makishima et al. 1990, ApJ, 365, L59). Using (2.2.1), the neutron star magnetic field is estimated as 2.5×10^{12} gauss.

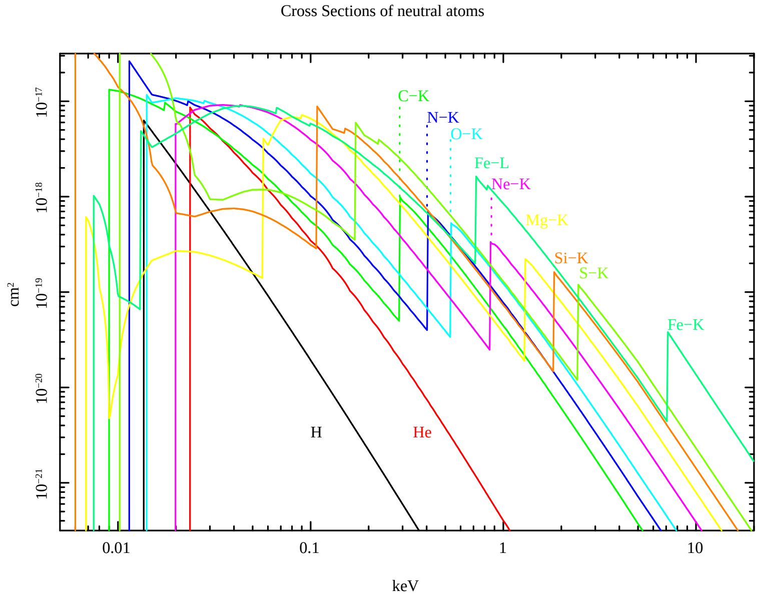

Figure 2.3: Cross-section due to neutral elements. Plotted using the data from $HEADAS/../ftools/spectral/xspec/manager/mansig.dat in the heasoft package provided by NASA/GSFC.

2.2.3 Photoelectric absorption by ionized matter (warm absorber)

As atoms get more highly ionized, edge energies increase, since the orbital electrons are more strongly bound. Also, electrons in the outer shell are ionized, so matter are more transparent for low energy X-rays. In particular, when all the elections in a particular shell are ionized, photoelectric absorption by that shell diminish. in Figure 2.4, when iron is ionized to Fe XVII (Ne-like; L-shell is filled, but M-shell is empty), iron will be transparent to X-rays below Fe XVII L-edge $\sim$ 1.3 keV. Similarly, for Fe XXV (He-like; K-shell is filled, but L-shell is empty), X-rays below Fe XXV K-edge, $\sim$ 8.8 keV are not absorbed.

In realistic ionized plasma, various elements are ionized at various ionization states, so complex X-ray spectra with many absorption lines and/or emission lines are observed. In particular, when there are vacancies in the upper-shell, resonance absorption lines are produced when electrons are excited by absorbing the X-ray corresponding to the energy gap (L-shell $\rightarrow$ M-shell, or K-shell $\rightarrow$L-shell)、

2.3 Basic of Astrophysics

2.3.1 Eddington luminosity

Matter falling to stellar objects may receive photon-pressure due to the radiation. In the case of spherical symmetry, the *Eddington limit* gives the maximum luminosity, when the gravity and the photon-pressure balance.

Here, for simplicity, we consider only hydrogen, where m_H is the hydrogen atomic mass.

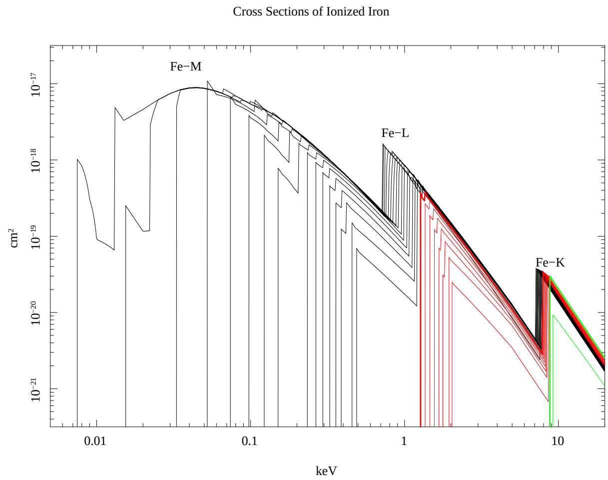

Figure 2.4: Photoelectric absorption cross-sections of ionized iron. Black lines show those from Fe I (neutral) to Fe XVI (Na-like), red lines from Fe XVII (Ne-like) to Fe XXIV (Li-like), green lines for Fe XXV (He-like) and Fe XXVI (H-like). Stables ions, Fe XVII (Ne-like) and Fe XXV (He-like), shown with thick lines. Data taken from $HEADAS/../ftools/spectral/xspec/manager/mansig.dat.

The balance of gravity and photon-pressure may be written as

$$\frac{\sigma_T}{c}\frac{L_{Edd}}{4\pi r^2} = \frac{GMm_H}{r^2}. \tag{2.15}$$

Here, $\sigma_T = 6.65 \times 10^{-25}$ cm^2 is the Thomson cross section (2.10).

Thus,

$$L_{Edd} = \frac{4\pi cGM}{\sigma_T/m_H} = \frac{4\pi c\, GM}{\kappa_T}. \tag{2.16}$$

Here, κ_T is the opacity due to Thomson scattering, $\sim$0.4 cm^2/g (2.11), so

$$L_{Edd} = \frac{4\pi c^3}{\kappa_T}\frac{GM_\odot}{c^2}\left(\frac{M}{M_\odot}\right) \approx 1.3 \times 10^{38}\left(\frac{M}{M_\odot}\right) \text{ [erg/s]}. \tag{2.17}$$

Consider the compact objects, namely white dwarfs, neutron stars and black holes. Maximum mass of the white dwarfs is the *Chandrasekhar limit*, $1.4M_\odot$, that is an average luminosity of neutron stars. Maximum mass of the neutron stars is $\sim 3M_\odot$; more massive compact objects are black holes. In fact, bright neutron star X-ray binaries have luminosities of $\sim 10^{38}$ ergs/s. Galactic black holes have luminosities up to $\sim 10^{39}$ erg/s.

Roughly speaking, neutron stars are more luminous than white dwarfs, and so are black holes than neutron stars. The more massive black holes become, the brighter.

2.3.2 The compact objects

White dwarfs

- White dwarfs are sustained by the degenerate pressure of electrons, of which maximum mass is the *Chandrasekhar limit* that is $\approx 1.4M_\odot$.
  Chandrasekhar obtained the Nobel prize in 1983.

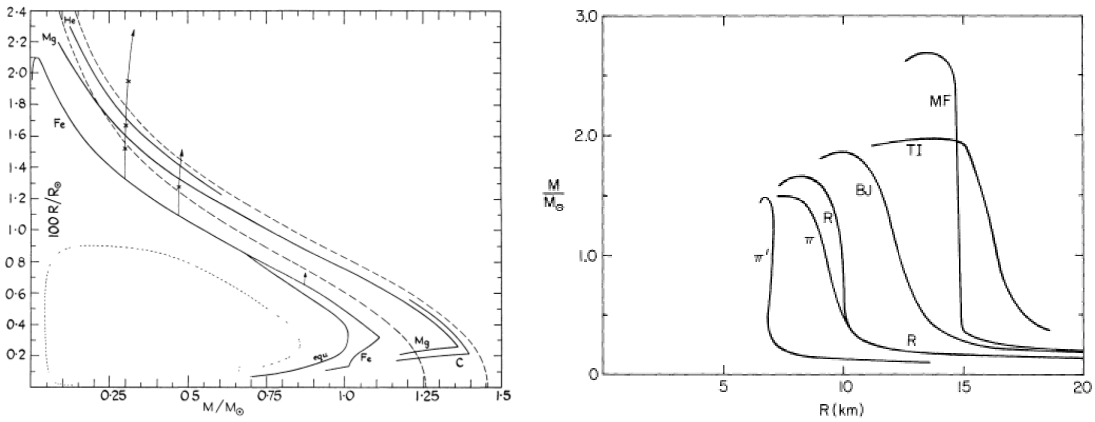

Figure 2.5: Mass-radius relations for white-dwarfs (left; Hamada and Salpeter 1961,ApJ, 134, 683) and neutron stars (right; Baym and Pethick ARAA 1979, 415).

- Typical mass is $\approx 1M_\odot$
- Typical radius $\approx$ 6000 km
  Remember, white dwarfs are as massive as Sun and as large (or small) as Earth.
- There is mass-radius relationship for given abundances and equation of states. *More massive they get, more compact they become* (Figure 2.5).

Neutron stars

- Typical mass $\approx 1.4M_\odot$
  This corresponds to the Chandrasekhar limit of the degenerate core of evolved stars (progenitors of Type II supernova).
- Typical radius $\approx$ 10 km
- Central density, an order of $\sim 10^{15}$ [g/cm^3], that is the densest matter in the universe.
- Maximum mass to sustain by the degenerate pressure of neutrons, $\approx 3M_\odot$
- There is mass-radius relationship for given abundances and equation of states. *More massive they get, more compact they become* (Figure 2.5).
- Magnetic and rotating neutron stars are observed as *pulsars.* Isolated pulsars emit from radio to $\gamma-$rays due to synchrotron emission. Binary X-ray pulsars mostly emit in X-rays.
- Typical magnetic fields of neutron stars, $\sim 10^{12}$ gauss. *Magnetars*, which are known by peculiar X-ray characteristics, has magnetic fields as large as $\sim 10^{15}$ gauss.

Black holes

- Minimum mass, $\sim$ maximum mass of neutron stars $\sim 3M_\odot$
- Dynamically measured most massive stellar black hole; 15.7 $M_\odot$ (M33 X-7)[2]. The most massive stellar black hole in our Galaxy; $\sim 14M_\odot$ (GRS1915+105).
- Using gravitational wave, a black hole merger was discovered, where $36M_\odot$ and $29M_\odot$ black holes merged, and 62 $M_\odot$ black hole is created (Abbott et al. 2016, PRL, 116, 061102)
- Black hole at Sgr A*, $(3.7 \pm 0.2) \times 10^6 [R_0/(8 \text{ kpc})]^3 M_\odot$ (Ghez et al. 2005, ApJ, 620, 744)
- Theoretical upper-limit of the black holes created in the stellar evolution; $\sim 40M_\odot$ (Fryer 1999, ApJ, 522, 413)
- There are "stellar black holes" ($\sim 10M_\odot$) and 'super-massive black holes" ($\gtrsim 10^6 M_\odot$) in the center of galaxies. It is under discussion if there are "intermediate-mass black hole" with the mass of 100 – 1000 $M_\odot$)
- Origin of Ultra-luminous or Hyper-luminous X-ray Sources (ULXs, HLXs) in luminosities of $10^{40} \sim 10^{42}$ erg/s unresolved yet.
- Schwarzschild radius for the object with mass M is $2GM/c^2 \approx 3(M/M_\odot)$ [km]. Roughly, this may be regarded as black hole "radius".
- Schwarzschild radius of Earth, $\sim$ 9 mm.
- Schwarzschild radius appears in the Schwarzschild metric, that is a solution of the Einstein equation. However, it coincides with the radius where the escape velocity becomes the light velocity in Newtonian mechanics;

$$\frac{1}{2} v_{escape}^2 = \frac{GM}{r}, \tag{2.18}$$

  where, if we put $v_{escape} = c$, we get

$$r = \frac{2GM}{c^2}. \tag{2.19}$$

- Schwarzschild black holes are non-rotating black holes, where the angular momentum $a = 0$. Kerr black holes are rotating black holes, where $0 < a \leq 1$.
- Terminal spin value, $a = 0.998$.

[2] http://chandra.harvard.edu/photo/2007/m33x7/

2.3.3 More about black holes

Timescale of variation around black holes

Light-crossing time of Schwarzschild radius;

$$\Delta t \approx \frac{2GM/c^2}{c} = \frac{2GM_\odot/c^2}{c}\frac{M}{M_\odot}$$

$$\approx \frac{3\ \mathrm{km}}{3\times 10^5 \mathrm{km/s}}\frac{M}{M_\odot} \approx 100\ \mu\mathrm{sec}\frac{M}{10M_\odot} = 100\ \mathrm{sec}\frac{M}{10^6 M_\odot}.$$

For stellar mass black holes, very high time resolution is needed to study X-ray time-variation close to the black holes. The RXTE satellite, having a time-resolution of $\sim$ μsec, carried out precise timing study of many bright Galactic black hole binaries and neutron star binaries.

For AGNs, $\sim$100 sec is sufficient to study X-ray time-variation close to the black holes. However, since AGNs are not as bright as Galactic X-ray binaries, high sensitivity is needed. Today, XMM-Newton satellite is the most suitable for this purpose.

Apparent size of black holes

Assuming the distance to a black hole d and the mass of the black hole M, the apparent size of the black hole (Schwarzschild radius) may be estimated as,

$$\Delta\theta = \frac{2GM/c^2}{d} = \frac{30\ \mathrm{km}(M/10M_\odot)}{10\ \mathrm{kpc}(d/10\ \mathrm{kpc})}$$

$$\approx 10^{-16}\frac{(M/10M_\odot)}{(d/10\ \mathrm{kpc})} \approx 2\times 10^{-11}\ \mathrm{arcsec}\ \frac{(M/10M_\odot)}{(d/10\ \mathrm{kpc})}.$$

We do not know any technologies to achieve such a spatial resolution and resolve *Galactic stellar-mass black holes*, at least in the foreseeable future.

On the other hand, let's consider *super-massive black holes*, the one in the nucleus in our Galaxy (Sgr A*), and the other one in a near by AGN, M87. For the black hole in Sgr A*, d= 8 kpc and $M = 3.7\times 10^6 M_\odot$,

$$\Delta\theta \approx 8\mu\mathrm{arcsec}.$$

The black hole in the center of M87 is located at $d \approx 18$ Mpc (v=0.00437 km/s, H=72 km/s/Mpc), and $M \approx 3\times10^9 M_\odot$ (Macchetto et al. 1997, ApJ, 489, 579). We see the apparent size is $\sim$ 3 μarcsec.

Currently, sub-mm VLBI offers the best spatial resolution in observational astronomy [3]. In general, spatial resolution of the astronomical instrument is given by

$$\Delta\theta \approx \lambda/D,$$

where λ is the observational wave-length and D is the diameter of the telescope, or base-line in the case of interferometer. Let's assume λ is 1 mm and D is 10,000 km[4],

$$\Delta\theta \approx \lambda/D = 1[\mathrm{mm}]/10,000[\mathrm{km}] = 10^{-10} \approx 20\mu\mathrm{arcsec}.$$

[3] `http://www.eventhorizontelescope.org/technology/building_a_larger_array.html`

[4] Distance between Mauna Kea in Hawaii and ALMA in Chile.

This may not be sufficient to spatially resolve the black hole in Sgr A* or M87.

X-ray interferometer satellites, if technically feasible, will offer the best spatial resolution[5]. Let's assume the base-line of $d \sim 20$ m, using X-rays with $\lambda \sim 1$Å. The spatial resolution will be

$$\Delta\theta \approx \lambda/D = 1\AA/20 \text{ m} \approx 5 \times 10^{-12} \approx 1\mu\text{arcsec},$$

which may be sufficient to spatially resolve the super-massive black holes at Sgr A* and M81.

Black hole "densities"

Let's assume that a black hole is a classical sphere having the Schwarzschild radius R_s, and calculate the black hole "density";

$$\rho = \frac{M}{4\pi R_s^3/3} \approx 2 \times 10^{16} \left(\frac{M}{M_\odot}\right)^{-2} \;\; [\text{g/cm}^3],$$

where we used the solar mass $M_\odot \approx 2 \times 10^{33}$ [g]. For a 1 $M_\odot$ black hole, which does not exist in the universe, will have an extreme density $\sim 10^{16}$ [g/cm^3], which is not physical either[6].

As black hole mass increases, the density decreases as $\rho \propto M^{-2}$. Eventually, for super-massive black holes with $M \gtrsim 10^8 M_\odot$, the density becomes less than 1 [g cm^{-3}], smaller than that of water! *Black holes do not necessarily have high densities.*

It is a remarkable characteristic of black holes that the mass is proportional to the radius ($R_S = 2GM/c^2$), while the mass tends to be proportional to the volume (cube of the radius) for ordinary matters.

Innermost Stable Circular Orbit (ISCO) and the energy conversion efficiency

In Newtonian mechanics, there are no limits of the minimum radius of the Kepler motion around the central object. In fact, Keplerian motion with an infinitesimal radius is possible, where the gravitational potential ($-GM/r$) shall diverge; the Newtonian mechanics apparently break here.

In general relativity, there are Innermost Stable Circular Orbit; ISCO) of Keplerian motion around the central object (black hole), which depends on the angular momentum of the black holes[7].

For Schwarzschild black holes ($a = 0$),

$$R_{ISCO} = 3R_S = \frac{6GM}{c^2}. \tag{2.20}$$

When the directions of the black hole spin and the Keplerian motion around the black hole are the same (prograde motion) R_{ISCO} decreases with increasing the black hole spin. When $a = 1$,

$$R_{ISCO} = 0.5R_S = \frac{GM}{c^2}. \tag{2.21}$$

[5] `http://bhi.gsfc.nasa.gov`

[6] Remember, central density of the neutron star, $\sim 10^{15}$ [g/cm^3] is the densest matter in the universe.

[7] `https://duetosymmetry.com/tool/kerr-isco-calculator`

When the directions of the black hole spin and the Keplerian motion around the black hole are the opposite (retrograde motion) R_{ISCO} increases with increasing the black hole spin. When $a = -1$,

$$R_{ISCO} = 4.5 R_S = \frac{9GM}{c^2}. \tag{2.22}$$

Let's consider a case that matter with the mass m falls to the black hole through an *accretion disk*. Innermost radius of the accretion disk may be identified with ISCO. Total energy of the matter E at the ISCO may be roughly estimated with Newtonian mechanics, as

$$E \approx -\frac{GMm}{R_{ISCO}} + \frac{1}{2} m v^2, \tag{2.23}$$

$$= -\frac{GMm}{2R_{ISCO}}, \tag{2.24}$$

where v is the velocity and we used the Newtonian equation of motion,

$$m\frac{v^2}{r} = \frac{GMm}{r^2}. \tag{2.25}$$

Namely, for each mass m, the gravitational energy $\frac{GMm}{2R_{ISCO}}$ is released in the accretion disk. When the *accretion rate* is $\dot{m}$, the accretion disk luminosity is

$$L_{disk} \approx \frac{GM\dot{m}}{2R_{ISCO}}. \tag{2.26}$$

In the case of Schwarzschild black hole ($a = 0$), using (2.20),

$$L_{disk} \approx \frac{1}{12} \dot{m}\, c^2 \approx 0.08\, \dot{m}\, c^2 \ \ \text{(Schwarzschild black hole)} \tag{2.27}$$

In the case of extreme-Kerr black hole with prograde case ($a = 1$), using (2.21),

$$L_{disk} \approx 0.5\, \dot{m}\, c^2 \ \ \text{(Extreme Kerr black hole).} \tag{2.28}$$

These simple calculations are based on Newtonian mechanics, which is not correct. Precisely, using general relativity, these coefficients (=energy conversion efficiencies) will be

$$1 - \sqrt{8/9} \approx 0.057 \ \ \text{(Schwarzschild black hole)}$$

and

$$1 - \sqrt{1/3} \approx 0.42 \ \ \text{Extreme Kerr black hole).}$$

Note that *black holes, in particular fast rotating black holes, are very efficient mass-energy converter*. Compare with the case of thermal nuclear reaction inside stars; the energy conversion efficiency is only 0.009 (average from hydrogen to iron).

2.3.4 X-ray energy spectra

Units of the energy spectra

When we observe X-ray energy spectrum from an celestial object, the unit of the energy spectrum is "photon/s/cm^2/keV", before the photons are detected by the satellite. However, in fact, what we can measure is in the unit of "counts/s/channel".

From the observed energy spectrum in "counts/s/channel", which is affected by instrumental energy resolution and statistical noise (due to paucity of photons), we need to estimate the incident spectrum in "photons/c/cm^2", which is independent of instruments (but dependent on assumed spectral model). Relationship between them are given by two-dimensional "response matrix".

In addition to [counts/s/channel] and [photon/s/cm^2/keV], [erg/s/cm^2/keV] ([keV/s/cm^2/keV]) or erg^2/s/cm^2/keV ([keV^2/s/cm^2/keV]) are often used to indicate energy spectra.

X-ray Energy Spectrum of the Crab Nebula

The Crab nebula is often used as a "standard candle" in X-ray astronomy, since it has a nearly constant luminosity and simple power-law spectrum in the standard X-ray energy range (typically 2–10 keV[8]).

Within 1 keV ≈ 50 keV energy range, the energy spectrum of Crab may be expressed as

$$f(E) \approx 10\,(E/1\,\mathrm{keV})^{-2.1}\ [\mathrm{photons/s/cm^2/keV}]. \tag{2.29}$$

Remember, you get "∼10 photons per 1cm^2 per second at 1 keV" if you observed the Crab nebula.

Crab unit

Historically, energy flux of the Crab nebula ("one Crab") has been used as a unit of the energy flux[9]

Let' calculate the energy flux of the Crab nebula, which is "1 Crab" in definition. Using (2.29),

$$\int_2^{10} 10\,E^{-2.1}\,E\,dE = 13.9\ \mathrm{keV/s/cm^2} \approx 2\times10^{-8}\ \mathrm{erg/s/cm^2}. \tag{2.30}$$

Commonly, X-ray energy fluxes of the sources in 2 – 10 keV are expressed in the unit of "erg/s/cm^2"

2.3.5 Galactic interstellar space

Typical interstellar density

≈ 1 Hydrogen atom/cm^3

Using this, distance to the Galactic source d and the hydrogen column density (N_H) has a rough correlation : $N_=H \approx 3\times10^{21}$ (d/kpc) cm^{-2}

[8]Proportional counters using Ar or Xe have sensitivity in this energy band.

[9]For instance, "X-ray flux from LMC X-3 in 2-10 keV is variable within ∼10mCrab to ∼40mCrab".

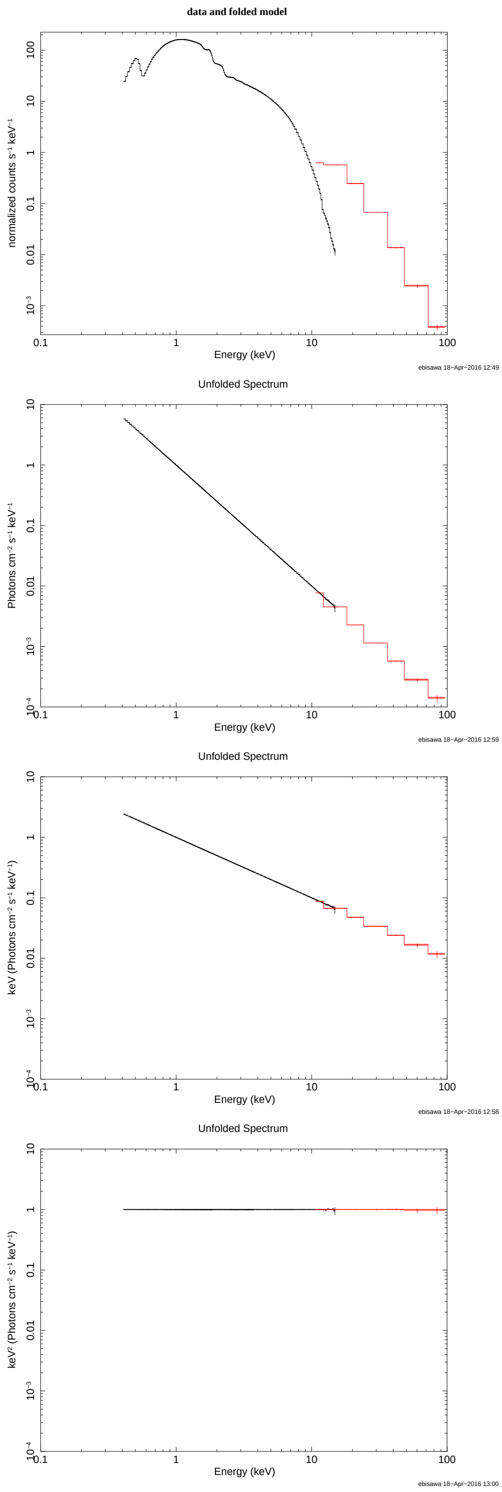

Figure 2.6: Energy spectra displayed in different units. The model is a power-law with E^{-2} [photons/s/cm^2/keV]. In the top ([counts/s/keV]), Suzaku XIS (0.4-12 keV) and PIN (10–80 keV) instrumental responses are adopted.

Interstellar Magnetic Fields and Energy Density

Typical interstellar magnetic field strength is $B \approx 3\mu$ Gauss。 Using (**??**), the corresponding energy density is $\approx 3.6 \times 10^{-13}$ erg cm^{-3} ≈ 0.2 eV cm^{-3}。

Energy density of the Cosmic Microwave Background is ≈ 0.3 eV/cm^{3}indexCosmic Microwave Background which is comparable to that of the stellar magnetic energy density.

On the other hand, energy density of Galactic cosmic ray is $\approx$ 1 eV/cm^3, which is most significant energy density in the Galactic interstellar space.

X-ray Absorption and Interstellar Extinction

X-rays are absorbed by photoelectric absorptions by interstellar heavy elements such as C, N, O, Ne, Mg and Fe. Degree of the interstellar absorption is estimated using the hydrogen column density, N_H, assuming cosmic elemental abundance. Note that hydrogen and helium hardly contribute the X-ray absorption.

Meanwhile, optical and infrared lights are affected by interstellar dusts, so the interstellar "extinction" and "reddening" take place.

Amount of interstellar heavy elements and dusts are correlated, so that there are empirical relationship between the interstellar extinction and the hydrogen column density ;

$$N_H/A_V \approx 1.9 \times 10^{21} \ \ \mathrm{cm}^{-2}\ \mathrm{mag}^{-1} \tag{2.31}$$

$$N_H/A_J \approx 5.6 \times 10^{21} \ \ \mathrm{cm}^{-2}\ \mathrm{mag}^{-1} \tag{2.32}$$

$$N_H/A_K \approx 1.1 \times 10^{22} \ \ \mathrm{cm}^{-2}\ \mathrm{mag}^{-1}. \tag{2.33}$$

As you go to the longer wavelength ($V \rightarrow J \rightarrow K$), the hydrogen column densities required to extinguish the light by one magnitude will be larger. Namely, you will be able to observed the Galactic plane "deeper".

Interstellar Extinctions and Optical Depths

Let's assume the interstellar extinction A, and the corresponding optical depth is τ. Let's put the flux and magnitude before affected by the extinction are f_b, m_b, and those after the extinction are f_a, m_a.

$$f_a = f_b\, e^{-\tau}$$

$$m_b = -2.5 \log f_b + C, m_a = -2.5 \log f_a + C$$

Thus,

$$A = m_a - m_b = 2.5 \log(f_b/f_a) = 2.5\, \tau\ \log e = 1.09\, \tau \approx \tau. \tag{2.34}$$

Namely, amount of the dust to reduce the light by 1 magnitude has the optical depth $\sim$unity.

Penetrating Power of X-rays and K-band Infrared-light

From (2.33) and (2.34), we can see that the interstellar dusts which reduce the K-band infrared-light by 1 magnitude ($\tau \approx 1$ in K-band) correspond to $N_H \approx 1.1 \times 10^{22}$ cm^{-2}. X-ray photo-absorption cross-sections by interstellar-matter are calculated (Figure 2.7), and it is $\sim$9 $\times 10^{-23}$ cm^2 at 1.5 keV. Namely, the interstellar matter with $N_H \approx 1.1 \times 10^{22}$ cm^{-2} gives $\tau \approx 1$ also at 1.5 keV.

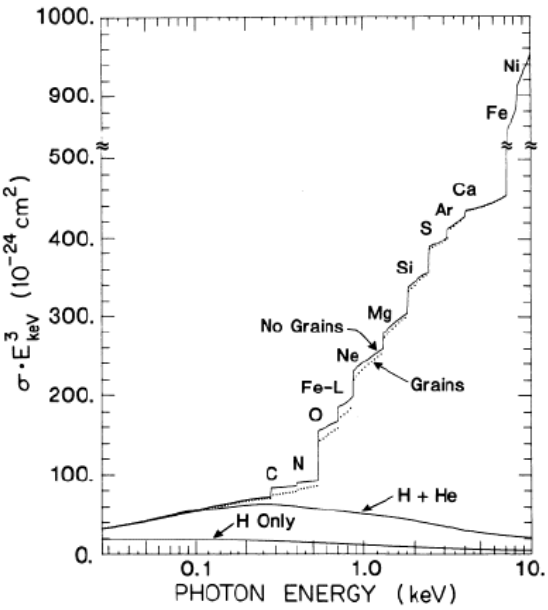

Figure 2.7: X-ray cross-sections of interstellar matter (from Morrison and McCammon, 1983, ApJ, 270, 119).

Consequently, the *K-band infrared-light and 1.5 keV X-ray have similar penetrating power toward the Galactic plane.* Thus, Galactic X-ray sources are often followed-up by K-band infrared observations, where optical counterparts are not visible due to heavy extinction[10].

[10]See e.g, Ebisawa et al. 2015, ApJ, 635, 214; Morihana et al. 2016, PASJ

Chapter 3

Basic of Accretion Disk

3.1 X-ray Astronomy and the Standard Accretion Disk

Look at the text book "High Energy Astrophysics" by Katz, which was published in 1987: 'There are few astronomical objects in which the continuum radiation from an accretion disk can be unambiguously identified. ... The theory of discs is in a much more primitive state than that of stars. This resembles the problem of stellar structure prior to the development of nuclear physics in 1930's. We may be worse off than this, because so few direct observations of discs are possible. ... It may be appropriate to compare our present understanding of discs to Galileo's understanding of sunspots and solar activity." Surprisingly, this was the situation regarding observation of accretion disks in med 1980's.

The Japanese Ginga satellite, which was operational from 1987 to 1991, confirmed that several Galactic black hole binaries, including LMC X-3, GS2000+25 and GS1124–68[1], have rather constant innermost disk radii while their luminosities are largely variable (in other words, the disk luminosity is proportional to the disk temperature to the power of fourth), and the innermost radius is about the size of three times Schwarzschild radius; ISCO in the Schwarzschild black hole (eq. 2.20; Figure 3.1).

Ginga confirmed that the standard optically thick accretion disks do exist in Galactic black hole binaries. "High Energy Astrophysics" second edition (1994) by Longair states as follows; "This is a remarkable result, but it is clearly dependent upon a number of assumptions, particularly that the accretion disk is optically thick." In fact, before Ginga, presence of the optically thick accretion disk around Galactic black holes was not certain. Following Ginga, RXTE and other satellites have confirmed presence of the remarkably constant innermost radius of the optically thick accretion disk, which is identified as ISCO (Figure 3.2).

3.2 Accretion Disk Models as Mathematical Solutions

Accretion disk models are obtained by solving equations of gravitation, pressure balance, radiation etc. Those solutions are often indicated on the 2-dimensional plane of surface density Σ [g/cm^2] and mass accretion rate $\dot{M}$ [g/s] (Figure 3.3).

In Figure 3.3, the line $H = r$ indicates the height (H) and radius (r) of the disk are equal; closer to this line, the disk is geometrically thicker, further from this line, the disk is

[1]GS stands for Ginga Satellite.

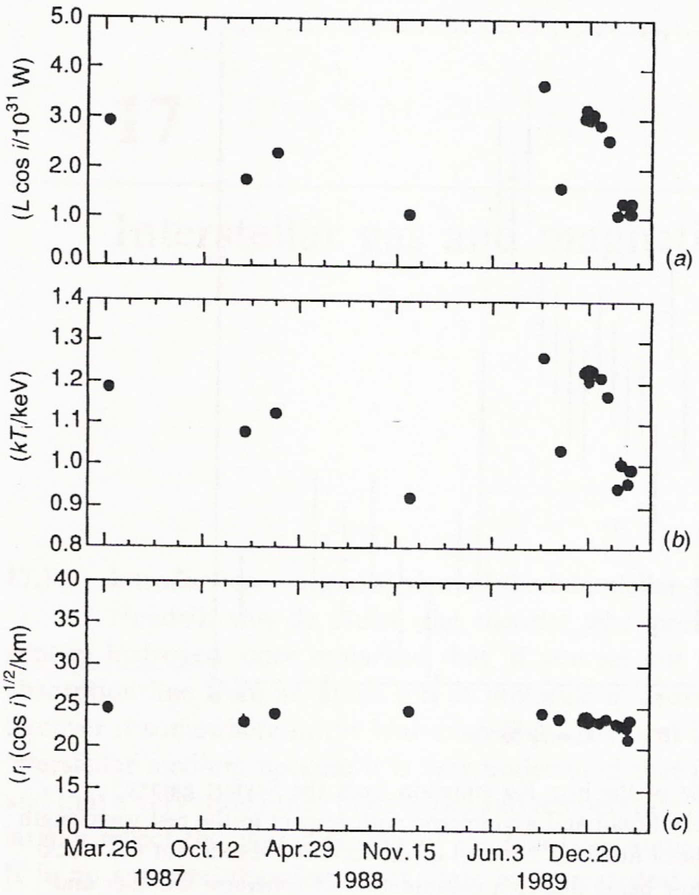

Figure 16.22. Time histories of the best-fit parameters to the soft component of the X-ray spectrum of LMC X-3 obtained by the Japanese Ginga satellite. (*a*) The bolometric luminosity of the sources; (*b*) the inferred temperature at the inner radius of the acccretion disc; (*c*) the inferred inner radius, r_i, of the accretion disc. i is the inclination angle of the plane of the orbit to the plane of the sky. (From H. Inoue (1992). *Proc. Texas/ESO-CERN Symposium on Relativistic astrophysics, cosmology and fundamental particles*, eds J.D. Barrow, L. Mestel and P.A. Thomas, pp. 86–103. New York: New York Academy of Sciences.)

Figure 3.1: Spectral variation of LMC X-3 observed with Ginga. Top panel indicates the disk luminosity, the middle panel is disk temperature, and the bottom panel is the innermost disk radius, where model fit was made with the innermost disk radius (r_{in}) and the temperature (T_{in}) being free parameters. The disk luminosity is derived as $L_{disk} \propto r_{in}^2\ T_{in}^4$ (eq. 3.15). Taken from Longair, "High Energy Astrophysics, volume 2" second edition (1994), together with the figure caption, which cites the original Ginga paper.

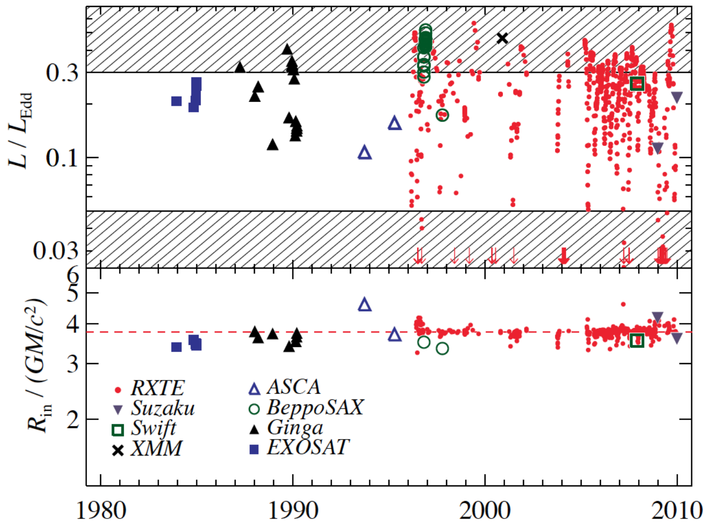

Figure 3.2: Accretion disk luminosity (top) and innermost radius (bottom) of LMC X-3 observed by various satellites including Ginga. Taken from McClintock, Narayan and Steiner, 2014, Space Science Reviews, 183, 295.

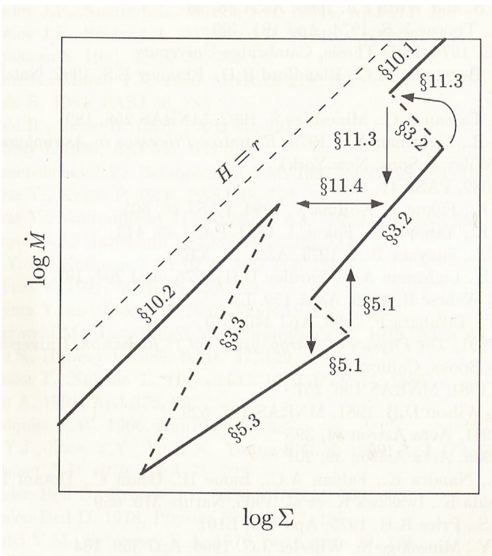

Figure 3.3: Mathematical solutions of accretion disks on the $\log \Sigma$ vs. $\log \dot{M}$ plane. Taken from Kato, Fukue and Mineshige "Black-hole Accretion Disks". Labels correspond to section numbers in the book.

geometrically thinner. If you go right-hand side, the surface density is larger and the disk is more optically thick; in left-hand side, the disk is optically thinner.

Labels in Figure 3.3 correspond to sections in the book, particular states of the accretion disk; §3.2 corresponds to the "Optically Thick Disks", which is so-called the standard accretion disk model. Observationally, this explains X-ray emission in the "high/soft" state of Galactic black hole binaries, where the innermost radius corresponds to ISCO (Figures 3.1, 3.2; section 3.5). §3.3 is the "Optically Thin Disks", which is thermally unstable.

§5.1 corresponds to "Thermal-Ionization Instability", such that the hydrogen is ionized in the upper-branch and not ionized in the lower-branch. The "limit-cycle"' takes place between the two branches, which explains "dwarf novae" observed in optical and UV lights in terms of the "disk instability model".

§5.3 corresponds to "Emission-Line Formation during Quiescence", which corresponds to the quiescence state of dwarf novae, when the Doppler-shifted emission lines are observed from the accretion disk.

§10.1 is the "Radiation-Pressure-Dominated Disks", which is optically thick and the advection is dominant. This is also coled Optically thick Advection Dominated Accretion Flow (ADAF), or "slim-disk". Slim-disk may explain the Ultra-Luminous X-ray (ULX) sources (section 3.7).

§10.2 is the "Optically-Thin One-Temperature", or optically thin ADAF, corresponding to hot, optically thin, and geometrically thick disk, which is considered to to explain the low/hard state of the black hole binaries.

§11.3 is "Relaxation Oscillations in Hot Accretion Disks", which explains limit-cycle oscillation between the slim-disk state and the standard-disk state, which presumably explain the quasi-periodic variations observed from GRS1915+105.

§11.4 is "Advection-Dominated Flow in X-ray Novae", which explain the transition between the high/soft state and the low/hard state of black hole binaries.

3.3 Thickness, Temperature, and Potential of the Disk

Consider the accretion disk where gas-pressure is dominant. Assuming pressure P, density ρ, temperature T and the gas particle mass (mostly hydrogen) m, the equation of state gives,

$$P \approx \frac{\rho k T}{m}. \tag{3.1}$$

Assuming the height of the disk, h, gravitational balance in the vertical direction gives,

$$\frac{dP}{dh} \approx -\frac{GM\rho}{r^2}\frac{h}{r}.$$

We may estimate orders of the parameters such as,

$$\frac{P}{h} \approx \frac{GM\rho}{r}\frac{h}{r^2}. \tag{3.2}$$

Combining (3.1) and (3.2), we get

$$\frac{kT}{GMm/r} \approx \left(\frac{h}{r}\right)^2. \tag{3.3}$$

Look at the left-hand side; the denominator gives the gravitational potential of a particle, and the numerator is the thermal energy. Namely, we can see that *geometrically thin disk* ($h/r \ll 1$)*, which is the case for the standard accretion disk (section 3.4), gives the thermal energy (disk temperature) much lower than the gravitational potential energy of a particle*, and that *geometrically thicker disk gives higher disk temperature.*

The gravitational energy of a particle around a black hole may be estimated at the Schwarzschild radius $R_S = 2GM/c^2$, such that,

$$\frac{GMm}{R_s} = \frac{GMm}{2GM/c^2} \approx mc^2 \approx 1 \text{ GeV}, \tag{3.4}$$

whereas typical standard disk temperature of Galactic black holes is ~ 1 keV (section 3.5.3), that is much lower, in fact.

The geometrically thin and cool disk corresponds to the high/soft state of the black hole binaries (§3.2"Optically Thick Disks" in Figure 3.3), and the geometrically thick and hot disk corresponds to the low/hard state (§10.2 "Optically-Thin One-Temperature"). The slim-disk (§10.1) is hotter and geometrically thicker than the standard accretion disk, which may explain the relatively high temperature (hard X-ray energy spectra) of the Ultra-luminous X-ray sources.

3.4 The Standard Accretion Disk Model

The paper by Shakura and Sunyaev (1973, A&A, 24, 337) is historical, where the "standard accretion disk model" is established[2]. Here, accretion disk solutions are obtained assuming that (1) the disk is optically thick and geometrically thin, (2) the released gravitational energy is converted to the radiation (no advection), and (3) the viscous tensor is proportional to the viscous parameter α and the pressure (eq. 3.7).

In short, there are 11 equations to connect the following 11 parameters of the disk. For given $M, \dot{M}, \alpha$, the 11 parameters are solved as functions of the disk radius r.

1. $\Omega = \sqrt{\frac{GM}{r^3}}$ — angular velocity by Keplerian motion
2. h — disk height
3. Σ — disk surface density
4. ρ — disk density
5. v_r — vertical velocity
6. T_c — temperature inside (mid-point) of the disk
7. τ — disk optical depth in the vertical direction
8. ν — kinematic viscosity
9. v_s —sound velocity

[2] As of June 6, 2016, ADS shows 7521 citations.

10. p — disk pressure

11. $\bar{\kappa}$ — average opacity

In particular, the six parameters following Ω are obtained as functions of $M, \dot{M}, \alpha, r$, with which the rest four parameters are expressed.

3.4.1 Rotation velocity and infall velocity

While rotating in the disk with Keplerian motion, the matter gradually falls toward black hole due to kinematic viscosity. The viscous tensor which works between the azimuthal direction and the radial direction is written as

$$t_{r\varphi} \approx \rho\, v_{turb}^2 \approx \rho\, v_r v_\varphi, \tag{3.5}$$

where ρ is density, v_{turb} is the turbulent velocity, v_r is the radial velocity, $v_\varphi(=\sqrt{GM/r})$ is the azimuthal velocity.

We may assume that the turbulent velocity is smaller than the sound velocity, $v_s \approx \sqrt{P/\rho}$, so that

$$t_{r\varphi} \lesssim \rho\, v_s^2 = P. \tag{3.6}$$

It is remarkable that Shakura and Sunyaev (1973) defined the viscous parameter α as

$$t_{r\varphi} \equiv \alpha P, \tag{3.7}$$

where α takes values between 0 and 1, P is pressure. Due to eq. (3.7), equations of standard accretion disk can be solved[3].

From (3.5), (3.6) and (3.7),

$$\alpha = \frac{v_r\, v_\varphi}{v_s^2}. \tag{3.8}$$

Using (3.2),

$$\frac{P}{h} \approx \frac{GM\rho}{r}\frac{h}{r^2} \approx v_\varphi^2 \frac{\rho h}{r^2}. \tag{3.9}$$

Since $P/\rho \approx v_s^2$,

$$v_\varphi \approx v_s \left(\frac{r}{h}\right). \tag{3.10}$$

In the standard accretion disk, which is geometrically thin, $r/h \gg 1$, so that *the rotation velocity is much larger than sound velocity.* Also, from (3.8) and (3.10),

$$v_r \approx \alpha\, v_s \left(\frac{h}{r}\right) \approx \alpha\, v_\varphi \left(\frac{h}{r}\right)^2. \tag{3.11}$$

Namely, *the in-falling velocity will be higher as α gets greater, but it is much smaller than the rotational velocity even at the maximum ($\alpha = 1$).*

[3]Today, the viscosity is considered to be caused by magneto-viscous effects, and Magnetic Hydro-Dynamics (MHD) simulation can solve accretion disk equations without α and eq. (3.7.

3.5 X-ray Emission from the Standard Disk

3.5.1 Radial dependence of the disk temperature

Let's consider the standard accretion disk around a black hole having the mass M, where the mass accretion rate is $\dot{M}$. While matter falls dr in the disk, half the gravitational potential is released (Virial theorem), the disk is thermalized, and converted to the emission.

Assuming the black body emission from both surfaces,

$$2 \cdot 2\pi r\, dr\, \sigma T^4 \propto \frac{1}{2} d\left(-\frac{GM\dot{M}}{r}\right) = \frac{GM\dot{M}}{2\,r^2}\, dr,$$

$$T(r) \propto \left(\frac{GM\dot{M}}{8\pi\sigma r^3}\right)^{1/4}. \tag{3.12}$$

In the above equation, the radial dependence is correct, but the inner-boundary condition is not taken into account. If we consider the inner-boundary condition (zero temperature at the innermost radius), the precise equation is,

$$T(r) = \left(\frac{3GM\dot{M}}{8\pi\sigma r^3}\left(1 - \sqrt{r_{in}/r}\right)\right)^{1/4}. \tag{3.13}$$

In any case, emission from the innermost region is not significant because of the low temperature and the small area. It is essential that the *disk temperature is proportional to* $r^{-3/4}$ *in the standard accretion disk*[4].

3.5.2 Luminosity of the multicolor blackbody disk

Ignore the inner-most boundary condition, and assume the radial dependence of the temperature $T(r) \propto r^{-3/4}$. Consider the accretion disk which emits the black body emission at each radius with the temperature $T(r)$. This model is called "multicolor disk blackbody" model, which is simple but explain the observations sufficiently enough

Let's obtain the luminosity of the multicolor disk blackbody model. Assuming the innermost radius and the temperature r_{in} and T_{in},

$$T(r) = T_{in}\,(r/r_{in})^{-3/4}. \tag{3.14}$$

Considering both surfaces and integrating from the innermost radius to the outer edge (r_{out}), we get

$$\begin{aligned} L_{disk} &= 2\int_{r_{in}}^{r_{out}} 2\pi r\sigma T(r)^4 dr \\ &= 4\pi\sigma T_{in}^4 r_{in}^3 \int_{r_{in}}^{r_{out}} r^{-2} dr \\ &= 4\pi\sigma T_{in}^4 r_{in}^3 (1/r_{in} - 1/r_{out}) \approx 4\pi\sigma r_{in}^2 T_{in}^4, \end{aligned} \tag{3.15}$$

where, we assumed $r_{out} \gg r_{in}$.

[4] As the mass-accretion rate increases, the disk will be "slim disk" and the exponent varies from $-3/4$ to -0.5.

3.5.3 Maximum disk temperature around black holes

Let's estimate the maximum disk temperature, T_{in}, in the case of Schwarzschild metric. Now, $R_{ISCO} = 3R_s$ (eq. 2.20), which may be identified as r_{in} in (3.15). We assume that the standard accretion disk is shining at the Eddington limit, which is a valid assumption (section 3.7).

From

$$L_{Edd} = \frac{4\pi \, c\,GM}{\kappa} = 4\pi \, \sigma \, (3R_s)^2 \, T_{in}^4, \tag{3.16}$$

$$\begin{aligned} T_{in} &\approx \left(\frac{c^3}{18\sigma\kappa}\right)^{1/4} \left(\frac{2GM_\odot}{c^2}\right)^{-1/4} \left(\frac{M}{M_\odot}\right)^{-1/4} \\ &\approx 2 \text{ keV} \left(\frac{M}{M_\odot}\right)^{-1/4} \approx 1 \text{ keV} \left(\frac{M}{10M_\odot}\right)^{-1/4}. \end{aligned} \tag{3.17}$$

Namely, *the standard accretion disk around a* $\sim 10M_\odot$ *black hole shining at the Eddington limit has the temperature* ~ 1 *keV, to be observed in the X-ray band.*

Note that *the maximum accretion disk temperature decreases as the black hole mass increases as* $\propto M^{-1/4}$ (eq. 3.17). For instance, the super-massive black hole with $M = 10^9 M_\odot$ has the maximum disk temperature ~ 10 eV, which may be observed in the UV band. This is considered to be origin of the *UV-bump* often observed in the Active Galactic Nuclei.

3.6 Measurement of the Black Hole Spin

From eq. (3.16), we see T_{in} will be higher for smaller R_{ISCO}. Namely, rotating black holes ($0 < a \leq 1$), having smaller R_{ISCO} (eq. 2.21), will have higher disk temperature. Retrograde disk, where the disk is rotating in opposite direction to black hole, R_{ISCO} is larger than the Schwarzschild case (eq. 2.22), and the disk temperature will be lower. Accretion disk temperature is measured in X-ray, where relativistic effects should be taken into account to precisely compare the X-ray observation and the accretion disk model[5]. For the Galactic black hole binaries of which distance, mass and inclination angles are known, X-ray observation can constrain R_{ISCO}, and thereby the black hole spin. See for details, e.g., McClintock, Narayan and Steiner, 2014, Space Science Reviews, 183, 295; Morningstar et al. 2014, ApJ, 784, L18.

3.7 Maximum Luminosity of the Slim-Disk

We have seen that luminosity from the spherically accreting and emitting object is limited by the Eddington limit (section 2.3.1). Let's consider maximum luminosities of accretion disk which is obviously not spherically symmetric.

Considering balance in the vertical direction, assuming the flux per disk area F,

$$\frac{F\sigma_T}{c} \lesssim \frac{GMm_H}{r^2}\frac{h}{r}, \tag{3.18}$$

[5] The relativistic effects are significantly dependent on the disk inclination angle.

where σ_T is the Thomson cross-section and m_H is the hydrogen mass. The disk luminosity, L_{disk} may be obtained by radially integrating F for both surfaces from r_{in} to r_{out};

$$L_{disk} = 2 \times 2\pi \int_{r_{in}}^{r_{out}} rF dr. \tag{3.19}$$

Consequently,

$$\begin{aligned} L_{disk} &\leq \frac{4\pi cGMm_H}{\sigma_T} \int_{r_{in}}^{r_{out}} \frac{1}{r}\frac{h}{r} dr \\ &\approx L_{Edd}\left(\frac{h}{r}\right) \int_{r_{in}}^{r_{out}} \frac{1}{r} dr \approx L_{Edd}\left(\frac{h}{r}\right) \ln\left(\frac{r_{out}}{r_{in}}\right), \end{aligned} \tag{3.20}$$

where we made an assumption that $h/r = \text{const}$.

Approximately, $\ln(r_{out}/r_{in}) \sim 10$, thus geometrically thin standard disk $(h/r \approx 0.1)$ gives $L_{disk} \leq L_{Edd}$.

On the other hand, when the disk is geometrically thicker $(h/r \approx 1)$, $L_{disk} \leq 10L_{Edd}$, namely, the disk can have *super-Eddington luminosities.* Hence, slim-disk, which is optically thick and geometrically thicker than the standard disk, can emit super-Eddington luminosities, and considered to explain the *Ultra-Luminous X-ray sources (ULXs)* with 10^{40-41} erg/s, that cannot be explained by stellar-mass black holes with sub-Eddington luminosities.

Chapter 4

Astronomical Observation using Artificial Satellites

In order to observe Universe in X-rays, we need to go to space, since we cannot observe from ground. Similarly, UV, far-infrared, gamma-ray observations are carried out from space. Even in optical wave-length, there is a merit to observe from space, since the atmospheric seeing does not exist in space[1]. Let's learn how to observe using astronomical satellites. First, we need to learn different celestial coordinates. Then, we learn satellite attitudes and orbits. This is necessary to understand the Attitude and Orbit Control System (AOCS) of the satellite, which is critical for satellite operation/observation.

4.1 Celestial Coordinates

In astronomy, we adopt a virtual *celestial sphere* to consider apparent locations on the sky. We are at the center of the sphere, and if we extrapolate the spin-axis of the earth, we may define the *North pole* of the celestial sphere. If we extrapolate the equator of the earth, we may define the *Equator* of the celestial sphere.

The spin-axis of the earth is not perpendicular to the orbital plane of the earth, but tilted by $23.^\circ 44$[2]。 Path of Sun on the celestial sphere is *ecliptic* , which is inclined by $23.^\circ 44$ relative to equator. Crossing points of the equator and the ecliptic are the *spring equinox* (Sun crosses the equator from south to north) and the *autumn equinox* (Sun crosses the equator from north to sought). The point on the ecliptic where Sun is the most north is *summer solstice*, and the point on the ecliptic where Sun is the most south is *winter solstice*. Spring equinox, autumn equinox, summer solstice, winter solstice are terminologies for the locations on celestial sphere, as well as for the corresponding dates in calendar.

Like global longitude ($0^\circ \sim 360^\circ$) and latitude ($-90^\circ \sim +90^\circ$), we define *Right ascension*

[1]Typically, atmospheric seeing blurs a star about $1''$ in optical band. If you need better spatial resolution in optical band, you either need to go to space or use adaptive optics.

[2]The inclination varies from $22.^\circ 2$ to $24.^\circ 5$ at a period of 41000 year, and the spin axis shows a *precession* such that the spin axis rotates around a fixed axis with a period of 25800 year. Thus, the equatorial coordinates change with time, and we must specify which *equinox* we are referring to. Today, commonly equinox 2000 is used (J2000). A few tens of year ago, it was more common to use the equinox 1950 (B1950). In a few tens of year, equinox 2050 will be more common. As an example, location of the black hole binary Cyg X-1 is ($299.^\circ 590$, $35.^\circ 201$) (J2000), or ($299.^\circ 120$,$35.^\circ 065$)(B1950).

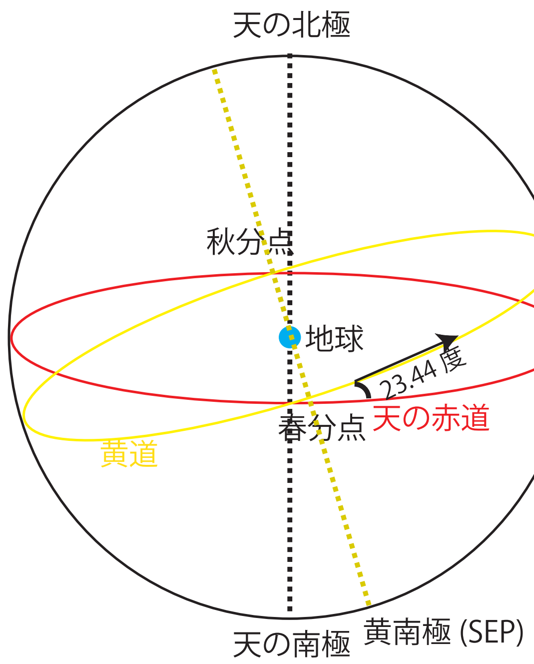

Figure 4.1: Celestial sphere, equator, ecliptic

($0° \sim 360°$) and Declination ($-90° \sim +90°$) on the celestial sphere. Like the location of the Greenwich observation is at the global longitude $0°$, origin of the Right Ascension is the Sprint equinox. In this manner, *Equatorial Coordinates* are defined [3]。 Similarly, we may define the *Ecliptic Coordinates*, based on the ecliptic plane and ecliptic poles.

Similar to the earth surface, we use north (direction of North Pole), south (direction of Sought Pole), east (direction of increasing the Right Ascension) and west (direction of decreasing the Right Ascension) on the celestial sphere. Be careful that *directions of east and west are opposite on the earth (we are outside of the globe) and on the celestial sphere (we are inside of the sphere).* On a map of the earth, when north is up, right is east; on a map of the celestial sphere, when north is up, left is east.

Also, we often use *Galactic coordinates*, which is based on the Galactic Plane (Milky Way). Direction of the Galactic center is the origin, where Galactic Longitude and latitude is (0,0). The Galactic latitude increases as you go left on the Galactic plane. ,

Any positions on the celestial sphere may be expressed with Equatorial Coordinates, Ecliptic Coordinates, or Galactic Coordinates. Figure 4.2 shows presents grids of all the

[3]Since rotation of the celestial sphere is used as a "clock", we may express the Right Ascension from 0 hour to 24 hour, instead of 0○ to 360○. In this case, an hour corresponds to 15°. As usual, an hour is 60 minutes, and a minute is 60 seconds. Using hh, mm, ss for hour, minutes, and seconds, Right Ascension may be expressed as hh:mm:ss.s. Also, one degree is 60 arcmin, and 1 arcmin is 60 srcsec, namely, $1° = 60', 1' = 60''$.

In this manner Right Ascension and Declination of a celestial target may be written as $(281.°00, -4.°07)$ or, identically, $(18:44:0.0, -4°4'12'')$

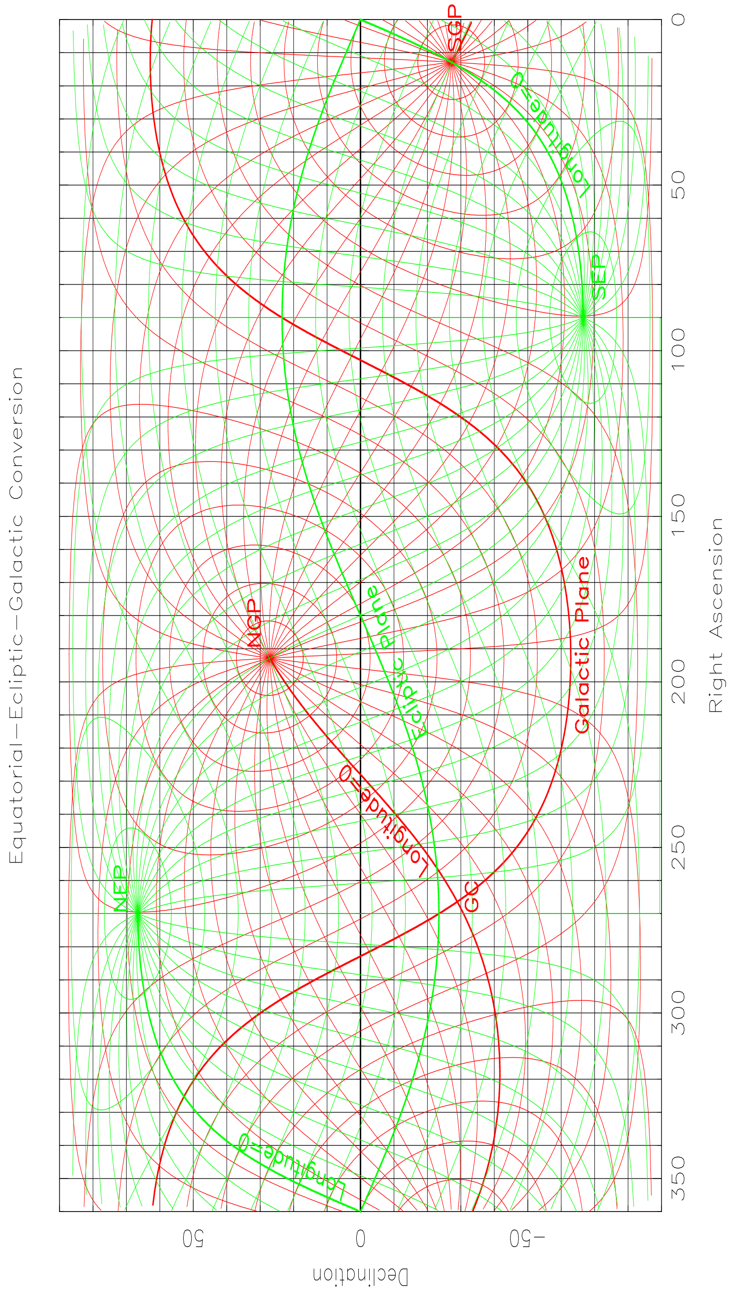

Figure 4.2: Equatorial coordinates, Ecliptic coordinates, and Galactic coordinates

three coordinates [4].

For example, the following coordinate indicates the same position; [5].

$$\begin{gathered}(\text{RA、DEC})=(\alpha,\delta)=(281.^\circ 00,\ -4.^\circ 07)\\ (\text{Galactic longitude, Galactic latitude})=(l,b)=(28.^\circ 463,\ -0.^\circ 204)\\ (\text{Ecliptic longitude, Ecliptic latitude }=(\lambda,\beta)=(281.^\circ 608,\ 18.^\circ 927)\end{gathered}$$

Below, we consider how we calculate these coordinate conversions[6].

4.2 Satellite Attitudes

4.2.1 Satellite Axes and Satellite Coordinate

Consider the "satellite coordinates" XYZ, which is fixed to the satellite (Figure 4.3). Science satellites developed at JAXA/ISAS have such a definition of the satellite attitude that the spin axis and the telescope are along the +Z-axis, the solar-panel is toward the +Y-axis. You should be careful that the definition of the satellite coordinate is dependent on different satellites or institutes.

The solar-panel should be toward the sun to produce electric power, and the Sun moves on the ecliptic with season. Consequently, the observation targets (+Z-axis) should be on the great circles which are orthogonal to the ecliptic. Also, we can see that North Ecliptic Pole (NEP) and South Ecliptic Pole (SEP) are always observable all year around.

Some satellites, such as ROSAT (X-ray) and Akari (infrared), carry out *all-sky survey*, continuously spinning around the Y-axis. These scan paths are the great circles through NEP and SEP. See, example, `http://apod.nasa.gov/apod/ap000819.html`, `http://www.ir.isas.jaxa.jp/AKARI/Archive/Images/FIS_AllSkyMap/`. You can vaguely see many scan-paths, which concentrate on the NEP and SEP.

The ASCA satellite was not designed for all-sky survey, but the *attitude maneuver* or *slew* are performed always facing the Y-axis toward the Sun. Consequently, the large attitude maneuver/scan paths are along the great circles through NEP and SEP. In Figure 4.4, we show exposure map (exposure time on each sky pixel) of the ASCA slew operations throughout the mission period (from 1993 to 2000) in the Galactic coordinates and ecliptic coordinates. We can see that NEP and SEP are most exposed as well as Galactic plane region.

4.2.2 Satellite attitudes and Euler angles

Satellite attitudes relative to the sky coordinates are described with the "Euler angles". Let's put the initial attitude of the satellite that the +Z-axis is toward the North-pole, +X-axis is toward the sprint equinox. We sequentially rotate the satellite by ϕ around +Z-axis, θ around the +Y-axis, and ψ around the +Z-axis. Now, the resultant satellite attitude is represented

[4] The Fortran program to draw this figure is put at `http://www.isas.jaxa.jp/home/ebisawalab/ebisawa/TEACHING/2007Komaba/PlotCoordinates.f` Here, I used the pgplot library.

[5] "GALACTIC_RIDGE" observation with Suzaku. See, `http://darts.jaxa.jp/astro/tables/SUZAKU_LOG.html`, where the sequence numbers are 500009010 and 500009020, and the Euler angles are (281.0000,94.0700,184.4698).

[6] There are many tools available to carry out the coordinate conversion. For instance, `http://heasarc.gsfc.nasa.gov/cgi-bin/Tools/convcoord/convcoord.pl`.

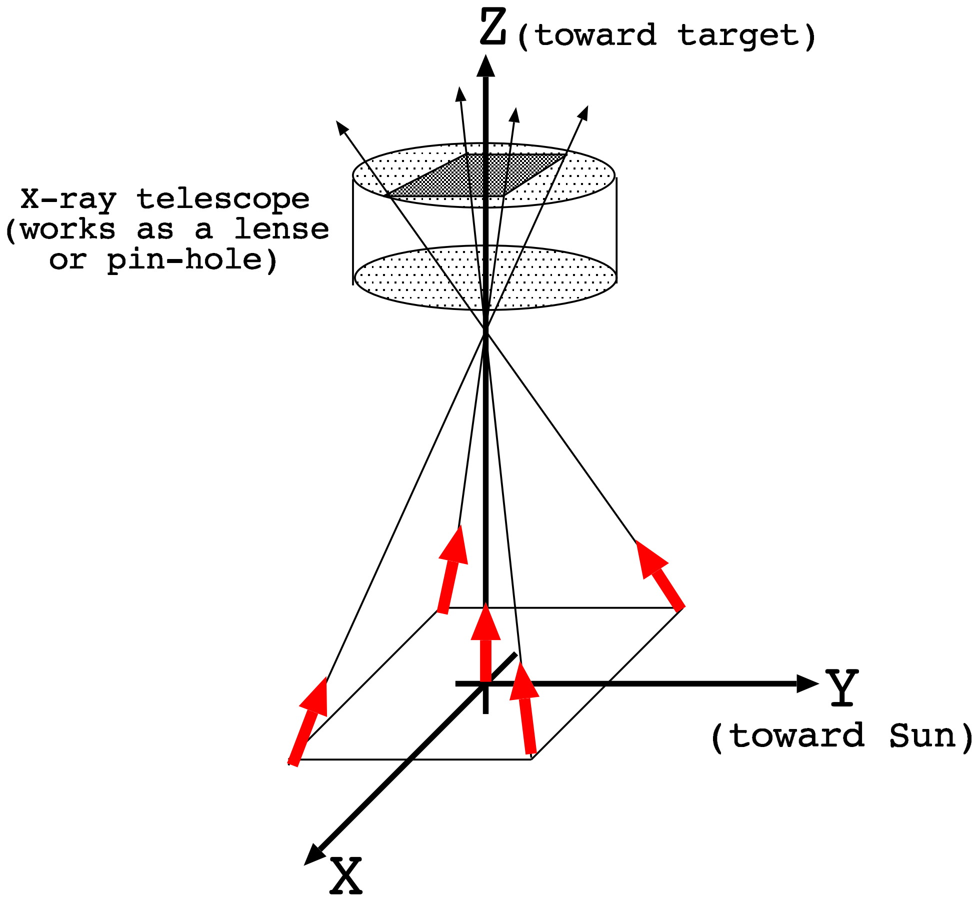

Figure 4.3: Satellite coordinates and field of view.

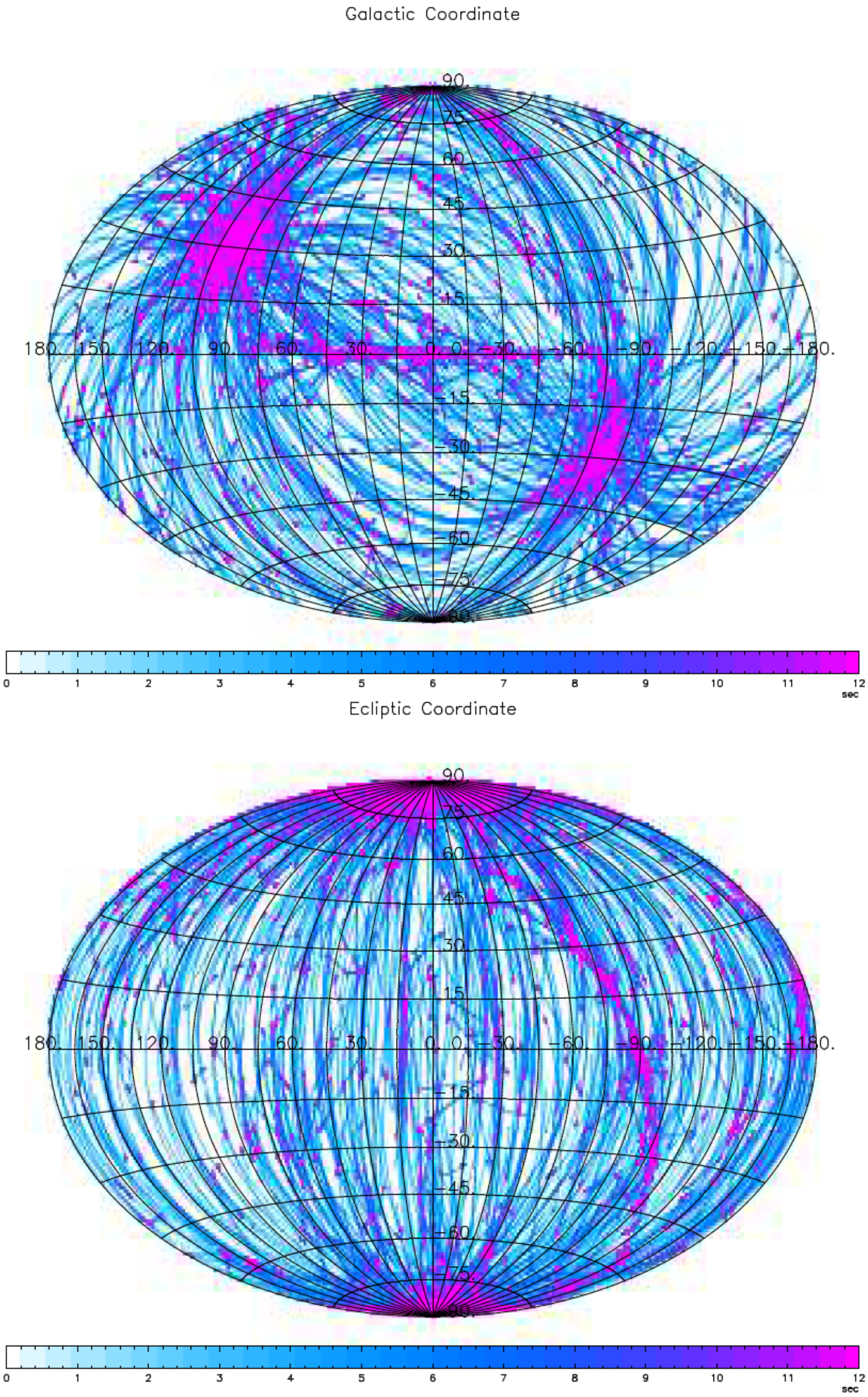

Figure 4.4: Exposure map of the ASCA slew survey in the Galactic coordinates (top) and the ecliptic coordinates (bottom). Taken from "ASCA Slew Survey", Ebisawa, Fujimoto and Ueda 2003 (DOI: 10.1002/asna.200310058).

with (ϕ, θ, ψ) Euler angles with ZYZ rotation. Remember, definition of Euler angles is not unique, and we need to specify the the order and axis of the rotation. In any case, any satellite attitudes can be represented with three angles.

Let' consider relationship between the Euler angles and field of view of the satellite. Put the ZYZ Euler angles (ϕ, θ, ψ), and the telescope is pointing the +Z direction. Right Ascension and Declination of the pointing direction are given as

$$R.A. = \phi, Dec. = 90^\circ - \theta. \tag{4.1}$$

The third Euler angle ψ determines the *roll-angle* of the field of view. Commonly, we measure the roll-angle from North toward the instrument +Y-axis (DETY) counter-clock-wise[7]。

Relation between the third Euler angle and roll-angle is given by[8]

$$Roll = 90^\circ - \psi. \tag{4.2}$$

4.2.3 Observation and season

When observing with satellites, the first two Euler angles are determined from the target position. The third Euler angle is constrained from the condition that the Solar-panel (+Y-axis) is toward the Sun. Consequently, when the same target is observed at different seasons, the third Euler angle is different in different seasons.

NEP is a popular area to observe, since it is observable all the year round. Let's consider the Euler angles to observe NEP in different seasons. Ecliptic is tilted by 23.°4 relative to the its equator, where they intersect at the spring equinox and the autumn equinox (Figure 4.1). Namely, if we rotate the equatorial coordinates (x-axis toward the spring equinox, the z-axis is toward the north pole) by 23.°4 around x-axis, you will get the ecliptic coordinates (x-axis toward the spring equinox, the z-axis is toward the NEP) . You can see that the equatorial coordinates of the NEP is $(\alpha, \delta) = (270^\circ, 66.^\circ6)$ (see also Figure 4.2). Since we use ZYZ Euler angles to describe the satellite attitude, the first two Euler angles are $\phi = 270^\circ, \theta = 23.^\circ4$. Starting from the initial attitude (+X toward spring equinox, +Z toward the North pole), note that now the satellite Z-axis is toward the NEP, and Y-axis is toward the spring equinox. According the the third Euler angle ψ around +Z axis, the +Y axis move on the ecliptic with the same direction of the Sun. Now we can tell the third Euler angle to observe the NEP depending on season[9]:
At sprint equinox, $\psi = 0^\circ$
At summer solstice, $\psi = 90^\circ$
At autumn equinox, $\psi = 180^\circ$
At winter solstice, $\psi = 270^\circ$。

Let's look at actual example of the NEP observation with Suzaku. Here are the dates and Euler angles of the Suzaku NEP observations with sequential numbers:

---

[7]Be careful that this is opposite on the earth, where the directional angle, or CAP, is measure clock-wise from North.

[8]This is illustrated with animation in `http://www.isas.jaxa.jp/home/ebisawalab/ebisawa/TEACHING/roll-angle.ppt`.

[9]Assuming that the solar-panel (Y-axis) completely faces toward the Sun. In fact, the solar-panel can be slightly off the Sun within the allowance technically determined (Solar-angle).

2013-11-14 (270.08, 23.40, 232.40), sequence number =708014010
2009-11-15 (270.05, 23.44, 232.82), sequence number =504070010
2009-12-07 (270.05, 23.43, 255.35), sequence number =504072010
2009-12-15 (270.05, 23.43, 261.93), sequence number =504074010
2009-12-28 (270.04, 23.42, 284.63), sequence number =504076010
2015-01-30 (270.03, 23.43, 307.48), sequence number =109016010
2015-02-03 (270.04, 23.42, 307.48), sequence number =109016020

Also, please note that the instrument field of view rotate *clock-wise* with season, since the Euler angle increases with season and the roll-angle decreases (eq. 4.2) .

4.3 Coordinate Conversion and Euler angles

4.3.1 Directional vector and coordinate conversion

Consider the *directional vector* with the unit-length toward the direction (α, δ) in the equatorial coordinates. The xyz coordinates are as follows;

$$\begin{pmatrix} x \\ y \\ z \end{pmatrix} = \begin{pmatrix} \cos\delta\cos\alpha \\ \cos\delta\sin\alpha \\ \sin\delta \end{pmatrix}. \tag{4.3}$$

Confirm $x^2 + y^2 + z^2 = 1$. Assuming the base vectors of the x, y, z-axes being $\mathbf{e_x}, \mathbf{e_y}, \mathbf{e_z}$, we may write,

$$\mathbf{p} = x\mathbf{e_x} + y\mathbf{e_y} + z\mathbf{e_z} = (\mathbf{e_x}, \mathbf{e_y}, \mathbf{e_z}) \begin{pmatrix} x \\ y \\ z \end{pmatrix}. \tag{4.4}$$

Let's put ecliptic coordinate three axes as x',y',z', and base vectors $\mathbf{e'_x}, \mathbf{e'_y}, \mathbf{e'_z}$. Similarly, the Galactic coordinate three axes x'',y'',z'', and base vectors $\mathbf{e''_x}, \mathbf{e''_y}, \mathbf{e''_z}$.

The same directional vector (4.4) can be expressed with the ecliptic coordinate or the Galactic coordinates;

$$\mathbf{p} = (\mathbf{e_x}, \mathbf{e_y}, \mathbf{e_z}) \begin{pmatrix} x \\ y \\ z \end{pmatrix} = (\mathbf{e'_x}, \mathbf{e'_y}, \mathbf{e'_z}) \begin{pmatrix} x' \\ y' \\ z' \end{pmatrix} = (\mathbf{e''_x}, \mathbf{e''_y}, \mathbf{e''_z}) \begin{pmatrix} x'' \\ y'' \\ z'' \end{pmatrix}. \tag{4.5}$$

If we put the Galactic coordinates of $\mathbf{p}$ as (l, b),

$$\begin{pmatrix} x'' \\ y'' \\ z'' \end{pmatrix} = \begin{pmatrix} \cos b\ \cos l \\ \cos b\ \sin l \\ \sin b \end{pmatrix}. \tag{4.6}$$

This can be solved for l and b, that

$$\begin{pmatrix} l \\ b \end{pmatrix} = \begin{pmatrix} \tan^{-1}\left(y''/x''\right) \\ \tan^{-1}\left(z''/\sqrt{x''^2 + y''^2}\right) \end{pmatrix}. \tag{4.7}$$

In summary, in order to convert the equatorial coordinates (α, δ) to the Galactic coordinates (l, b), first obtain the (x, y, z) components with (4.3), convert to (x'', y'', z'') with (4.5), then use (4.7).

4.3.2 Orthogonal transformation and orthogonal matrix

Consider orthogonal transformation from the orthogonal coordinate system represented with the base vectors $(\mathbf{e_1}, \mathbf{e_2}, \mathbf{e_3})$ to that represented with $(\mathbf{e'_1}, \mathbf{e'_3}, \mathbf{e'_3})$.

Since base vectors are orthogonal,

$$\mathbf{e_1}^2 = \mathbf{e_2}^2 = \mathbf{e_3}^2 = 1, \mathbf{e_1} \cdot \mathbf{e_2} = \mathbf{e_2} \cdot \mathbf{e_3} = \mathbf{e_3} \cdot \mathbf{e_1} = 0 \tag{4.8}$$

$$\mathbf{e'_1}^2 = \mathbf{e'_2}^2 = \mathbf{e'_3}^2 = 1, \mathbf{e'_1} \cdot \mathbf{e'_2} = \mathbf{e'_2} \cdot \mathbf{e'_3} = \mathbf{e'_3} \cdot \mathbf{e'_1} = 0. \tag{4.9}$$

Base vectors of the one system are represented with those of the other system.

$$\mathbf{e'_1} = a_{11}\mathbf{e_1} + a_{12}\mathbf{e_2} + a_{13}\mathbf{e_3}, \tag{4.10}$$

$$\mathbf{e'_2} = a_{21}\mathbf{e_1} + a_{22}\mathbf{e_2} + a_{23}\mathbf{e_3}, \tag{4.11}$$

$$\mathbf{e'_3} = a_{31}\mathbf{e_1} + a_{32}\mathbf{e_2} + a_{33}\mathbf{e_3}, \tag{4.12}$$

or, equivalently,

$$(\mathbf{e'_1}, \mathbf{e'_2}, \mathbf{e'_3}) = (\mathbf{e_1}, \mathbf{e_2}, \mathbf{e_3}) \begin{pmatrix} a_{11} & a_{21} & a_{31} \\ a_{12} & a_{22} & a_{32} \\ a_{13} & a_{23} & a_{33} \end{pmatrix}. \tag{4.13}$$

From the condition (4.9), we see the following constrains among the elements of the *conversion matrix*;

$$a_{11}^2 + a_{12}^2 + a_{13}^2 = 1, a_{21}^2 + a_{22}^2 + a_{23}^2 = 1, a_{31}^2 + a_{32}^2 + a_{33}^2 = 1, \tag{4.14}$$

$$a_{11}a_{21} + a_{12}a_{22} + a_{13}a_{23} = 0, a_{21}a_{31} + a_{22}a_{32} + a_{23}a_{33} = 0, a_{31}a_{11} + a_{32}a_{12} + a_{33}a_{13} = 0 \tag{4.15}$$

If we take the inner product of (4.10), (4.11), (4.12) and $\mathbf{e_1}, \mathbf{e_2}, \mathbf{e_3}$, we can see

$$\mathbf{e'_1} \cdot \mathbf{e_1} = a_{11},\ \mathbf{e'_1} \cdot \mathbf{e_2} = a_{12},\ \mathbf{e'_1} \cdot \mathbf{e_3} = a_{13}, \tag{4.16}$$

$$\mathbf{e'_2} \cdot \mathbf{e_1} = a_{21},\ \mathbf{e'_2} \cdot \mathbf{e_2} = a_{22},\ \mathbf{e'_2} \cdot \mathbf{e_3} = a_{23}, \tag{4.17}$$

$$\mathbf{e'_3} \cdot \mathbf{e_1} = a_{31},\ \mathbf{e'_3} \cdot \mathbf{e_2} = a_{32},\ \mathbf{e'_3} \cdot \mathbf{e_3} = a_{33}. \tag{4.18}$$

Namely, nine elements of the conversion matrix defined by (4.13) are the *direction cosine* between the three base vectors before the conversion and three base vectors after the conversion.

Similarly, inverse of 式 (4.10),(4.11),(4.12) may be obtained as,

$$\mathbf{e_1} = a_{11}\mathbf{e'_1} + a_{21}\mathbf{e'_2} + a_{31}\mathbf{e'_3}, \tag{4.19}$$

$$\mathbf{e_2} = a_{12}\mathbf{e'_1} + a_{22}\mathbf{e'_2} + a_{32}\mathbf{e'_3}, \tag{4.20}$$

$$\mathbf{e_3} = a_{13}\mathbf{e'_1} + a_{23}\mathbf{e'_2} + a_{33}\mathbf{e'_3}, \tag{4.21}$$

or, equivalently,

$$(\mathbf{e_1}, \mathbf{e_2}, \mathbf{e_3}) = (\mathbf{e'_1}, \mathbf{e'_2}, \mathbf{e'_3}) \begin{pmatrix} a_{11} & a_{12} & a_{13} \\ a_{21} & a_{22} & a_{23} \\ a_{31} & a_{32} & a_{33} \end{pmatrix}. \tag{4.22}$$

From the condition (4.8), corresponding to 4.14), (4.15), we get

$$a_{11}^2 + a_{21}^2 + a_{31}^2 = 1, a_{12}^2 + a_{22}^2 + a_{32}^2 = 1, a_{13}^2 + a_{23}^2 + a_{33}^2 = 1 \tag{4.23}$$

`

$$a_{11}a_{12}+a_{21}a_{22}+a_{31}a_{32} = 0, a_{12}a_{13}+a_{22}a_{23}+a_{32}a_{33} = 0, a_{13}a_{11}+a_{23}a_{21}+a_{33}a_{31} = 0. \tag{4.24}$$

If we compare (4.13) and (4.22), we can see that the *transpose* of the conversion matrix is the inverse-matrix. In fact, this is one of the characteristics of the orthogonal matrix.

4.3.3 Notation of orthogonal matrix and transformation

We introduce **Kronecker's delta**;

$$\delta_{ij} = \begin{cases} 1 & (i = j) \\ 0 & (i \neq j) \end{cases} \tag{4.25}$$

Also, we introduce a rule to sum over the same indices in an equation (omit the Σ symbol).
In this manner, (4.8),(4.9) may be written as,

$$\mathbf{e_i} \cdot \mathbf{e_j} = \delta_{ij}, \mathbf{e'_i} \cdot \mathbf{e'_j} = \delta_{ij}. \tag{4.26}$$

Also, the following relations hold;

$$\mathbf{e'_i} \cdot \mathbf{e_j} = a_{ij},\ \mathbf{e'_i} = a_{ij}\mathbf{e_j},\ \mathbf{e_i} = a_{ji}\mathbf{e'_j}, \tag{4.27}$$

$$a_{ik}a_{jk} = \delta_{ij}, a_{ki}a_{kj} = \delta_{ij}. \tag{4.28}$$

4.3.4 Scalar triple product and determinant

There is another important character of the orthogonal matrix; *the determinant of the* 3×3 *orthogonal matrix is unity.* Let's take a look.
Let's review basic vector analysis. Outer product of the three dimensional vectors **A** and **B** is written as

$$\mathbf{O} = \mathbf{A} \times \mathbf{B}. \tag{4.29}$$

O is orthogonal to both **A** and **B**, toward the direction when a screw is rotated from the direction of **A** to **B**, and the length is $|A||B|\sin\theta$ where θ is the angle between **A** and **B** (area of the parallelogram made with **A** and **B**). The three components of **O** are

$$\begin{pmatrix} O_x \\ O_y \\ O_z \end{pmatrix} = \begin{pmatrix} A_yB_z - A_zB_y \\ A_zB_x - A_xB_z \\ A_xB_y - A_yB_x \end{pmatrix}. \tag{4.30}$$

In general *Scalar triple product* of the vectors $\mathbf{A}, \mathbf{B}, \mathbf{C}$ is defined as

$$\mathbf{A} \cdot (\mathbf{B} \times \mathbf{C}) = \mathbf{B} \cdot (\mathbf{C} \times \mathbf{A}) = \mathbf{C} \cdot (\mathbf{A} \times \mathbf{B}). \tag{4.31}$$

When the vectors $\mathbf{A}, \mathbf{B}, \mathbf{C}$ forms the right-handed coordinates, the scalar triple products give volume of the parallelepiped formed by these vectors. The scalar triple product of may be written as,

$$\mathbf{A} \cdot (\mathbf{B} \times \mathbf{C}) = A_x B_y C_z + A_y B_z C_x + A_z B_x C_y - A_x B_z C_y - A_y B_x C_z - A_z B_y C_x \tag{4.32}$$

$$= \begin{vmatrix} A_x & A_y & A_z \\ B_x & B_y & B_z \\ C_x & C_y & C_z \end{vmatrix} = \begin{vmatrix} A_x & B_x & C_x \\ A_y & B_y & C_y \\ A_z & B_z & C_z \end{vmatrix}, \tag{4.33}$$

where $|\mathbf{A}|$ gives the determinant of the matrix $\mathbf{A}$. The parallelepiped formed by the base vectors $\mathbf{e_1}, \mathbf{e_2}, \mathbf{e_3}$ or $\mathbf{e'_1}, \mathbf{e'_2}, \mathbf{e'_3}$ is a cubic of which the each side is unity and thus the volume is unity. Consequently, the scalar triple product of the unit vector, or determinant of the conversion matrix is unity.

$$\begin{vmatrix} a_{11} & a_{12} & a_{13} \\ a_{21} & a_{22} & a_{23} \\ a_{31} & a_{32} & a_{33} \end{vmatrix} = 1 \tag{4.34}$$

Equivalently,

$$a_{11}a_{22}a_{33} + a_{12}a_{23}a_{31} + a_{13}a_{21}a_{32} - a_{13}a_{22}a_{31} - a_{12}a_{21}a_{33} - a_{11}a_{23}a_{32} = 1. \tag{4.35}$$

4.3.5 Coordinate conversion

Combining (4.5) and (4.22),

$$\mathbf{p} = (\mathbf{e_x}, \mathbf{e_y}, \mathbf{e_z}) \begin{pmatrix} x \\ y \\ z \end{pmatrix} = (\mathbf{e'_x}, \mathbf{e'_y}, \mathbf{e'_z}) \begin{pmatrix} a_{11} & a_{12} & a_{13} \\ a_{21} & a_{22} & a_{23} \\ a_{31} & a_{32} & a_{33} \end{pmatrix} \begin{pmatrix} x \\ y \\ z \end{pmatrix} = (\mathbf{e'_x}, \mathbf{e'_y}, \mathbf{e'_z}) \begin{pmatrix} x' \\ y' \\ z' \end{pmatrix}. \tag{4.36}$$

Consequently,

$$\begin{pmatrix} x' \\ y' \\ z' \end{pmatrix} = \begin{pmatrix} a_{11} & a_{12} & a_{13} \\ a_{21} & a_{22} & a_{23} \\ a_{31} & a_{32} & a_{33} \end{pmatrix} \begin{pmatrix} x \\ y \\ z \end{pmatrix}. \tag{4.37}$$

This relation gives the conversion between the three components (x, y, z) and (x', y', z') in the two coordinates.

4.3.6 Euler angles and coordinate conversion

Let's consider the ZYZ Euler angles. When rotated ϕ around z, let's put the new axes $x'y'z'$ (of course, $z = z'$)。Next, when rotated θ around y', let's put the new axes $x''y'''z'''$ (of course, $y' = y''$)。Finally, rotate ψ around z'', then we get x''',y''',z'''. The Euler angles (ϕ, θ, ψ) gives the coordinate conversion from the xyz coordinates to the $x'''y'''z'''$ coordinates.

The conversion matrices given (4.13) or (4.22) can be expressed using the Euler angles. The first rotation around z-axis gives the following;

$$(\mathbf{e'_1}, \mathbf{e'_2}, \mathbf{e'_3}) = (\mathbf{e_1}, \mathbf{e_2}, \mathbf{e_3}) \begin{pmatrix} \cos\phi & -\sin\phi & 0 \\ \sin\phi & \cos\phi & 0 \\ 0 & 0 & 1 \end{pmatrix}. \tag{4.38}$$

Similarly, θ rotation around y' axis gives,

$$(\mathbf{e_1''}, \mathbf{e_2''}, \mathbf{e_3''}) = (\mathbf{e_1'}, \mathbf{e_2'}, \mathbf{e_3'}) \begin{pmatrix} \cos\theta & 0 & \sin\theta \\ 0 & 1 & 0 \\ -\sin\theta & 0 & \cos\theta \end{pmatrix}. \tag{4.39}$$

Finally, ψ rotation around z'' axis gives,

$$(\mathbf{e_1'''}, \mathbf{e_2'''}, \mathbf{e_3'''}) = (\mathbf{e_1''}, \mathbf{e_2''}, \mathbf{e_3''}) \begin{pmatrix} \cos\psi & -\sin\psi & 0 \\ \sin\psi & \cos\psi & 0 \\ 0 & 0 & 1 \end{pmatrix}. \tag{4.40}$$

We may combine these three equations;

$$(\mathbf{e_1'''}, \mathbf{e_2'''}, \mathbf{e_3'''}) = (\mathbf{e_1}, \mathbf{e_2}, \mathbf{e_3}) \begin{pmatrix} \cos\phi & -\sin\phi & 0 \\ \sin\phi & \cos\phi & 0 \\ 0 & 0 & 1 \end{pmatrix} \begin{pmatrix} \cos\theta & 0 & \sin\theta \\ 0 & 1 & 0 \\ -\sin\theta & 0 & \cos\theta \end{pmatrix} \begin{pmatrix} \cos\psi & -\sin\psi & 0 \\ \sin\psi & \cos\psi & 0 \\ 0 & 0 & 1 \end{pmatrix} \tag{4.41}$$

$$= (\mathbf{e_1}, \mathbf{e_2}, \mathbf{e_3}) \begin{pmatrix} \cos\phi\cos\theta\cos\psi - \sin\phi\sin\psi & -\sin\phi\cos\psi - \cos\phi\cos\theta\sin\psi & \cos\phi\sin\theta \\ \sin\phi\cos\theta\cos\psi + \cos\phi\sin\psi & \cos\phi\cos\psi - \sin\phi\cos\theta\sin\psi & \sin\phi\sin\theta \\ -\sin\theta\cos\psi & \sin\theta\sin\psi & \cos\theta \end{pmatrix}. \tag{4.42}$$

This is an orthogonal matrix, which satisfies (4.28) and (4.34).

4.3.7 Conversion from equatorial coordinates to ecliptic coordinates

Ecliptic coordinates are given with rotation around x axis (pointing the sprint equinox) by $\theta = 23.^\circ 43929$. Here, the original base vectors are $\mathbf{e_x}, \mathbf{e_y}, \mathbf{e_z}$, and the new base vectors are $\mathbf{e_x'}, \mathbf{e_y'}, \mathbf{e_z'}$.

$$(\mathbf{e_x'}, \mathbf{e_y'}, \mathbf{e_z'}) = (\mathbf{e_x}, \mathbf{e_y}, \mathbf{e_z}) \begin{pmatrix} 1 & 0 & 0 \\ 0 & \cos\theta & -\sin\theta \\ 0 & \sin\theta & \cos\theta \end{pmatrix} = (\mathbf{e_x}, \mathbf{e_y}, \mathbf{e_z}) \begin{pmatrix} 1 & 0 & 0 \\ 0 & 0.91748 & -0.39778 \\ 0 & 0.39778 & 0.91748 \end{pmatrix}. \tag{4.43}$$

$$(\mathbf{e_x}, \mathbf{e_y}, \mathbf{e_z}) = (\mathbf{e_x'}, \mathbf{e_y'}, \mathbf{e_z'}) \begin{pmatrix} 1 & 0 & 0 \\ 0 & 0.91748 & 0.39778 \\ 0 & -0.39778 & 0.91748 \end{pmatrix}. \tag{4.44}$$

We put the components of the directional vector in the equatorial coordinates (x, y, z), and those in the ecliptic coordinates (x', y', z'). From (4.37),

$$\begin{pmatrix} x' \\ y' \\ z' \end{pmatrix} = \begin{pmatrix} 1 & 0 & 0 \\ 0 & 0.91748 & 0.39778 \\ 0 & -0.39778 & 0.91748 \end{pmatrix} \begin{pmatrix} x \\ y \\ z \end{pmatrix}. \tag{4.45}$$

This gives conversion from the equatorial coordinates to ecliptic coordinates.

Consider an example shown in p.44. For $(\alpha, \delta) = (281.000, -4.070)$, the directional vector given by (4.3) is $(0.19033, -0.97915, -0.0709752)$. Using (4.45), the directional vector in the ecliptic coordinates is $(0.19033, -0.92658, 0.32437)$. Similarly to (4.7),

$$\lambda = \tan^{-1}\left(\frac{-0.92658}{0.19033}\right) = -78.3923 = 281.608.$$

$$\beta = \tan^{-1}\left(\frac{0.32437}{\sqrt{-0.92658^2 + 0.19033^2}}\right) = 18.927.$$

4.3.8 Conversion from equatorial coordinates to Galactic coordinates

The Galactic center is located at $(\alpha, \delta) = (266.40500, -28.93617)$, so that rotation around z-axis by $\phi = 266.40500$ followed by rotation around y'-axis by $\theta = 28.93617$ gives the x''-axis pointing to the Galactic center. Furthermore, we need to specify the inclination of the Galactic plane, that is $\psi = 58.59866$ around the x''-axis (Figure 4.5).

In the following, triple-dash means the base vectors in the Galactic coordinates. Similar to (4.41),

$$(\mathbf{e}_\mathbf{x}''', \mathbf{e}_\mathbf{y}''', \mathbf{e}_\mathbf{z}''') = (\mathbf{e}_\mathbf{x}, \mathbf{e}_\mathbf{y}, \mathbf{e}_\mathbf{z}) \begin{pmatrix} \cos\phi & -\sin\phi & 0 \\ \sin\phi & \cos\phi & 0 \\ 0 & 0 & 1 \end{pmatrix} \begin{pmatrix} \cos\theta & 0 & \sin\theta \\ 0 & 1 & 0 \\ -\sin\theta & 0 & \cos\theta \end{pmatrix} \begin{pmatrix} 1 & 0 & 0 \\ 0 & \cos\psi & -\sin\psi \\ 0 & \sin\psi & \cos\psi \end{pmatrix}. \tag{4.46}$$

The inverse conversion is the following;

$$(\mathbf{e}_\mathbf{x}, \mathbf{e}_\mathbf{y}, \mathbf{e}_\mathbf{z}) = (\mathbf{e}_\mathbf{x}''', \mathbf{e}_\mathbf{y}''', \mathbf{e}_\mathbf{z}''') \begin{pmatrix} 1 & 0 & 0 \\ 0 & \cos\psi & \sin\psi \\ 0 & -\sin\psi & \cos\psi \end{pmatrix} \begin{pmatrix} \cos\theta & 0 & -\sin\theta \\ 0 & 1 & 0 \\ \sin\theta & 0 & \cos\theta \end{pmatrix} \begin{pmatrix} \cos\phi & \sin\phi & 0 \\ -\sin\phi & \cos\phi & 0 \\ 0 & 0 & 1 \end{pmatrix}. \tag{4.47}$$

$$= (\mathbf{e}_\mathbf{x}''', \mathbf{e}_\mathbf{y}''', \mathbf{e}_\mathbf{z}''') \begin{pmatrix} -0.0548755 & -0.873437 & -0.483835 \\ 0.49411 & -0.44483 & 0.746982 \\ -0.867666 & -0.198076 & 0.455984 \end{pmatrix}. \tag{4.48}$$

Namely, when the components in the equatorial coordinates are (x, y, z), those in the Galactic coordinates are (x''', y''', z'''),

$$\begin{pmatrix} x''' \\ y''' \\ z''' \end{pmatrix} = \begin{pmatrix} -0.0548755 & -0.873437 & -0.483835 \\ 0.49411 & -0.44483 & 0.746982 \\ -0.867666 & -0.198076 & 0.455984 \end{pmatrix} \begin{pmatrix} x \\ y \\ z \end{pmatrix} \tag{4.49}$$

gives conversion from the equatorial coordinates to the Galactic coordinates.

Let's again consider an example shown in p.44, where $(\alpha, \delta) = (281.000, -4.070)$ and the direction vector is $(0.19033, -0.97915, -0.0709752)$. Using (4.49), we get components of the direction vector in the Galactic coordinate $(0.879122, 0.476581, -0.00355986)$. Consequently,

$$l = \tan^{-1}\left(\frac{0.476581}{0.879122}\right) = 28.463$$

$$b = \tan^{-1}\left(\frac{-0.00355986}{\sqrt{0.879122^2 + 0.476581^2}}\right) = -0.204.$$

4.3.9 Conversion from satellite coordinates to sky coordinates

Similarly, we may convert from satellite coordinates to sky coordinates using Euler angles. For instance, detectors are fixed on the satellite, and we often need to calculate the sky location corresponding to an arbitrary position on the detector.

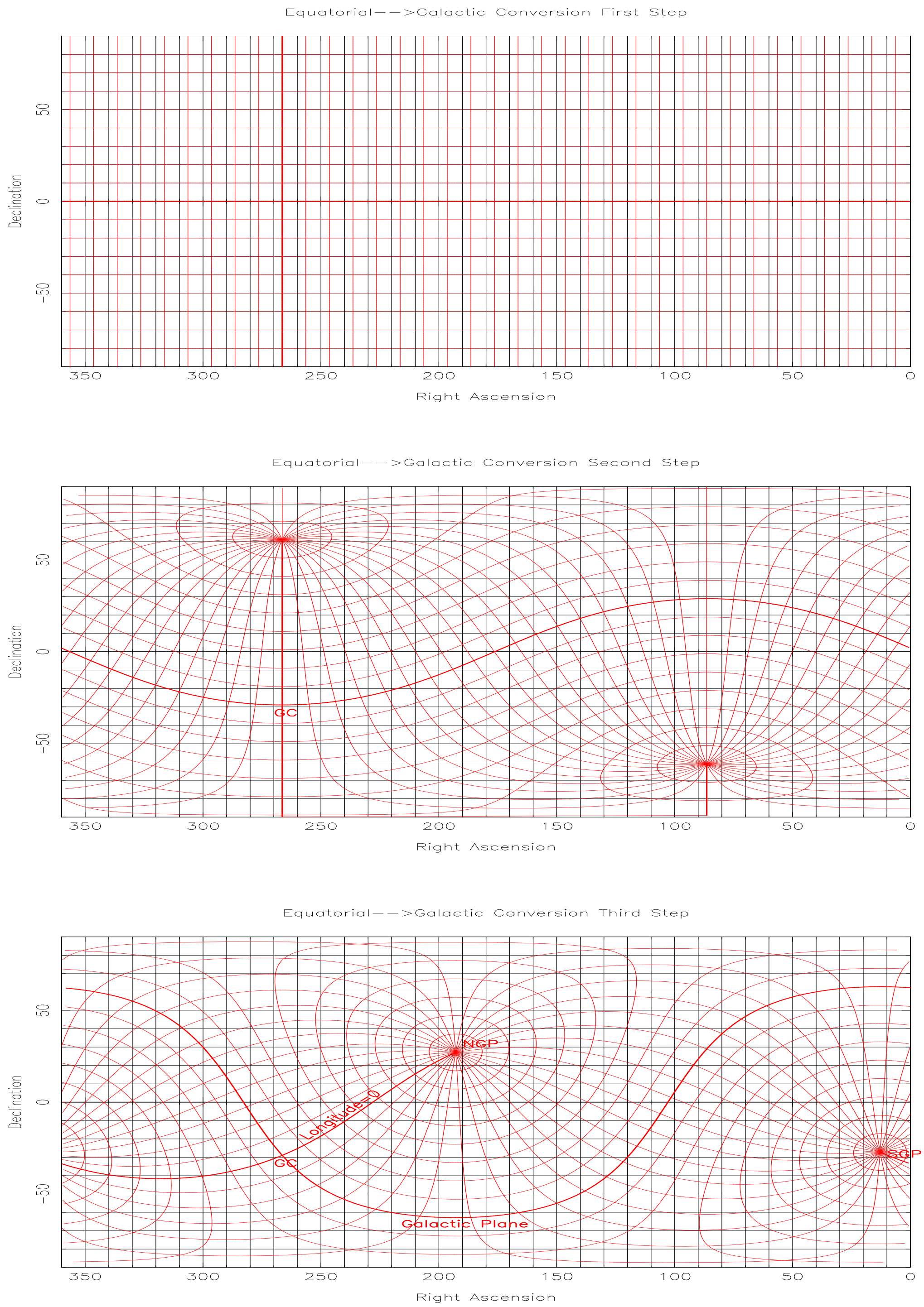

Figure 4.5: Conversion from the equatorial coordinates to the Galactic coordinates in three steps.

Equation (4.42) gives conversion between the base vectors in the equatorial coordinates and those in the satellite coordinates. Let's put the satellite ZYZ Euler angles (ϕ, θ, ψ). Having components of a direction vector in the satellite coordinates (x''', y''', z''') and those in the equatorial coordinates (x, y, z), the conversion between the two coordinates is given as

$$\begin{pmatrix} x \\ y \\ z \end{pmatrix} = \begin{pmatrix} \cos\phi\cos\theta\cos\psi - \sin\phi\sin\psi & -\sin\phi\cos\psi - \cos\phi\cos\theta\sin\psi & \cos\phi\sin\theta \\ \sin\phi\cos\theta\cos\psi + \cos\phi\sin\psi & \cos\phi\cos\psi - \sin\phi\cos\theta\sin\psi & \sin\phi\sin\theta \\ -\sin\theta\cos\psi & \sin\theta\sin\psi & \cos\theta \end{pmatrix} \begin{pmatrix} x''' \\ y''' \\ z''' \end{pmatrix}. \tag{4.50}$$

Let's consider a practical example. Suzaku CCD camera has $18' \times 18'$ square field of view, which is aligned to the XY-axes. As shown in Figure 4.3, the CCD square field of view (FOV) corresponds to a square sky region. The pointing vector corresponds to the FOV center has the satellite coordinate $(0, 0, 1)$. For other locations on the CCD, the direction vector is slightly tilted. We should obtain the satellite coordinate of the direction vector, then convert to the sky coordinate using the Euler angles.

Let's take a look at the Suzaku observation carried out on 2006 October 15 to 17 (sequence number is 500009020). From `http://darts.isas.jaxa.jp/astro/judo2/meta_info_page/html/SUZAKU/500009020.html`, we see the Euler angles are

$$\phi = 281.004, \theta = 94.078, \psi = 184.470. \tag{4.51}$$

Since Suzaku CCD camera has $18' \times 18'$ FOV along the X and Y-axes, the four corners have the following satellite XY coordinates;

$$(0.^\circ 15, 0.^\circ 15), (-0.^\circ 15, 0.^\circ 15), (-0.^\circ 15, -0.^\circ 15), (0.^\circ 15, -0.^\circ 15). \tag{4.52}$$

We see that four directional vectors corresponding to the four CCD corners are the following (shown in red in Figure 4.3)[10];

$$\begin{pmatrix} 2.61799 \times 10^{-3} \\ 2.61799 \times 10^{-3} \\ 0.9999931 \end{pmatrix}, \begin{pmatrix} 2.61799 \times 10^{-3} \\ -2.61799 \times 10^{-3} \\ 0.9999931 \end{pmatrix}, \begin{pmatrix} -2.61799 \times 10^{-3} \\ -2.61799 \times 10^{-3} \\ 0.9999931 \end{pmatrix}, \begin{pmatrix} -2.61799 \times 10^{-3} \\ 2.61799 \times 10^{-3} \\ 0.9999931 \end{pmatrix}. \tag{4.53}$$

Put (4.51) in (4.50), conversion from the satellite coordinates to the equatorial coordinates is

$$\begin{pmatrix} x \\ y \\ z \end{pmatrix} = \begin{pmatrix} -0.0629713 & -0.979686 & 0.190394 \\ -0.084471 & -0.184856 & -0.979129 \\ 0.994434 & -0.0777398 & -0.0711144 \end{pmatrix} \begin{pmatrix} x''' \\ y''' \\ z''' \end{pmatrix}. \tag{4.54}$$

Putting (4.53), we can obtain the four directional vectors in equatorial coordinates corresponding the four CCD corners;

$$\begin{pmatrix} 0.187663 \\ -0.979827 \\ -0.0687141 \end{pmatrix}, \begin{pmatrix} 0.192793 \\ -0.978859 \\ -0.068307 \end{pmatrix}, \begin{pmatrix} 0.193123 \\ -0.978417 \\ -0.0735139 \end{pmatrix}, \begin{pmatrix} 0.187993 \\ -0.979385 \\ -0.0739209 \end{pmatrix}. \tag{4.55}$$

To convert to right ascension and declination, we use (4.7). Consequently, we obtain the coordinate of the for CCD corners,

$$(\alpha, \delta) = (280.842, -3.940), (281.142, -3.917), (281.166, -4.216), (280.866, -4.239).$$

[10] Note that $0.15^\circ = 2.61799 \times 10^{-3}$ rad.

You may confirm using, for instance, JUDO2[11].

4.4 Quaternion, Coordinate Conversion and Satellite Attitudes

4.4.1 Euler's rotation theorem

Euler angles are convenient to describe satellite attitudes, since they are intuitive (equations 4.1 and 4.2). However, satellite attitude is not controlled in that manner, sequential rotation around Z-, Y-, and Z-axis. Instead, satellite attitude can be controlled by a *single* rotation around a rotation axis, because of the following *Euler's rotation theorem.*

Theorem I *: Any displacement in three dimensional space with a fixed point can be achieved by a single rotation around an axis through the point.*

Assuming that such a rotation axis exists, put the direction vector on the axis (x_0, y_0, z_0). This vector is invariable with the rotation, so that

$$\begin{pmatrix} x_0 \\ y_0 \\ z_0 \end{pmatrix} = \begin{pmatrix} a_{11} & a_{12} & a_{13} \\ a_{21} & a_{22} & a_{23} \\ a_{31} & a_{32} & a_{33} \end{pmatrix} \begin{pmatrix} x_0 \\ y_0 \\ z_0 \end{pmatrix} = A \begin{pmatrix} x_0 \\ y_0 \\ z_0 \end{pmatrix}. \tag{4.56}$$

Here, A is an orthogonal matrix. Namely, (x_0, y_0, z_0) is an eigen vector of A, and the eigen value is 1. Using the unit matrix I, the above may be written as

$$(A - I) \begin{pmatrix} x_0 \\ y_0 \\ z_0 \end{pmatrix} = A \begin{pmatrix} 0 \\ 0 \\ 0 \end{pmatrix}. \tag{4.57}$$

Namely, matrix $A - I$ does not have an inverse matrix, which is equivalent that the determinant is null.

$$|A - I| = 0 \tag{4.58}$$

Also, transpose of A is inverse of A;

$$(A - I)\, {}^t\!A = I - {}^t\!A. \tag{4.59}$$

Take the determinants of the both sides, using that the determinant of the transpose is the same as the determinant of the original matrix, determinant of the orthogonal matrix is unity (4.34), we see

$$|A - I| = |I - A|\,. \tag{4.60}$$

Meanwhile, in general for a $n \times n$ matrix B,

$$|-B| = (-1)^n\, |B|\,. \tag{4.61}$$

Currently, we consider 3x3 matrices, so $|I - A| = -\,|A - I|$. Namely, (4.60) indicates (4.58).

[11] `http://darts.isas.jaxa.jp/astro/judo2/?center_lng=281.005&center_lat=-4.0776&zoom=40&coord=J2000&selectedLayer=SUZAKU_PUBLIC_FOV,Constellation&Base=AL_P_2MASS_color&Top=SUZAKU_IMAGE&TopAlpha=100&GraphicAlpha=100`

4.4.2 Quaternion

Let's take a look at inside of "attitude files" of the satellites. The following is a part of the ASCA attitude file in 1993/09/28 taken from `ftp://ftp.darts.isas.jaxa.jp/pub/asca2/10010120/aux/fa930928_0641.1435.gz`;

```
 2.335207979544103E+07  -3.664577454889666E-01
                         4.253754826778572E-01
                         5.598341700062809E-01
                         6.093850355900631E-01
 2.335208379541934E+07  -3.664573182646553E-01
                         4.253649060520620E-01
                         5.598375141751545E-01
                         6.093896030552058E-01
 2.335208779543787E+07  -3.664571463319929E-01
                         4.253647582397316E-01
                         5.598375515033529E-01
                         6.093897753298769E-01
 2.335209179521501E+07  -3.664635097319999E-01
                         4.253653064430918E-01
                         5.598271266903228E-01
                         6.093951430157092E-01
 2.335209579523355E+07  -3.664768211073824E-01
                         4.253597832398843E-01
                         5.598082237138666E-01
                         6.094083582093963E-01
```

The first column is the elapsed time (in second) from the beginning of 1993 (ASCA time). The second column is the *unit quaternion* , which describe the satellite attitude at the time. Make sure the norm of each unit quaternion is unity.

Using *quaternion*, you can smoothly calculate rotation in three dimensional space. Most importantly, quaternion gives the rotation axis and the rotation angle directly for a displacement with a fixed point (Theorem I). Also, since quaternion has only four numbers while the rotation matrix has 9 elements, amount of the calculation is reduced using quaternion. Thus, quaternion is used in satellite operation, computer graphics and many other fields involving computation of rotation in 3D space.

4.4.3 Characteristics of quaternion[12].

Quaternion is discovered by Hamiltonian in 19th century. Besides mathematical implication, practically, *unit quaternion describes rotation in 3D space.*

Quaternion is defined as follows;

$$q \equiv \mathbf{i}x + \mathbf{j}y + \mathbf{k}z + w, \quad \text{where} \;\; \mathbf{i}^2 = \mathbf{j}^2 = \mathbf{k}^2 = \mathbf{ijk} = -1. \tag{4.62}$$

Here, x, y, z, w are real.

[12]See `ftp://ftp.cis.upenn.edu/pub/graphics/shoemake/quatut.ps.Z`

Multiply $\mathbf{i}$ from the left of $\mathbf{ijk} = -1$, using $\mathbf{i}^2 = -1$,

$$\mathbf{jk} = \mathbf{i}. \tag{4.63}$$

Similarly, multiply $\mathbf{k}$ from the right, using $\mathbf{k}^2 = -1$,

$$\mathbf{ij} = \mathbf{k}. \tag{4.64}$$

Multiply (4.64) from the left of (4.63), using $\mathbf{j}^2 = -1$,

$$-\mathbf{ik} = \mathbf{ki}. \tag{4.65}$$

Similarly, multiply $\mathbf{k}$ from the right of (4.63),

$$-\mathbf{j} = \mathbf{ik} = -\mathbf{ki}. \tag{4.66}$$

Multiply $\mathbf{i}$ from right,

$$\mathbf{k} = -\mathbf{ji}. \tag{4.67}$$

Finally multiply $\mathbf{j}$ to (4.64) from right,

$$-\mathbf{i} = \mathbf{kj}. \tag{4.68}$$

In summary, the following relationships are obtained:

$$\begin{cases} \mathbf{i}^2 = \mathbf{j}^2 = \mathbf{k}^2 = \mathbf{ijk} = -1 \\ \mathbf{ij} = -\mathbf{ji} = \mathbf{k} \\ \mathbf{jk} = -\mathbf{kj} = \mathbf{i} \\ \mathbf{ki} = -\mathbf{ik} = \mathbf{j} \end{cases} \tag{4.69}$$

A quaternion may be expressed as follows;

$$q = [\mathbf{v}, w] = [(x, y, z), w] = [x, y, z, w]. \tag{4.70}$$

$\mathbf{v}$ is a three dimensional vector. If $q = [\mathbf{v}, w], q' = [\mathbf{v}', w']$, summation of two quaternions to make a new quaternion is defined as follows;

$$q + q' = [\mathbf{v}, w] + [\mathbf{v}', w'] \equiv [\mathbf{v} + \mathbf{v}', w + w']. \tag{4.71}$$

Multiplication of two quaternion is defined as follows;

$$qq' = [\mathbf{v}, w][\mathbf{v}', w'] = (x\mathbf{i} + y\mathbf{j} + k\mathbf{z} + w)(x'\mathbf{i} + y'\mathbf{j} + z'\mathbf{z} + w') \tag{4.72}$$

$$\begin{aligned} &= xx'\mathbf{i}^2 + xy'\mathbf{ij} + xz'\mathbf{ik} + xw'\mathbf{i} + yx'\mathbf{ji} + yy'\mathbf{j}^2 + yz'\mathbf{jk} + yw'\mathbf{j} \\ &+zx'\mathbf{ki} + zy'\mathbf{kj} + zz'\mathbf{k}^2 + zw'\mathbf{k} + wx'\mathbf{i} + wy'\mathbf{j} + wz'\mathbf{k} + ww' \end{aligned} \tag{4.73}$$

$$\begin{aligned} &= -xx' + xy'\mathbf{k} - xz'\mathbf{j} + xw'\mathbf{i} - yx'\mathbf{k} - yy' + yz'\mathbf{i} + yw'\mathbf{j} \\ &+zx'\mathbf{j} - zy'\mathbf{i} - zz' + zw'\mathbf{k} + wx'\mathbf{i} + wy'\mathbf{j} + wz'\mathbf{k} + ww' \end{aligned} \tag{4.74}$$

$$\begin{aligned} &= (yz' - zy')\mathbf{i} + (zx' - xz')\mathbf{j} + (xy' - yx')\mathbf{k} \\ &+w(x'\mathbf{i} + y'\mathbf{j} + z'\mathbf{k}) + w'(x\mathbf{i} + y\mathbf{j} + z\mathbf{k}) + ww' - xx' - yy' - zz' \end{aligned} \tag{4.75}$$

$$= [\mathbf{v} \times \mathbf{v}' + w\mathbf{v}' + w'\mathbf{v}, ww' - \mathbf{v} \cdot \mathbf{v}']. \tag{4.76}$$

Here, (4.69) is used.

We should be careful that order of the multiplication of two quaternion cannot be switched ($qq' \neq q'q$), corresponding to the fact that order of two 3D rotations around different axes cannot be switched.

On the other hand, if $q'' = [\mathbf{v}'', w'']$,

$$(qq')q'' = q(q'q'') \tag{4.77}$$

holds[13].

Constants and three dimensional vectors can be represented as quaternions. If s is real constant, its quaternion representation is $[0, 0, 0, s] = [\mathbf{0}, s]$。If $\mathbf{v}$ is a three dimensional vector, its quaternion representation is $[\mathbf{v}, 0]$. The following will be trivial:

$$sq = [\mathbf{0}, s][\mathbf{v}, w] = [s\mathbf{v}, sw] = qs, \tag{4.78}$$

$$\mathbf{v}\mathbf{v}' = [\mathbf{v}, 0][\mathbf{v}', 0] = [\mathbf{v} \times \mathbf{v}', -\mathbf{v} \cdot \mathbf{v}']. \tag{4.79}$$

If s, s' are constant quaternions, and p, q, q' are any quaternions, the following linear relationships hold;

$$p(sq + s'q') = spq + spq', \tag{4.80}$$

$$(sq + s'q')p = sqp + s'q'p. \tag{4.81}$$

Definition and characteristics of *conjugate* are the following;

$$q^* = [\mathbf{v}, w]^* \equiv [-\mathbf{v}, w]. \tag{4.82}$$

$$(q^*)^* = q, \tag{4.83}$$

$$\begin{aligned}(pq)^* = \left\{[\mathbf{v}, w][\mathbf{v}', w']\right\}^* &= [\mathbf{v} \times \mathbf{v}' + w\mathbf{v}' + w'\mathbf{v}, ww' - \mathbf{v} \cdot \mathbf{v}']^* \\ &= [\mathbf{v}' \times \mathbf{v} - w\mathbf{v}' - w'\mathbf{v}, ww' - \mathbf{v} \cdot \mathbf{v}'] \\ &= [-\mathbf{v}', w][-\mathbf{v}, w'] = q^* p^*,\end{aligned} \tag{4.84}$$

$$(p + q)^* = p^* + q^*. \tag{4.85}$$

Definition and characteristic of *norm* are the following;

$$N(q) \equiv qq^* = q^*q = w^2 + \mathbf{v} \cdot \mathbf{v} = w^2 + x^2 + y^2 + z^2, \tag{4.86}$$

$$N(qq') = (qq')^*(qq') = q'^*q^*qq' = N(q)q'^*q' = N(q)N(q^*), \tag{4.87}$$

$$N(q^*) = N(q). \tag{4.88}$$

In particular, quaternion with norm=1 is called *unit quaternion.*

Inverse quaternion of q is defined as

$$q^{-1} = q^*/N(q). \tag{4.89}$$

When q is a unit-quaternion,

$$q^{-1} = q^*. \tag{4.90}$$

[13]To prove this relation, you need (4.31) on scalar triple product and relations on *vector triple product*, $\mathbf{A} \times (\mathbf{B} \times \mathbf{C}) = (\mathbf{A} \cdot \mathbf{C})\mathbf{B} - (\mathbf{A} \cdot \mathbf{B})\mathbf{C}$, $(\mathbf{A} \times \mathbf{B}) \times \mathbf{C} = (\mathbf{A} \cdot \mathbf{C})\mathbf{B} - (\mathbf{B} \cdot \mathbf{C})\mathbf{A}$. You may remember this relation as follow: If you expand the vector triple products, (1) that is a linear combination of two vectors in the parenthesis, (2) coefficient of each vector is the inner-product of the other two vectors, and (3) sign is plus for the vector in the middle of the triple products, other wise negative.

4.4.4 Quaternion and rotation [14]

The following theorem holds.

Theorem II *: Put* $\mathbf{u}$ *as a unit-vector in three dimensional space. Consider a unit quaternion,* $q = [\mathbf{u}\sin\Omega, \cos\Omega]$*, and* $p = [\mathbf{v}, 0]$ *where* $\mathbf{v}$ *is an any three dimensional vector. Put* $p' = qpq^{-1} = [\mathbf{v}', 0]$*. Then* $\mathbf{v}'$ *is the vector when* $\mathbf{v}$ *is rotated by* 2Ω *around* $\mathbf{u}$*.*

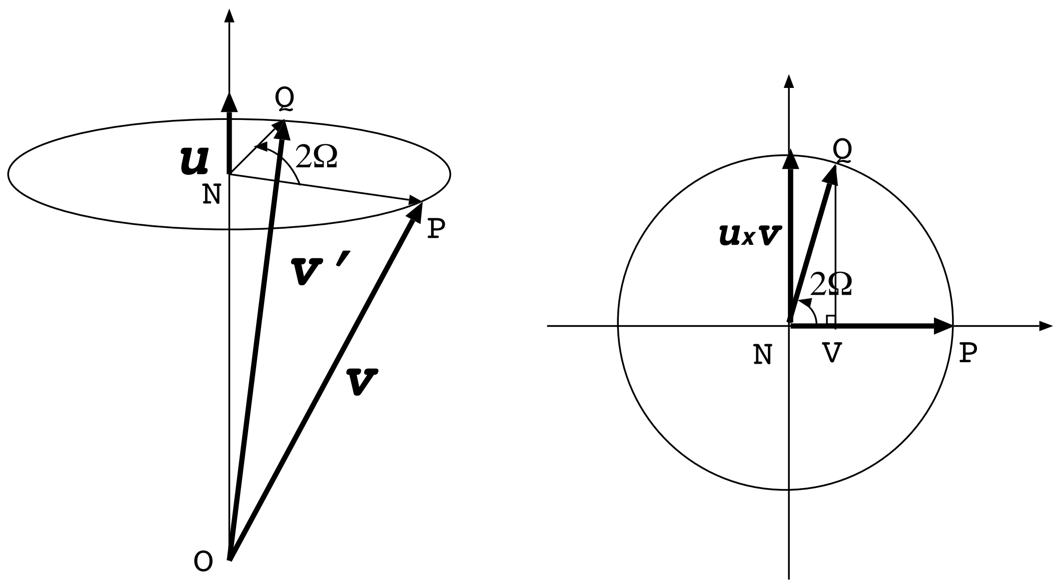

Figure 4.6: explanation of Theorem II.

Figure 4.6 illustrates the situation geometrically. If $\mathbf{v} = \overrightarrow{OP}$ is rotated around $\mathbf{u}$ by 2Ω, $\mathbf{v}' = \overrightarrow{OQ}$ is made. Here, note $\overrightarrow{OQ} = \overrightarrow{ON} + \overrightarrow{NV} + \overrightarrow{VQ}$.

Also, $\overrightarrow{ON} = (\mathbf{u}\cdot\mathbf{v})\mathbf{u}$, $\overrightarrow{NV} = \cos 2\Omega\,(\mathbf{v} - (\mathbf{u}\cdot\mathbf{v})\mathbf{u})$, and $\overrightarrow{VQ} = \sin 2\Omega\ \mathbf{u}\times\mathbf{v}$. Consequently,

$$\begin{aligned}\mathbf{v}' &= (\mathbf{u}\cdot\mathbf{v})\mathbf{u} + \cos 2\Omega\,(\mathbf{v} - (\mathbf{u}\cdot\mathbf{v})\mathbf{u}) + \sin 2\Omega\ \mathbf{u}\times\mathbf{v}\\ &= (1-\cos 2\Omega)\,(\mathbf{u}\cdot\mathbf{v})\mathbf{u} + \cos 2\Omega\ \mathbf{v} + \sin 2\Omega\ \mathbf{u}\times\mathbf{v}.\end{aligned} \tag{4.91}$$

On the other hand, multiplication of quaternions can be directly calculated as,

$$p' = qpq^{-1} = [\mathbf{u}\sin\Omega, \cos\Omega][\mathbf{v}, 0][-\mathbf{u}\sin\Omega, \cos\Omega]$$

$$= [\mathbf{u}\sin\Omega, \cos\Omega][-\sin\Omega(\mathbf{v}\times\mathbf{u}) + \cos\Omega\ \mathbf{v}, \sin\Omega\ \mathbf{u}\cdot\mathbf{v}]$$

$$= [-\sin^2\Omega\mathbf{u}\times(\mathbf{v}\times\mathbf{u}) + \sin\Omega\cos\Omega\mathbf{u}\times\mathbf{v} - \sin\Omega\cos\Omega(\mathbf{v}\times\mathbf{u}) + \cos^2\Omega\mathbf{v} + \sin^2\Omega(\mathbf{u}\cdot\mathbf{v})\mathbf{u}, 0]. \tag{4.92}$$

Focus on the spacial vector, and use vector triple products, then,

$$\mathbf{v}' = -\sin^2\Omega\mathbf{v} + \sin^2\Omega(\mathbf{u}\cdot\mathbf{v})\mathbf{u} + 2\sin\Omega\cos\Omega\mathbf{u}\times\mathbf{v} + \cos^2\Omega\mathbf{v} + \sin^2\Omega(\mathbf{u}\cdot\mathbf{v})\mathbf{u}$$

$$= 2\sin^2\Omega(\mathbf{u}\cdot\mathbf{v})\mathbf{u} + (\cos^2\Omega - \sin^2\Omega)\mathbf{v} + 2\sin\Omega\cos\Omega\ \mathbf{u}\times\mathbf{v}$$

[14] See, "Classical Mechanics" by H. Goldstein.

$$= (1 - \cos 2\Omega)(\mathbf{u}\cdot\mathbf{v})\mathbf{u} + \cos 2\Omega\ \mathbf{v} + \sin 2\Omega\ \mathbf{u}\times\mathbf{v}. \tag{4.93}$$

We see (4.91) and (4.93) free agree. Thus, Theorem II is proven.

Let's consider two sequential rotations. For $p = [\mathbf{v}, 0]$, rotate with q, followed by another rotation q';

$$q'(qpq^{-1})q'^{-1} = q'qpq^{-1}q'^{-1} = (q'q)p(q'q)^{-1}. \tag{4.94}$$

Here, we used (4.77) and (4.84). Consequently, the following theorem is obtained.

Theorem III *Following a rotation q, when new rotation q' is executed, the total rotation is represented with $q'q$.*

Remember that successive rotations using Euler angles required complicated matrix calculations (e.g., 4.42). Using quaternions, successive rotation can be simply represented by multiplication of quaternions.

4.4.5 Quaternion and conversion matrix

Put $\mathbf{v} = x\mathbf{e_x} + y\mathbf{e_y} + z\mathbf{e_z}$, consider xyz components of (4.91) or (4.93). Here, we assume

$$q = [\mathbf{u}\sin\Omega, \cos\Omega] \equiv [q_1, q_2, q_3, q_4]. \tag{4.95}$$

Since this is a unit-quaternion,

$$q_1^2 + q_2^2 + q_3^2 + q_4^2 = 1. \tag{4.96}$$

In the following, we use $\sin\Omega\mathbf{u} = q_1\mathbf{e_x} + q_2\mathbf{e_y} + q_3\mathbf{e_z}$.

$$\mathbf{v}' = 2(\sin\Omega\mathbf{u})\cdot\mathbf{v}\ \sin\Omega\mathbf{u} + (2\cos^2\Omega - 1)\mathbf{v} + 2\cos\Omega\ (\sin\Omega\mathbf{u})\times\mathbf{v}$$

$$= 2(q_1x + q_2y + q_3z)(q_1\mathbf{e_x} + q_2\mathbf{e_y} + q_3\mathbf{e_z}) + (q_4^2 - q_1^2 - q_2^2 - q_3^2)(x\mathbf{e_x} + y\mathbf{e_y} + z\mathbf{e_z})$$
$$+2q_4\left\{(q_2z - q_3y)\mathbf{e_x} + (q_3x - q_1z)\mathbf{e_y} + (q_1y - q_2x)\mathbf{e_z}\right\}$$
$$= (\mathbf{e_x}, \mathbf{e_y}, \mathbf{e_z})\begin{pmatrix} q_1^2 - q_2^2 - q_3^2 + q_4^2 & 2q_1q_2 - 2q_3q_4 & 2q_1q_3 + 2q_2q_4 \\ 2q_1q_2 + 2q_3q_4 & -q_1^2 + q_2^2 - q_3^2 + q_4^2 & 2q_2q_3 - 2q_1q_4 \\ 2q_1q_3 - 2q_2q_4 & 2q_2q_3 + 2q_1q_4 & -q_1^2 - q_2^2 + q_3^2 + q_4^2 \end{pmatrix}\begin{pmatrix} x \\ y \\ z \end{pmatrix} \tag{4.97}$$

$$\equiv (\mathbf{e_x}, \mathbf{e_y}, \mathbf{e_z})\ A\begin{pmatrix} x \\ y \\ z \end{pmatrix}. \tag{4.98}$$

Meaning of (4.98) is the following: In the coordinate system whose base-vectors are $(\mathbf{e_x}, \mathbf{e_y}, \mathbf{e_z})$, the vector $\mathbf{v}$ is represented as the coordinates (x, y, z). If this vector is rotated with the quaternion (4.95), $\mathbf{v}'$ is obtained, of which coordinates is $A\begin{pmatrix} x \\ y \\ z \end{pmatrix}$. Note that this is a rotation of a vector in the fixed coordinate system, and not the coordinate conversion.

Next, let's consider the coordinate conversion, and how a fixed vector is represented in the coordinate systems before and after the rotation.

The base vectors $(\mathbf{e_x}, \mathbf{e_y}, \mathbf{e_z})$ are rotated with the quaternion (4.95), and the new bases $(\mathbf{e'_x}, \mathbf{e'_y}, \mathbf{e'_z})$ are defined. The fixed vector $\mathbf{v}$ is represented by (x, y, z) before the rotation, and by (x', y', z') after the rotation. The rotation matrix is $A^{-1} = {}^tA$. Consequently,

$$\begin{pmatrix} x' \\ y' \\ z' \end{pmatrix} = \begin{pmatrix} a_{11} & a_{12} & a_{13} \\ a_{21} & a_{22} & a_{23} \\ a_{31} & a_{32} & a_{33} \end{pmatrix} \begin{pmatrix} x \\ y \\ z \end{pmatrix} = {}^tA \begin{pmatrix} x \\ y \\ z \end{pmatrix}$$

$$= \begin{pmatrix} q_1^2 - q_2^2 - q_3^2 + q_4^2 & 2q_1q_2 + 2q_3q_4 & 2q_1q_3 - 2q_2q_4 \\ 2q_1q_2 - 2q_3q_4 & -q_1^2 + q_2^2 - q_3^2 + q_4^2 & 2q_2q_3 + 2q_1q_4 \\ 2q_1q_3 + 2q_2q_4 & 2q_2q_3 - 2q_1q_4 & -q_1^2 - q_2^2 + q_3^2 + q_4^2 \end{pmatrix} \begin{pmatrix} x \\ y \\ z \end{pmatrix}. \tag{4.99}$$

Remember the Euler's rotation theorem (Theorem I). If we know the conversion matrix elements $(a_{11}, a_{12}, , , a_{33})$, how can we determine the corresponding rotation axis and the rotation angle? First, using (4.99), derive the quaternion $q = [q_1, q_2, q_3, q_4]$ from $(a_{11}, , a_{33})$. According to the Theorem II, if we put $q = [\mathbf{u} \sin\Omega, \cos\Omega]$, this gives the rotation around $\mathbf{u}$ by 2Ω.

4.4.6 Application to coordinate conversion

Conversion matrix from equatorial coordinate to Galactic coordinate is given in (4.49). Compare this with (4.99), and we may obtain the corresponding quaternion q_1, q_2, q_3, q_4:

$$q_1 = 0.4832,\ q_2 = -0.1963,\ q_3 = -0.6992,\ q_4 = 0.4889, \tag{4.100}$$

which gives the conversion from the equatorial coordinates to the Galactic coordinates.

Let' consider an example in p.53, where the directional vector in the equatorial coordinate $(0.19033, -0.97915, -0.0709752)$ is converted to that in the Galactic coordinate, (0.879122, 0.476581, -0.00355986,0).

Consider the quaternion

$$p = (0.19033, -0.97915, -0.0709752, 0),$$

which has the initial vector component. Apply the rotation by q above, then we will get,

$$q^{-1}pq = (0.879122, 0.476581, -0.00355986, 0). \tag{4.101}$$

We see that this gives the components in the Galactic coordinates.

Also from Theorem II, if we put $q = [\mathbf{u} \sin\Omega, \cos\Omega]$, this indicates rotation around $\mathbf{u} = (0.5539, -0.2250, -0.8016)$ by $2\Omega = 2 \times 60.^\circ 73$. In section 4.3.8, three Euler rotations were required from equatorial coordinate to Galactic coordinates. This is equivalent to the single rotation around $\mathbf{u}$ by 2Ω.

4.4.7 Application to satellite attitudes

Using quaternion, we may manipulate satellite attitudes in a straightforward manner. For example, we may know how to maneuver from one attitude to another attitude, calculate average of satellite attitudes or interpolate attitudes.

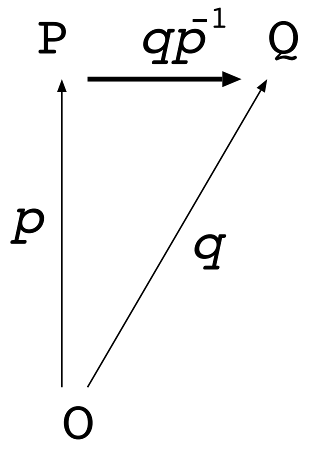

Figure 4.7:

Let's put the initial attitude O (satellite Z-axis is toward north pole, X-axis is toward the sprint equinox), apply the rotation p to achieve the new attitude P, followed by the application of q to achieve Q. What will be the most effective maneuver from P to Q? To change attitude from P to Q, this is represented with the quaternion qp^{-1} (Figure 4.7).

Given the quaternion qp^{-1}, represent it with $[\mathbf{u} \sin \Omega, \cos \Omega]$, which tells the rotation axis $\mathbf{u}$ and the rotation angle 2Ω. The average of the two attitude P and Q is simply given when the rotation angle is half (Ω).

We may interpolate the attitude between P and Q. For example, if the attitude P is at the time t_0, and attitude Q is at t_1, then any attitude at t between t_0 and t_1 is given by $[\mathbf{u} \sin \Omega(t), \cos \Omega(t)]$, where

$$\Omega(t) = \frac{t - t_0}{t_1 - t_0}. \tag{4.102}$$

4.5 Satellite Orbits

4.5.1 Two body problem and Kepler's law

Motion of artificial satellites around the earth, as well as that of planets around Sun, can be solved as *two body problem* in classical mechanics. Then naturally, we may derive *Kepler's three laws.* Let's take a look.

Assume mass of the earth (or Sun) M (position vector $\boldsymbol{r}_1$), that of satellite (or planet) m(position vector $\boldsymbol{r}_2$). We consider only gravity between them (gravitational constant G), and do not consider other bodies or forces (thus, two body problem). The force between the two body may be written as $\boldsymbol{F}$, then the equation of motions are

$$M \frac{d^2 \boldsymbol{r}_1}{dt^2} = \boldsymbol{F} \tag{4.103}$$

$$m \frac{d^2 \boldsymbol{r}_2}{dt^2} = -\boldsymbol{F}. \tag{4.104}$$

From these equations,

$$\frac{d^2(M\boldsymbol{r}_1 + m\boldsymbol{r}_2)}{dt^2} = 0 \tag{4.105}$$

$$\frac{mM}{m+M}\frac{d^2(\boldsymbol{r}_2 - \boldsymbol{r}_1)}{dt^2} = -\boldsymbol{F}. \tag{4.106}$$

(4.105) indicates that the center of gravity, $(M\boldsymbol{r}_1 + m\boldsymbol{r}_2)/(M+m)$, moves at a constant velocity move (or does not move). Equation (4.106) describes the motion of a planet that has a *reduced mass* $\mu \equiv mM/(m+M)$.

Position vector of the center mass is

$$\frac{M\boldsymbol{r}_1 + m\boldsymbol{r}_2}{M+m} = \frac{\boldsymbol{r}_1 + m/M\boldsymbol{r}_2}{1+m/M},$$

which is $\approx \boldsymbol{r}_1$, if $m/M \approx 0$. Also,

$$\mu = \frac{mM}{m+M} = \frac{m}{1+m/M},$$

which agrees with m when $m/M \approx 0$. Namely, when $m \ll M$, which always the case, the center of gravity is close to $\boldsymbol{r}_1$ and the reduce almost agrees with m.

Below, m is considered to be the reduced mass, and consider the position vector of the satellite relative to the earth, $\boldsymbol{r}_2 - \boldsymbol{r}_1 \equiv \boldsymbol{r}$.

Consider the polar coordinates, where $\boldsymbol{e}_r$ and $\boldsymbol{e}_\theta$ are base vectors. Velocity vector of the satellite is

$$d\boldsymbol{r}/dt = d(r\boldsymbol{e}_r)/dt = \dot{r}\boldsymbol{e}_r + r\dot{\boldsymbol{e}}_r = \dot{r}\boldsymbol{e}_r + r\dot{\theta}\boldsymbol{e}_\theta.$$

Put angular momentum of the satellite h, which is written as $h = mr^2\dot{\theta}$. The area which is made by the position vector $\boldsymbol{r}$ per unit-time is called *area velocity.* The area velocity may be written as $h/2m$. The acceleration vector is written as

$$d^2\boldsymbol{r}/dt^2 = (\ddot{r} - r\dot{\theta}^2)\,\boldsymbol{e}_r + (2\dot{r}\dot{\theta} + r\ddot{\theta})\,\boldsymbol{e}_\theta.$$

Consequently, we may write the equation of motion in the radial direction and azimuthal direction as,

$$m(\ddot{r} - r\dot{\theta}^2) = -\frac{GMm}{r^2} \tag{4.107}$$

$$m(2\dot{r}\dot{\theta} + r\ddot{\theta}) = 0. \tag{4.108}$$

From (4.108),

$$2\dot{r}\dot{\theta} + r\ddot{\theta} = \frac{1}{r}\frac{d}{dt}(r^2\dot{\theta}) = 0. \tag{4.109}$$

Since $mr^2\dot{\theta}$ is the angular momentum h, we can see that the angular momentum is constant. Since area velocity is $h/2m$, we see that *area velocity is constant* (Kepler's second law).

Using that h is constant, we may integrate (4.107) with r, and obtain the energy conservation equation which is

$$\frac{m}{2}\left(\frac{dr}{dt}\right)^2 + \frac{h^2}{2mr^2} - \frac{GMm}{r} = E. \tag{4.110}$$

Here, we put the total energy E.

Below, we will derive Kepler's fist law, namely, *orbit of the satellite is an ellipse where the earth locates at one of the two foci.*

In (4.110), we change the derivative by time to derivative by angle θ,

$$\frac{m}{2}(\frac{h}{mr^2}\frac{dr}{d\theta})^2 + \frac{h^2}{2mr^2} - \frac{GMm}{r} = E. \tag{4.111}$$

This derivative equation give the relation between r and θ. If r is represented as a function of θ, this gives an orbit of the satellite.

We switch the variable as $1/r = u$, then obtain a derivative equation of u and θ:

$$\pm\frac{du}{\sqrt{\frac{2mE}{h^2} + \frac{G^2M^2m^4}{h^4} - (u - \frac{GMm^2}{h^2})^2}} = d\theta. \tag{4.112}$$

We can directly integrate, then

$$\pm\cos^{-1}\left(\frac{u - \frac{GMm^2}{h^2}}{\sqrt{\frac{2mE}{h^2} + \frac{G^2M^2m^4}{h^4}}}\right) = \theta. \tag{4.113}$$

Here, we choose origin of the angle appropriately so that the integration constant is null. We may solve with r, such that

$$r = \frac{\frac{h^2}{GMm^2}}{1 + \sqrt{1 + \frac{2Eh^2}{G^2M^2m^3}}\cos\theta}. \tag{4.114}$$

Meanwhile, an ellipse can be expressed in the following;

$$r = \frac{l}{1 + e\cos\theta} \quad (0 \leq e < 1), \tag{4.115}$$

where r is distance from the focus, θ is angle from a line through the focus. Here e is eccentricity, and l is called *semi-latus rectum* (Figure 4.5.1). When $e = 0$, the ellipse will be a circle. As e is close to 1, the ellipse is more elongated.

If we put

$$l = \frac{h^2}{GMm^2} \tag{4.116}$$

$$e = \sqrt{1 + \frac{2Eh^2}{G^2M^2m^3}} \tag{4.117}$$

(4.114) and (4.115) agree.

Next, we will derive Kepler's third law, that *square of the orbital period is proportional to third power of the semi-major axis.*

To prepare, let's review general characteristics of ellipse. Consider an ellipse with the same-major axis a and semi-minor axis b. This ellipse is expressed as (4.115). Also, "sum of the distances from the two foci F and F' is constant on any points on ellipse", which is another definition of ellipse. If we consider points A or C, we can readily see the sum of the distances

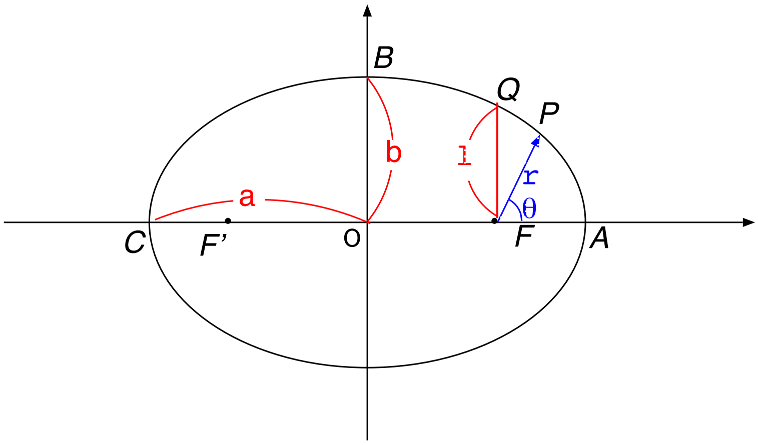

Figure 4.8: Satellite orbit (ellipse) and explanation of the nomenclatures used in the text.

from F and F' is $2a$. Meanwhile, using (4.115), $FA = l/(1+e)$ and $F'A = FC = 1/(1-e)$. From these relations, we get

$$2a = FA + F'A = \frac{l}{1+e} + \frac{l}{(1-e}, \tag{4.118}$$

$$a = \frac{l}{1-e^2}. \tag{4.119}$$

Also, we see,

$$OF = OA - FA = a - \frac{l}{1+e} = a - a(1-e) = ae. \tag{4.120}$$

At B,

$$BF + BF' = 2a = 2\sqrt{OB^2 + OF^2} = 2\sqrt{b^2 + (ae)^2}. \tag{4.121}$$

Using (4.119) to eliminate e, we finally get

$$b = \sqrt{al}. \tag{4.122}$$

The area of ellipse is given as πab. Having the area velocity T, we see that the area velocity is

$$h/2m = \frac{\pi ab}{T}. \tag{4.123}$$

Using (4.122) and that l is represented as (4.116),

$$T = \frac{2\pi a^{3/2}}{\sqrt{GM}}. \tag{4.124}$$

This is Kepler's third law.

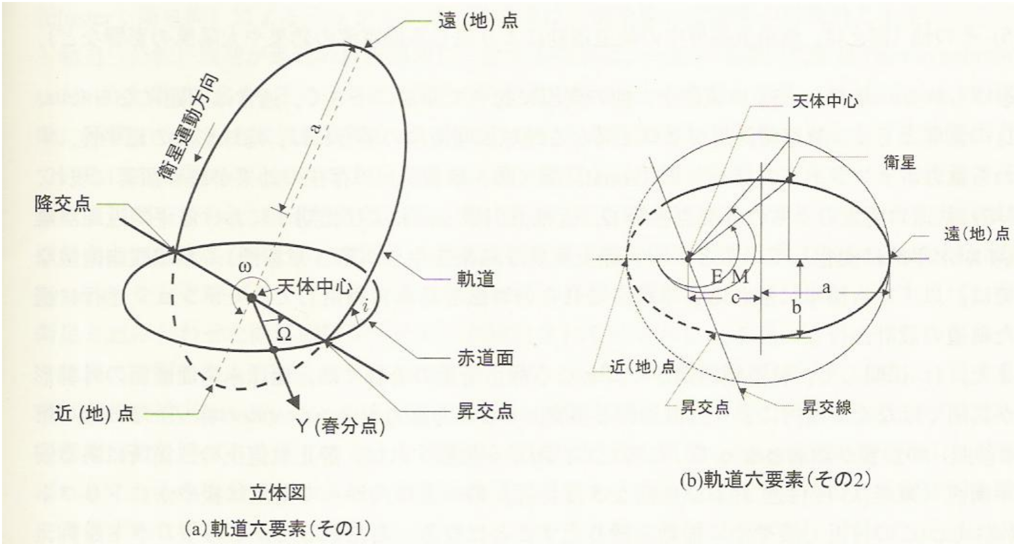

Figure 4.9: Explanation of the orbital six elements. Taken from "人工衛星の力学と制御ハンドブック"(ISBN:4563067563)

4.5.2 Orbital six elements

Satellite orbit and its location is fully described with the following *orbital six elements* [15]

- a: Semi-major axis. When circular orbit, this will be the radius.
- e: Eccentricity. When circular orbit, $e = 0$.
- i: Inclination). Angle between the equatorial plane and the satellite orbital plane.
- Ω: Right ascension of the ascending node. When $i \neq 0$, right ascension of the point where the equatorial plane and the satellite orbital plane crosses (ascending node).
- ω: Argument of perigee. When elliptical orbit, angle of the perigee from the ascending node。

  Orbit is determined from these five elements.

- M: Mean anomaly. Location of the satellite at a given time (epoch).

Figure 4.10 indicates time history of the orbital six-elements of the Ginga satellite, which was launched on 1987 February 5, and reentered on 1991 November 1.

We see the orbit is close to a circle, since $e \approx 0$. Since radius of the earth is about 6378 km, we see the altitude of the satellite at the launch is about 550 km. Inclination angle i corresponds to the latitude of the launch site, Uchinoura Space Station; the satellite was launched toward east to utilize the spin-velocity of the earth. Consequently, latitude of the launch station will be the inclination angle.

[15] See `http://spaceflight.nasa.gov/realdata/elements/`.

We see that Ω varied periodically, which indicates precession of the orbital plane, due to the non-spherical gravitational field of the earth.

Near the end of the mission, we see a drops rapidly, due to atmospheric friction. As a decreases, e decreases too (becomes closer to circle).

From Kepler's third law,

$$T = \frac{2\pi a^{3/2}}{\sqrt{GM}}, \tag{4.125}$$

orbital period and a are related. Using the Schwarzschild radius of the earth, $2GM_\oplus/c^2 = 8.87$ mm, we obtain

$$\begin{aligned} T &= \frac{2\sqrt{2}\pi a^{3/2}/c}{\sqrt{2GM/c^2}} = \frac{2\sqrt{2}\pi(a/6900\text{ km})^{3/2}(6900\text{ km})^{3/2}/(300000\text{ km/s})}{\sqrt{8.87\text{ mm}}} \\ &= 95\text{ min}(a/6900\text{ km})^{3/2}. \end{aligned} \tag{4.126}$$

Figure 4.11 shows the time history of the orbital period and a for the Ginga satellite. For low earth orbit (LEO) satellites like Ginga, orbital period is about 96 minutes.

4.5.3 Geosynchronous satellites

Spin period of the earth is 23 hour 56 minutes and 4.09 seconds [16]. From (4.126), we see that at $a = 42200$ km (altitude is about 35800 km), the orbital period of a satellite agrees with the spin period of the earth. If satellites are at this radius and the inclination is zero (on the equatorial plane), they look static from the earth surface. These satellites are called *geosynchronous satellites*. Weather satellites, communication satellites etc, which are required to be seen from particular location on the earth surface, are put in the geosynchronous orbits.

4.5.4 Two Line Elements

In order to represent orbital six-elements, *Two Line Elements* (TLE) are often used, which is a standard format of not only the six elements but also satellite name, international indentation number etc.

NORAD (NORth American aerospace Defense Command; `http://www.norad.mil`) is monitoring almost all the satellites (and whatever orbiting the earth), and release their orbital elements in the TLE format (Figure 4.12).

Be careful that "Mean Motion", which is the number of rotations per day, is used instead of a. Let's take a look at TLE of several satellites[17]:

```
SUZAKU
1 28773U 05025A   08013.93865221  .00000558  00000-0  37528-4 0  6575
2 28773  31.4061 323.8498 0007001 164.9250 195.1602 15.00529329137995
ASTRO-F (AKARI)
1 28939U 06005A   08014.23580039  .00000005  00000-0  11192-4 0  6030
2 28939  98.2316  16.5778 0008622   0.3484 359.7729 14.57435459100351
HINODE (SOLAR-B)
1 29479U 06041A   08013.94377495  .00000087  00000-0  26130-4 0  4426
```

[16] Not 24 hours, which is a day, period of the apparent solar motion seen from the earth.

[17] Latest TLE may be obtained from `http://celestrak.com`.

```
2 29479  98.0789  23.2007 0014564 229.4553 130.5382 14.62802560 69920
INTEGRAL
1 27540U 02048A   08012.45833333  .00000061  00000-0  10000-3 0  6500
2 27540  86.3672  23.5282 7969010 276.7243 358.3858  0.33418208  2558
HIMAWARI 6
1 28622U 05006A   08014.77456198 -.00000264  00000-0  10000-3 0  4588
2 28622   0.0211  76.8046 0002163  49.6656  46.0362  1.00271868 10549
```

We can readily see the following:

1. Suzaku, Akari, Hinode are LOE satellites, which orbits about 15 times a day. Himawari orbits once a day, since it is a geosynchronous satellite.

2. INTEGRAL, European gamma-ray satellite, has a large, eccentric orbit, where the orbital period is about three days. Other satellites have almost circular orbits.

3. Suzaku orbital inclination angle is 31.4 deg, corresponding to the latitude of the launch site, similar to Ginga. Inclination of Himawari is 0, since it is a geosynchronous satellite. Inclinations of Akari and Hinode are almost 90 degree, as they have the *Sun-synchronous orbit (SSO)*. Their orbital planes are always facing Sun, so that Hinode, solar observing satellite, can always observe Sun, and Akari, infrared satellite, can always observe the anti-direction of the earth[18].

[18] Earth is a strong source of the infrared noise.

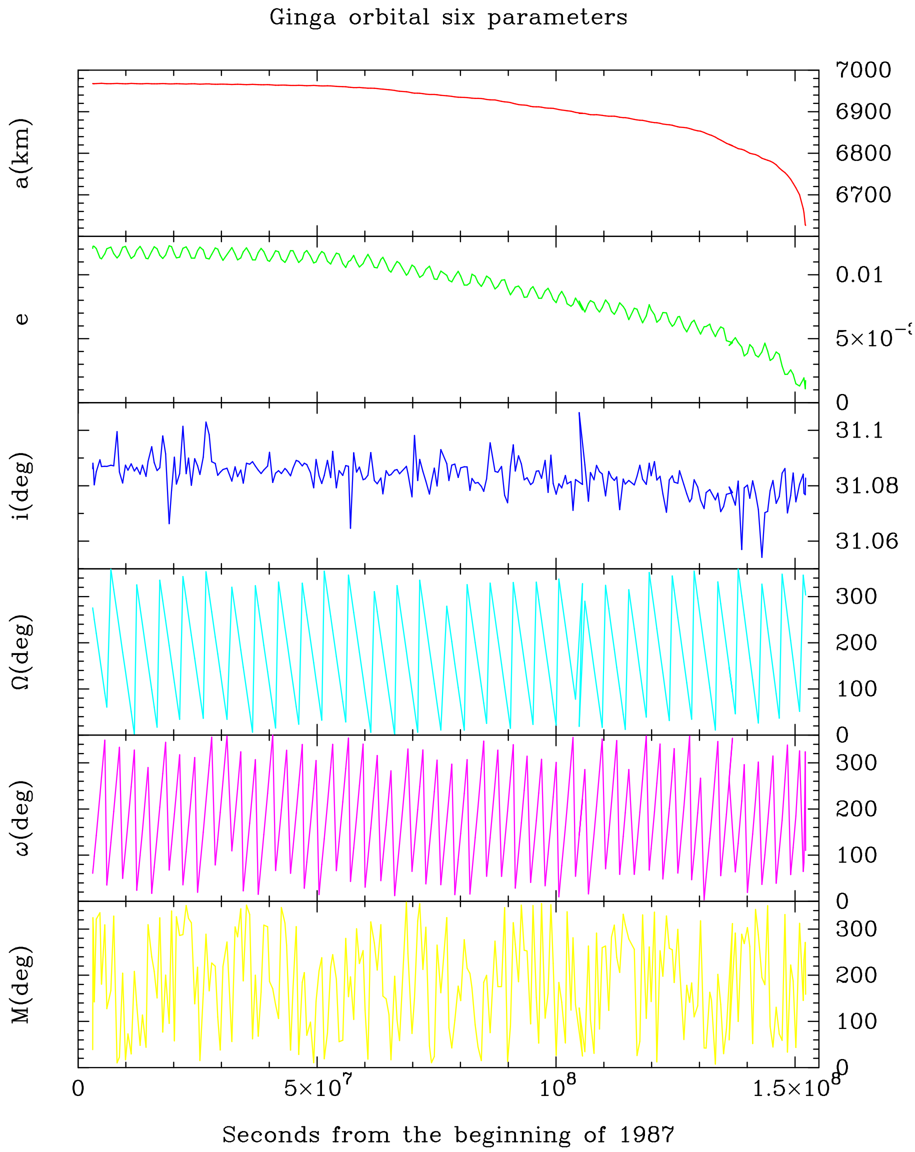

Figure 4.10: Variation of the orbital six-elements of Ginga satellite from the launch (1987/02/05) to the reentry (1991/11/01).

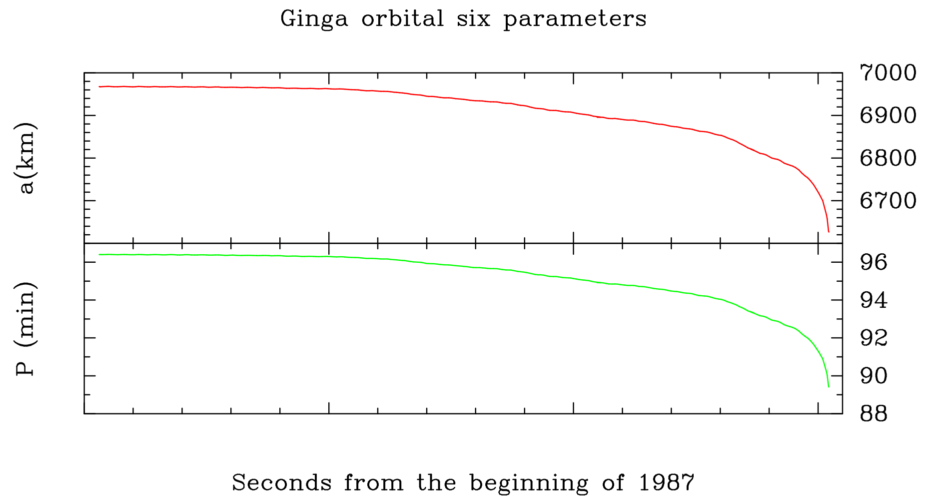

Figure 4.11: Variation of the semi-major axis and the orbital period of the Ginga satellite from the launch to the reentry。

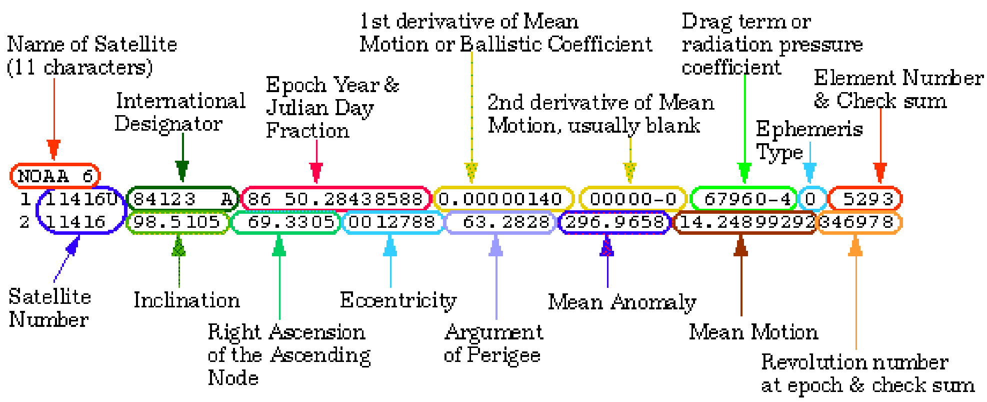

Figure 4.12: Definition of the Two Line Elements (TLE). Taken from `http://spaceflight.nasa.gov/realdata/sightings/SSapplications/Post/JavaSSOP/SSOP_Help/tle_def.html`.

Chapter 5

X-ray Production Mechanisms

5.1 Optical Depth

When radiation go through material with the optical depth τ, the flux will be weakened by $e^{-\tau}$. Thickness of the material being L [cm], hydrogen column density N_H [cm^{-2}], density ρ [g/cm^3], then

$$\tau = \alpha[\mathrm{cm}^{-1}]\, L[\mathrm{cm}] = \kappa[\mathrm{cm}^2/\mathrm{g}]\, \rho[\mathrm{g/cm}^3]\, L[\mathrm{cm}] = N_H[\mathrm{cm}^{-2}]\, \sigma_H[\mathrm{cm}^2], \tag{5.1}$$

where α is called *absorption coefficient*, κ *mass absorption coefficient; opacity*, σ_H is the *cross section per hydrogen atom*. In general these parameters are functions of location and wavelength (photon energy).

Consider each photon; *the probability that a single photon moves forward by* τ *without being absorbed is* $e^{-\tau}$. Also, *average optical depth of the photons is unity*. In fact,

$$\int_0^\infty e^{-\tau} d\tau = 1,$$

$$\langle \tau \rangle \equiv \int_0^\infty \tau e^{-\tau} d\tau = 1.$$

When $\tau > 1$, the material is *optically thick* and the photons are absorbed in the material. When $\tau < 1$, the materiel is *optically thin*, and the probability that a photon is absorbed in the material is $1 - e^{-\tau} \approx \tau$。

Average of the physical paths of photons, l, will be, from $\tau = \alpha\, l = 1$,

$$l = \frac{1}{\alpha}, \tag{5.2}$$

which is called mean free path。 From (5.1) and (5.2),

$$\tau = \frac{L}{l}. \tag{5.3}$$

5.2 Radiative Transfer

Using the emissivity j_ν [erg/s/cm^3/Hz/str]、and the absorption coefficient α_ν [cm^{-1}], the *source function* S_ν [erg/s/cm^2/Hz/str] is defined as,

$$S_\nu = \frac{j_\nu}{\alpha_\nu}. \tag{5.4}$$

You should remember the radiation transfer equation and the unite of I_ν and S_ν, erg/s/cm^2/Hz/str.

Equation of the *radiative transfer* is written as ,

$$\frac{dI_\nu}{d\tau_\nu} = -I_\nu + S_\nu. \tag{5.5}$$

In general, I_ν (specific intensity; brightness), S_ν (source function) is a function of frequency, location and optical thickness τ_ν that can be also a function of the frequency and location. If we considering *scattering* of photons, S will be dependent on I, and the radiation transfer equation will be more complicated (we do not consider the scattering here).

In the case of *local thermal equilibrium (LTE)*, the source function is determined only by temperature, and given as the Planck function $B_\nu(T)$

$$B_\nu(T) = \frac{2}{c^2}\frac{h\nu^3}{e^{h\nu/kT}-1} \ \ [\text{ergs/s/cm}^2/\text{Hz/str}]. \tag{5.6}$$

You should remember the functional form of the Planck function $B_\nu(T)$.

Equation (5.5) can be intuitively understood as follows:
When $I > S$, since $dI/d\tau < 0$, I decreases. When $I < S$, since $dI/d\tau > 0$, I increases. Namely, I is going to approach S, along τ. When τ is large enough (optically thick case), I will be S.

When $S_\nu = B_\nu$, it is called thermal emission. When $I_\nu = B_\nu$, it is blackbody emission. *Any thermal emission will become blackbody emission in the optically thick limit.*

In thermal emission, $S_\nu = B_\nu(T)$, and

$$\alpha_\nu = \frac{j_\nu}{B_\nu(T)} \tag{5.7}$$

holds. This is called the *Kirchhoff's law.*

In the simplest case when S_ν is constant not depending on τ_ν, (5.5) may be solved as,

$$I_\nu(\tau) = S_\nu(1 - e^{-\tau_\nu}) + I_\nu(0)e^{-\tau_\nu}. \tag{5.8}$$

Here, considering a matter (plasma) with the optical thickness τ, the input radiation is $I_\nu(0)$, and the output radiation is $I_\nu(\tau)$. From (5.8), when $\tau \gg 1$ (optically thick), as we have already seen,

$$I_\nu(\tau) = S_\nu. \tag{5.9}$$

In particular, in the case of thermal emission ($I_\nu(\tau) = B_\nu(T)$), whatever the composition of material (plasma), that will be the blackbody emission.

In the optically thin case ($\tau \ll 1$, (5.8) will be

$$I_\nu(\tau) = S_\nu\tau + I_\nu(0)(1 - \tau_\nu). \tag{5.10}$$

When there is no input radiation, the second term is zero, and *optically thin emission* proportional to the optical depth is observed from the first term.

In particular, if $\tau_\nu \gg 1$ at a particular frequency, an absorption line is observed at that frequency.

From (5.9) and (5.10), as long as thermal emission, $S_\nu = B_\nu(T)$, is concerned, always $I_\nu(\tau) \leq B_\nu$.. Namely, *strength of the thermal emission never exceeds that of the blackbody emission.*

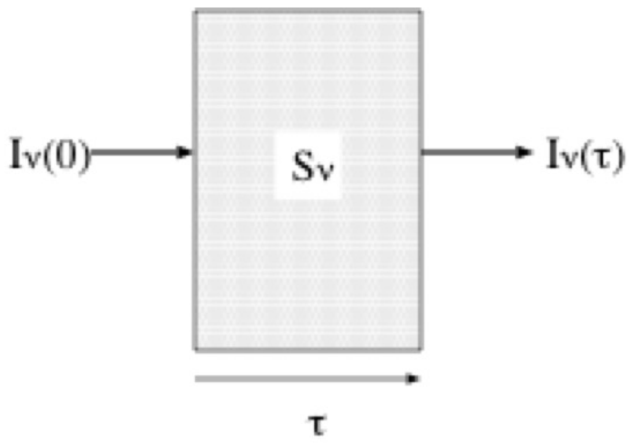

Figure 5.1: A simple configuration of radiation transfer.

5.3 Blackbody Radiation

5.3.1 Blackbody radiation and Einstein's A and B coefficients

Blackbody emission does not depend on composition of plasmas. Let's consider a simple case that two-level atoms (where the energy gap is $h\nu$) are in equilibrium in the blackbody radiation field with temperature T. If the number density of the upper-level atom is n_2 and that of the lower-level atom is n_1, since the atoms are in thermal equilibrium,

$$\frac{n_2}{n_1} = \exp(-h\nu/kT). \tag{5.11}$$

Atoms in the upper-level will have *spontaneously emission* to emit photons with the frequency ν and transit to the lower level at the rate of $A_{21}[\mathrm{s}^{-1}]$. In the radiation field J_ν, photons are absorbed by the lower-level atoms $B_{12}J_\nu$ per second. Also, we need to consider the *induced emission*, at the rate of $B_{21}J_\nu$. Here, A_{21}, A_{12}, B_{12} are called *Einstein's A and B coefficients.* Considering the detailed balance, we have

$$n_1 B_{12} J_\nu = n_2 A_{21} + n_2 B_{21} J_\nu. \tag{5.12}$$

This can be solved for J_ν, as

$$J_\nu = \frac{A_{21}/B_{21}}{(n_1/n_2)(B_{12}/B_{21}) - 1}. \tag{5.13}$$

Using (5.11),

$$J_\nu = \frac{A_{21}/B_{21}}{\exp(h\nu/kT)(B_{12}/B_{21}) - 1}. \tag{5.14}$$

Now, in general *Einstein's relationship* holds,

$$\begin{aligned} B_{12} &= B_{21}, \\ A_{21} &= \frac{2h\nu^3}{c^2} B_{21}. \end{aligned} \tag{5.15}$$

Using (5.15), 5.14) is rewritten as

$$J_\nu = \frac{2h\nu^3/c^2}{\exp(h\nu/kT) - 1} \ \ [\mathrm{erg/s/cm^2/Hz/str}]. \tag{5.16}$$

Now we obtained the Planck function, $B_\nu(T)$.

5.3.2 Characteristics of blackbody radiation

Frequency and wave-length to give the blackbody peak

Consider the blackbody radiation (5.6) or (5.16), which is given as a function of frequency. We may obtain the blackbody radiation as a function of wave-length, considering

$$B_\nu(T)\, d\nu = -B_\lambda(T)\, d\lambda.$$

Since $c = \lambda\nu$、 $d\nu/\nu = -\, d\lambda/\lambda$,

$$B_\lambda(T) = \frac{2hc^2/\lambda^5}{\exp(hc/\lambda kT) - 1} \ \ [\mathrm{erg/s/cm^2/Å/str}]. \tag{5.17}$$

Calculate derivative of (5.6) with ν, then we see the Planck function will be maximum at the peak frequency ν_{max};

$$h\nu_{max} = 2.82\ kT. \tag{5.18}$$

It is useful to remember that the *peak frequency of the blackbody energy spectrum is around three times the temperature.*

On the other hand, calculate derivative of (5.17) with λ, then we see the wavelength λ_{max}which gives the maximum blackbody flux is

$$\lambda_{max} = 0.201\ \frac{hc}{kT}. \tag{5.19}$$

Note that $\lambda_{max}\,\nu_{max} = 0.57c \neq c$、 Namely, *the peak frequency which gives the maximum blackbody flux per-frequency and the peak wave-length which give the maxim flux per wave-length are different..*

Approximation in the low/high-frequency limits

When $h\nu \ll kT$, from (5.6),

$$B_\nu(T) \approx \frac{2\nu^2 kT}{c^2}. \tag{5.20}$$

This is the *Rayleigh-Jeans law*

Note that h does not appear, and the intensity is proportional to T. Multiply $4\pi/c$, then the energy density is $(8\pi\nu^2/c^3)kT$. Remember that the classical electromagnetic natural vibration density is $8\pi\nu^2/c^3$. For each natural frequency, the thermal energy kT is associated.

When $h\nu \gg kT$,

$$B_\nu(T) \approx \frac{2h\nu^3}{c^2} e^{-kT/h\nu}, \tag{5.21}$$

which is *Wien's law.*

In radio astronomy, most emission is in the Rayleigh-Jeans regime, while in X-ray astronomy, where typical energy range is 2–10 keV, most emission is in the Wien's law side, since typical accretion disk temperature around stellar-mass black hole is ~ 1 keV and the X-ray burst of neutron stars have ~ 2 keV. We rarely see blackbody emission with higher temperatures.

5.3.3 Energy density and flux of blackbody emission

Energy density is given as

$$\begin{aligned} u &= \frac{4\pi}{c}\int_0^\infty B_\nu(T)d\nu \\ &= \frac{8\pi k^4}{h^3c^3}T^4\int_0^\infty \frac{x^3}{e^x-1}dx, \end{aligned}$$

where the integral is $\frac{\pi^4}{15}$, so

$$\begin{aligned} u &= a\,T^4, \\ a \equiv \frac{8\pi^5 k^4}{15h^3c^3} &= 7.56\times 10^{-15}\ \ [\text{erg cm}^{-3}\ \text{deg}^{-4}]. \\ &= 1.37\times 10^{14}\ \ [\text{erg cm}^{-3}\ \text{keV}^{-4}]. \end{aligned}$$

As an example, temperature of the Cosmic Microwave Background Radiation (CMBR) is 2.725 K, then the energy density is 4.17×10^{-13}erg/cm^3 ≈ 0.26 eV/cm^3.

Flux from the surface of the body emitting blackbody emission is given as

$$\begin{aligned} F &\equiv \int I\cos\theta\, d\Omega \\ &= 2\pi\int_0^{\pi/2}\left\{\int_0^\infty B_\nu(T)d\nu\right\}\cos\theta\sin\theta\, d\theta \\ &= \pi\int_0^\infty B_\nu(T)d\nu = \frac{c}{4}\,u = \frac{ac}{4}\,T^4 \equiv \sigma T^4, \qquad (5.22) \\ \sigma = \frac{2\pi^5k^4}{15h^3c^2} &= 5.67\times10^{-5}\ \ [\text{erg cm}^{-2}\ \text{deg}^{-4}\ \text{s}^{-1}] \\ &= 1.0\times10^{24}\ \ [\text{erg cm}^{-2}\ \text{keV}^{-4}\ \text{s}^{-1}], \end{aligned}$$

where σ is the Stephan-Boltzmann constant (see also section 2.1.1).

5.3.4 Photon number density of blackbody emission

Let n be the photon number density of the blackbody emission;

$$\begin{aligned} n &= \frac{4\pi}{c}\int_0^\infty B_\nu(T)/h\nu\; d\nu \\ &= \frac{8\pi k^3T^3}{h^3c^3}\int_0^\infty \frac{x^2}{e^x-1}dx. \end{aligned}$$

Since $\int_0^\infty \frac{x^2}{e^x-1}dx = 2.404$,

$$n = 60.4 \left(\frac{kT}{hc}\right)^3 = C\,T^3,$$

$$C = 20.3 \text{ [photons cm}^{-3}\text{ deg}^{-3}]$$

$$= 3.17 \times 10^{22} \text{ [photons cm}^{-3}\text{ keV}^{-3}].$$

For instance, in the case of CMBR (T=2.725 K), the photon density is ~ 410 photons/cm^3. Also, using (5.19),

$$1/n \approx 2\lambda_{max}^3.$$

$1/n$ is the volume per photon, so, schematically, the space is filled with the photons having the wave-length λ_{max}.

5.3.5 Three temperatures

Blackbody emission has the unique temperature, such that $T = T_{eff} = T_b. = T_{cold}$, where T_{eff}, T_b and T_{cold} are effective temperature, brightness temperature and color temperature, respectively, which are explained soon below. If emission is (slightly) different from the blackbody, we need to distinguish these three temperatures.

Effective temperature)

Let F be the flux from surface of the emitting body. Then the effective temperature T_{eff} is defined as

$$\sigma T_{eff}^4 \equiv F.$$

For instance, luminosity of the spherically emitting star with the radius R is given as $L = 4\pi R^2 F = 4\pi R^2 \sigma T_{eff}^4$. Put the distance to the star d, and the observed flux f, then $f = L/4\pi d^2$, and

$$\sigma T_{eff}^4 = F = \left(\frac{d}{R}\right)^2 f.$$

Namely, if d/R is known, effective temperature is derived from the observe flux; *otherwise we may not know the effective temperature from observation.*

Color temperature

Observed spectral "shape" is fitted with the Planck function, and the best-fit temperature is the *color temperature*, T_{col}, which does not dependent on distance to the source or area of the emission region.

What we may obtain from X-ray spectral fitting of the observed data is the color temperature, which is, in general, different from the effective temperature (see section 5.3.6).

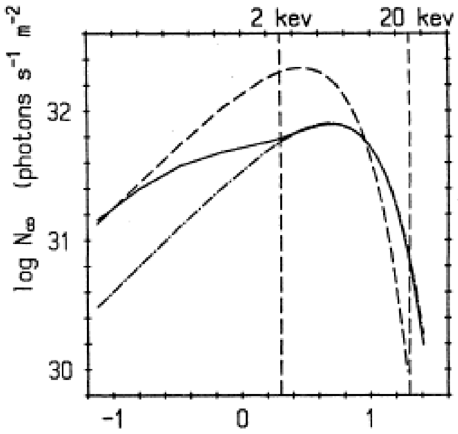

Figure 5.2: Model spectrum from bursting neutron star (solid line) numerically calculated taking account of inverse-Compton scattering in the upper-atmosphere. In the 2–20 keV energy range, this is approximated well with the "diluted blackbody", $(T_{eff}/T_{col})^4 B_\nu(T_{col})$ (dash-dotted line). The Planck function $B(T_{eff})$ is shown with the dashed line. Taken from Ebisuzaki 1987, PASJ, 39, 287.

Brightness temperature

At a given frequency ν, measure the specific intensity I_ν. The brightness temperature T_b is given by

$$I_\nu = B_\nu(T_b).$$

Brightness temperature is often used in radio astronomy where Rayleigh-Jeans approximation holds.

When medium (plasma) with temperature T is emitting thermal emission (say, thermal bremsstrahlung; section 5.4.1), since it is less efficient than blackbody emission (section 5.5), $T > T_b$. On the other hand, in the case of non-thermal emission (say, synchrotron emission; section 5.5) $T \ll T_b$ is common[1].

5.3.6 Correction for the difference between the color temperature and the effective temperature

In hot atmospheres such as accretion disk or neutron star surface, hot electrons near the surface inverse-Compton scatter the blackbody photons from inside. Consequently, the photons gain energies, and the blackbody spectra are distorted while preserving the total number of photons, such that lower energy photons appear in higher energies. The spectral peak shifts upward so that *the color temperature will be higher than the effective temperature* (Figure 5.2).

It is necessary to numerically solve radiation-transfer equations to obtain precise spectra when inverse-Compton scattering presents. Luckily, in the typical X-ray band (≈2–10 keV) the output spectrum affected by the inverse-Compton scattering s approximated with the

[1]For instance, $T_b \sim 10^{13}$ K is observed from the archetypal quasar 3C273. See `http://arxiv.org/abs/1601.05806`.

"diluted blackbody",

$$I_\nu = \left(\frac{T_{eff}}{T_{col}}\right)^4 B_\nu(T_{col}), \tag{5.23}$$

where the color temperature T_{col} is higher than the effective temperature T_{eff}. As in (5.22), we can obtain the flux from the unit surface,

$$F = \int \left\{ \int_0^\infty \left(\frac{T_{eff}}{T_{col}}\right)^4 B_\nu(T_{col})\, d\nu \right\} \cos\theta \, d\Omega$$

$$= \pi \left(\frac{T_{eff}}{T_{col}}\right)^4 \int_0^\infty B_\nu(T_{col})\, d\nu = \left(\frac{T_{eff}}{T_{col}}\right)^4 \sigma T_{col}^4 = \sigma {T_{eff}}^4. \tag{5.24}$$

So, definition of the effective temperature holds.

Let's consider the optically thick accretion disk around a stellar black hole (section 3.5.3). There, we assumed that the disk emits the blackbody emission, and derived the equation (3.15),

$$L_{disk} = 4\pi\sigma r_{in}^2 T_{in}^4. \tag{5.25}$$

Here, T_{in}, innermost disk temperature, should be the effective temperature, which we write as $T_{in}^{(eff)}$. However, what we can obtain from spectral shape (spectral model fitting) is the color temperature of the disk, which we may write as $T_{in}^{(col)}$.

Consequently,

$$L_{disk} = 4\pi\sigma r_{in}^2 (T_{in}^{(eff)})^4 = 4\pi\sigma r_{in}^2 \left(\frac{T_{in}^{(eff)}}{T_{in}^{(col)}}\right)^4 (T_{in}^{(col)})^4 = 4\pi\sigma (r_{in}^*)^2 (T_{in}^{(col)})^4, \tag{5.26}$$

where

$$r_{in} = r_{in}^* \left(\frac{T_{in}^{(col)}}{T_{in}^{(eff)}}\right)^2 \geq r_{in}^*. \tag{5.27}$$

Namely, the true innermost radius r_{in} is $\left(T_{in}^{(col)}/T_{in}^{(eff)}\right)^2$ times greater than the apparent innermost radius r_{in}^* derived from the color temperature $T_{in}^{(col)}$.

The value of T_{col}/T_{eff}, often called *hardening factor* should be numerically calculated. Luckily again, this value is rather constant at about ~ 1.7 over different radii and disk luminosities in the case of stellar-mass black holes (Shimura and Takahara 1995, ApJ, 445, 780).

The black hole mass is estimated by identifying r_{in} as R_{ISCO} that is $6GM/c^2$ in the case of Schwarzschild (non-rotating) black hole (section 2.3.3). Remember that what we can obtain from model fitting of the accretion disk spectra is $T_{in}^{(col)}$. If $T_{col}/T_{eff} \sim 1.7$ the actual black hole mass becomes $1.7^2 \approx 3$ times greater than the mass estimated (wrongly) assuming the blackbody emission with the temperature $T_{in}^{(col)}$.

5.4 Thermal Emission

5.4.1 Thermal bremsstrahlung

When free electrons are affected by Coulomb force of nuclei (mostly protons in astrophysical plasma), the electrical dipole will go through accelerated motion, and produce in electromagnetic radiation. This is called *bremsstrahlung*.

Optically think hot plasmas emit the radiation by *thermal bremsstrahlung*. From hot plasmas, not only the continuum emission due to thermal bremsstrahlung, but also many emission lines are emitted due to recombination of ions and electrons (Figure 5.5).

As explained in section 5.2, *any optically thick thermal emission will become the blackbody emission, that is most efficient.* Neutron star atmosphere, and the standard accretion disk (around black hole or neutron star) are optically thick, and emit blackbody emission[2].

On the other hand, thermal bremsstrahlung is observed from optically thin plasmas, such as Cataclysmic Variable (white dwarf binary), super-nova remnants (SNRs), galaxies, clusters of galaxies, etc. .

Since blackbody is the most efficient, very compact objects such as neutron star s of black holes, emitting blackbody emission, are bright X-ray sources. On the other hand, X-ray sources shinning with thermal bremsstrahlung are geometrically much bigger, otherwise they may not be observable.

Approximated formula of X-ray energy spectrum

Energy spectrum of thermal bremsstrahlung is given as (see Appendix),

$$\begin{aligned}\epsilon_\nu^{ff} \equiv \frac{dW}{dV\,dt\,d\nu} &= \frac{2^5\pi e^6}{3mc^3}\left(\frac{2\pi}{3km}\right)^{1/2} T^{-1/2} Z^2 n_e n_i e^{-h\nu/kT}\bar{g}_{ff}(T,\nu) \\ &= 6.8\times 10^{-38} T^{-1/2} Z^2 n_e n_i e^{-h\nu/kT}\bar{g}_{ff}(T,\nu) \ \ \text{[CGS unit]}. \end{aligned} \tag{5.28}$$

In X-ray observation, often $kT \approx h\nu$, in which case $\bar{g}_{ff}(T,\nu)$ is approximated as $\approx (h\nu/kT)^{-0.4}$. Consequently, X-ray energy spectrum of thermal bremsstrahlung may be approximated with

$$f_E(E) \propto E^{-0.4}\exp(-E/kT)\ \text{[erg/s/cm}^2\text{/keV]}. \tag{5.29}$$

Consequently, the photon spectrum is approximated as (Figure 5.3),

$$f_p(E) \propto E^{-1.4}\exp(-E/kT)\ \text{[photon/s/cm}^2\text{/keV]}. \tag{5.30}$$

Emissivity

If (A.23) is integrated by frequency, we may obtain emissivity of the thermal bremsstrahlung emission with temperature T per unit-time per unit-volume;

$$\begin{aligned}\int \epsilon_\nu^{ff} d\nu &= 6.8\times 10^{-38} T^{1/2} Z^2 n_e n_i \bar{g}_{ff}(T)\frac{k}{h} \ \ \text{[CGS unit]} \\ &= 1.4\times 10^{-27} T^{1/2} Z^2 n_e n_i \bar{g}_{ff}(T) \ \ \text{[CGS unit]}.\end{aligned}$$

[2]Affected by inverse-Compton scattering (section 5.3.5).

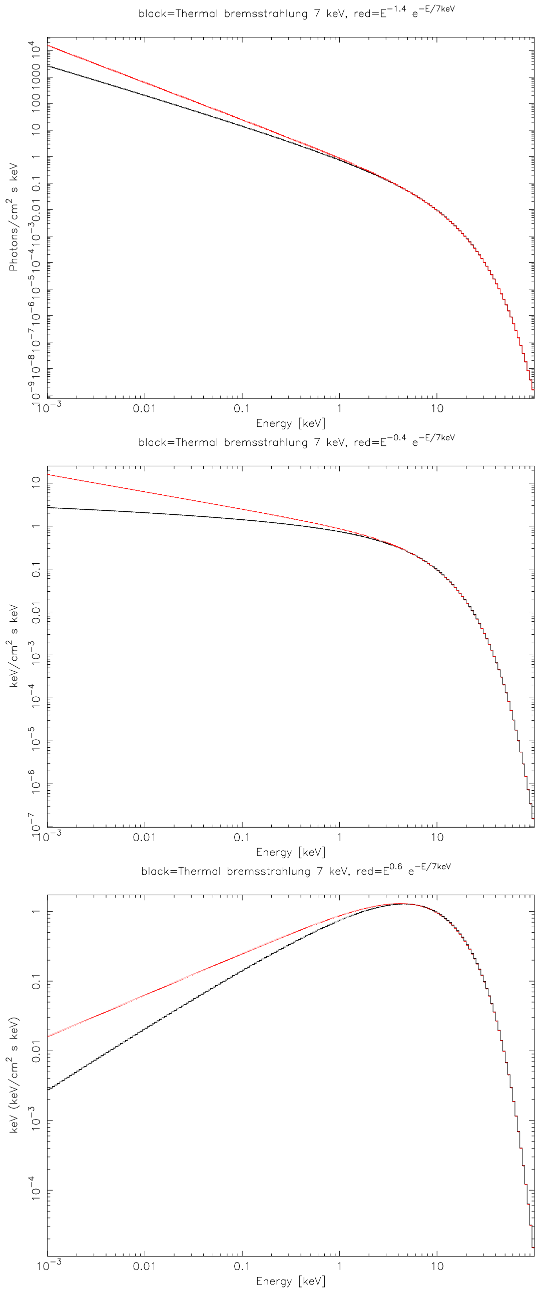

Figure 5.3: Comparison of kT=7 keV thermal bremsstrahlung spectra (black, `brems` model in xspec) and a cut-off power-law model $\propto E^{-p}\exp(-E/kT)$ where kT=7 keV (red). From top to bottom, unit of the Y-axis is [photon/s/keV/cm^2], [keV/s/keV/cm^2] and [keV^2/s/keV/cm^2], and the p value is $1.4, 0.4, -0.6$, respectively.

Here, a frequency averaged Gaunt factor is $\bar{g}_{ff}(T) \approx 1.2$, and assuming the cosmic abundance, $\sum_Z n_e n_Z Z^2 \approx 1.4 n_e^2$.[3] In the end, we can obtain the emissivity in [erg/s/cm^3] of thermal bremsstrahlung emission with T and n_e;

$$\int \epsilon_\nu^{ff} d\nu = 2.4 \times 10^{-27} T^{1/2} n_e^2 \ \text{[CGS unit]}. \tag{5.31}$$

Characteristics of thermal bremsstrahlung

- Broad energy spectra

  Let's compare a wide-band energy spectrum of thermal bremsstrahlung with that of the blackbody having the same temperature (Figure 5.4). We can see that the thermal bremsstrahlung is much "wider", in particular it extends toward lower energies. This is because those electron only slightly "curved" by the ions emit soft X-ray photons.

- Inefficiency compared to blackbody

  As we have already seen in 5.2, intensity of thermal emission never exceeds the black-body emission. In very early era of X-ray astronomy, bright sources like Sco X-1 was suggested to be white dwarfs emitting thermal bremsstrahlung emission. In order to explain the observed luminosity $\sim 10^{38}$ erg/s with thermal bremsstrahlung, using (5.31) with the temperature estimated from observation, $T = 2 \times 10^7$ K (~ 2 keV), an *emission measure* as large as $n_e^2 V \approx 10^{61}$ [cm^{-3}] is required. For dense plasma, the density is at most $\sim 10^{15}$ cm^{-3}, so $V \approx 10^{31}$ cm^3, or size of the emission region is $R \approx 10^{10}$ cm. This is much larger than the typical neutron star radius, $\sim 10^6$ cm, 10^9 cm, and even rather than white dwarfs ($R \lesssim 10^9$cm). Namely, so that such compact objects as neutron stars emit brightly, thermal bremsstrahlung is too inefficient, and optically thick emission (=black body) is required [4].

  Cataclysmic Variables, binaries of white-dwarf and late-type companion, are known to emit high-temperature ($kT \sim 10$ keV) thermal bremsstrahlung spectra. In this case, not the entire white dwarf surface, but only bottom part of the accretion column becomes optically thin and emit via thermal bremsstrahlung. If we put $R \sim 10^8$ cm^2, $n_e \sim 10^{15}$ cm^{-3} and $T \sim 10^8$ K, the luminosity will be $\sim 10^{31}$ erg/s from (5.31). We see that neutron star emitting with black body is $\sim$7 orders of magnitude brighter than white dwarfs, that is more than two orders of magnitude larger and an order of magnitude hotter than neutron stars.

- Line emission

  From hot plasmas, as long as they are not fully ionized, not only the thermal bremsstrahlung continuum, but also emission lines are observed from recombination (Figures 5.5 and 5.6). It is not easy to calculate line-dominated energy spectra from such hot plasmas, but theoretical plasma models are implemented in standard packages like XSPEC, and easily available.

[3] See, Zombeck, "Handbook of Space and Astrophysics".
[4] Or, non-thermal process like synchrotron emission is required.

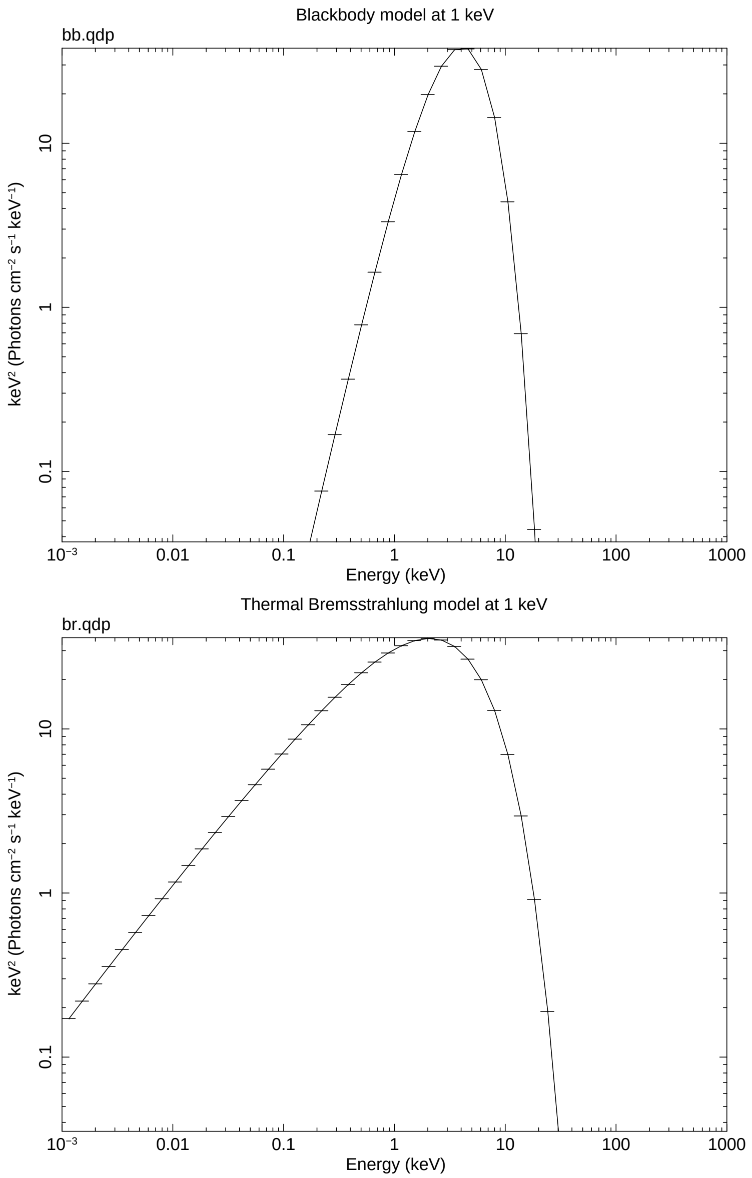

Figure 5.4: Blackbody spectrum with $kT = 1$ keV (top) and thermal bremsstrahlung spectrum with the same temperature (bottom) in the unite of $\mathrm{keV}^2/\mathrm{s}/\mathrm{cm}^2/\mathrm{keV}$. Both have peaks at around 3 kT (section 5.3.2). We can see thermal bremsstrahlung is much wide and particularly extends toward lower energies.)

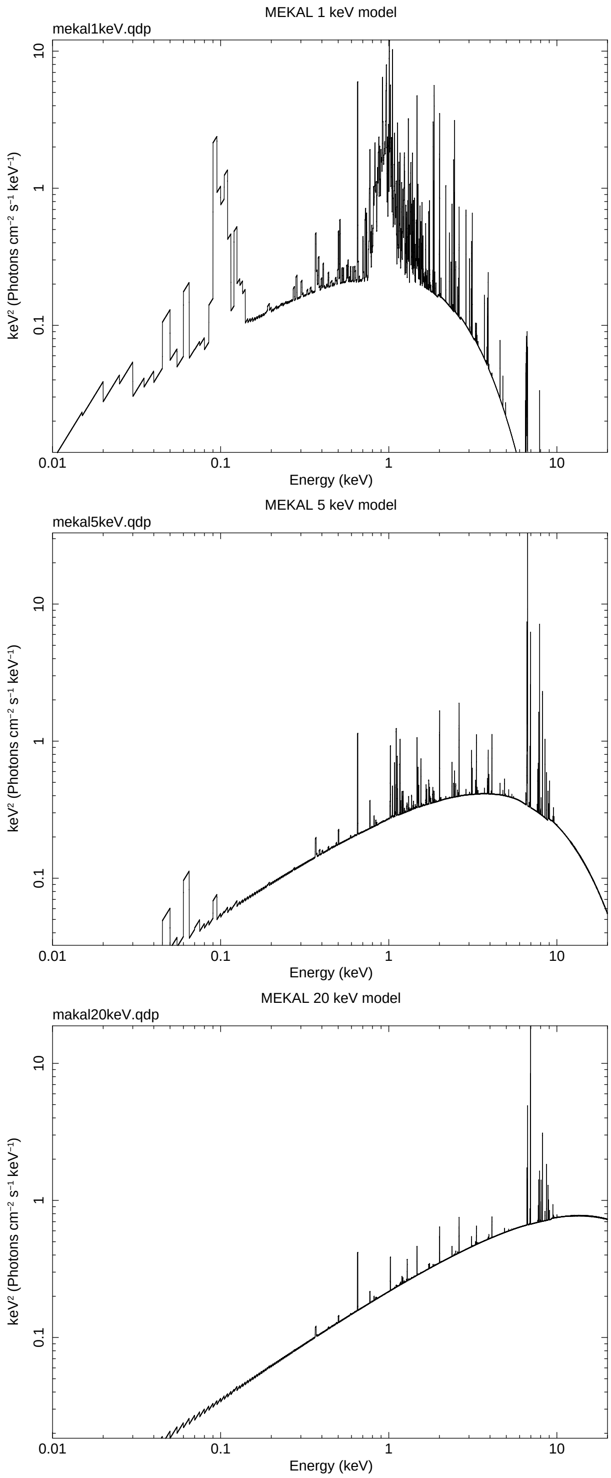

Figure 5.5: Theoretical energy spectra from thermal plasmas at 1 keV, 5 keV and 20 keV. The "mekal" model in XSPEC is used. We can see that, as the temperature increases, (1) the continuum peaks shift toward higher energies, and (2) emission lines from heavier elements are more prominent.

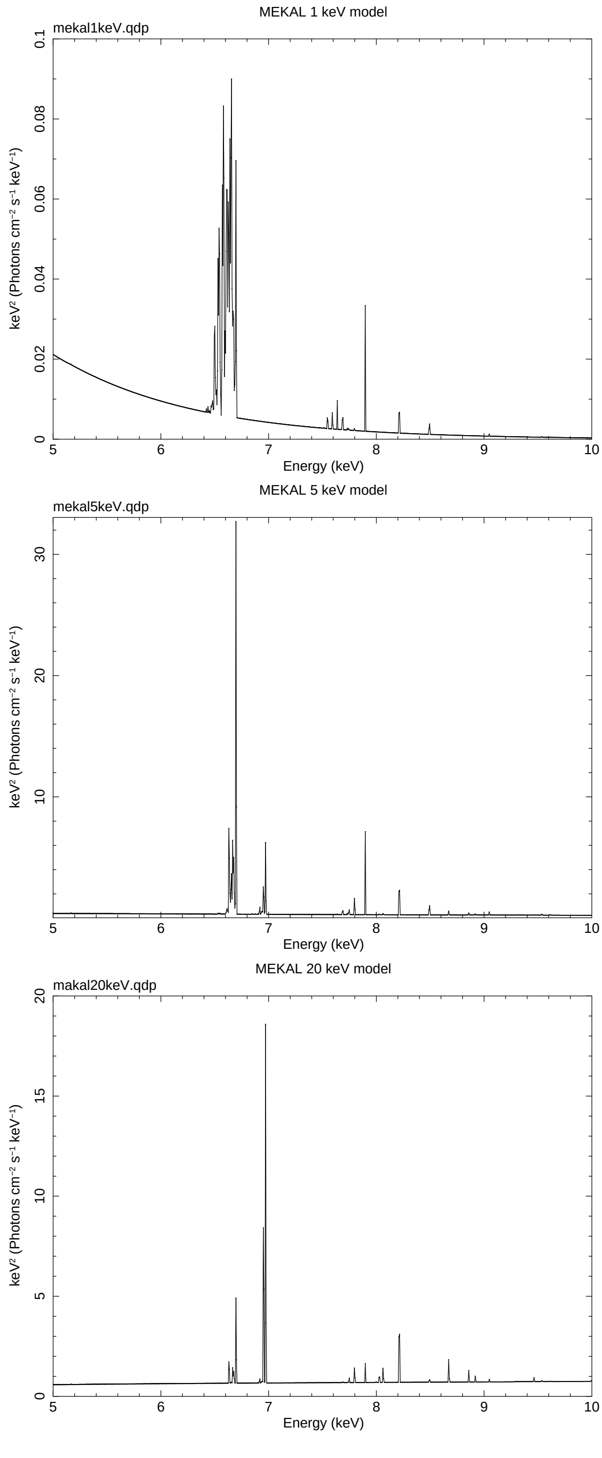

Figure 5.6: Expansion of the iron K-line region in the previous figure. Iron line missions from the 1 keV, 5 keV and 20 keV thermal plasmas are indicated. Around 6.6 – 6.7 keV, FeXXV (He-like) lines are seen, and around 7.0 keV, FeXXVI (H-like) lines are observed. As the plasma temperature increases, lines from more highly ionized ions are observed.

5.4.2 Thermal inverse Comptonization

In thermal (and non-thermal) *Comptonization*, photons are not created, but already existent photons are *scattered* by electrons in the plasmas. In Comptonization, number of photons are preserved. Let's review related terminologies:

Thomson scattering

Scattering of long-wavelength electromagnetic waves (= low energy photons) by free electrons. This is the long-wavelength (=low energy) limit of the Compton scattering. Thomson scattering is described by classical electromagnetic theory, such that electrons oscillate according to the input electromagnetic wave, and emit the electromagnetic wave with the same-frequency; namely, photons do not change energies due to Thomson scattering. Cross-section of Thomson scattering is $\sigma_T = \frac{8\pi}{3} r_0^2$, where r_0 is the classical electron radius (section 2.2.1).

Compton scattering (=Comptonization)

Scattering of high energy photons by electrons. When mono-energetic X-ray photons are scattered by electrons, low energy (longer wavelength) X-ray photons are observed by $\Delta\lambda = \lambda_C(1-\cos\theta)$, where θ is the scattering angle, and $\lambda_C = h/mc \approx 0.02426\mathring{A}$ is the Compton wavelength of electron (section 2.2.1). Compton scattering is considered as elastic collision between photons and electrons.

Cross-section of Compton scattering is given as *Klein-Nishina cross-section*, of which the low-energy (long-wave) limit is Thomson cross-section.

Inverse Compton scattering

In Compton scattering, high-energy photons lose energy through elastic-scattering with low energy electrons. In *inverse-Compton scattering*, low-energy photons gain energies through elastic-scattering with high-energy electrons. These two phenomena are identical if observed at the electron rest-frame. Therefore, often Compton scattering and inverse-Compton scattering are not distinguished, but may be just called Compton scattering or Comptonization.

In X-ray astronomy, we often observe inverse-Compton scattering of soft photons by high energy electrons.

Energy spectra of Thermal inverse Comptonization

Thermal electrons in hot-plasma ($\approx kT_e$) inverse-Compton scatter input low energy photons ($\approx E_{soft} \ll kT_e$), so that photons gain energies. In the energy range $E_{soft} \ll E \ll kT_e$, power-law spectra are observed due to superposition of multiple scattered photon spectra (Figure 5.7). In $E \gtrsim kT_e$, the spectrum falls exponentially.

The Compton y-parameter is defined as follows;

$$y = \frac{4kT_e}{mc^2}\ Max(\tau_{Scot}, \tau_{sct}^2), \tag{5.32}$$

where τ_{sct} is the scattering optical depth of the plasma. Here, $max\tau_{sct}, \tau_{sct}^2)$ is the number of scattering in the medium, and $4kT_e/mc^2$ is the energy each photon gains per scattering. The power-law spectrum becomes flatter as y increases. When $\tau_{sct} \gg 1$, inverse-Compton effect is *saturated*, and Wien peak appears at around $E \approx 3\ kT_e$ (Figure 5.8, left).

Thermal Comptonization explain energy spectra of *low-state* of Galactic black hole binaries (Figure 5.8, right), where hot, thermal plasma is believed to exist around black hole, while optically thick standard accretion disk terminates far from the black hole ($R_{in} \gg R_{ISCO}$)[5].

5.5 Non-thermal Emission

5.5.1 Radiation by relativistic electrons

Consider the case that electrons are accelerated up to much higher energies than the rest mass energy (511 keV), where electrons are called *relativistic* [6] . Energy of an electron with velocity v is $E = mc^2\gamma$, where $\gamma \equiv 1/\sqrt{1-(v/c)^2}$.

Often we consider the case that electron energy distribution, $N(E)$, is expressed with a power-law function such that

$$N(E)dE \propto \gamma^{-p}\, d\gamma. \tag{5.33}$$

For example, *Fermi acceleration* of elections is known to produce such power-law electron distribution.

If relativistic electrons are in the magnetic fields, they emit photons with the *synchrotron radiation* (section 5.5.2). If there are input soft-photons, they are Comptonized by the relativistic electrons, and the *relativistic inverse-Compton emission* is produced (section **??**). Both processes can take place at the same time. In particular, synchrotron photons may be comptonized by the very electrons to have created these photons, which is called *synchrotron self-compton (SSC)* mechanism[7].

In both synchrotron emission and non-thermal inverse-Comptonized emission from an electron with the energy $E = mc^2\gamma$, the following conditions are satisfied;

1. Typical emitted photon energy ($\equiv h\nu_c$) is proportional to γ^2 (see equations 5.37 and 5.41).

2. Luminosity that photons with frequency ν is emitted from a single electron is represented with $S(\nu/\nu_c)$.

In this case, if electron distribution is represented with (5.33) in a wide-energy range, the energy spectrum (in [erg/s/cm^2/Hz]) is written as

$$F(\nu) \propto \int S(\nu/\nu_c)\gamma^{-p}\, d\gamma.$$

Let's change the variable from γ to ν_c using $\nu_c \propto \gamma^2$, so that

$$\frac{d\gamma}{\gamma} \propto \frac{d\nu_c}{\nu_c} \propto \nu_c\, d\left(\frac{1}{\nu_c}\right).$$

[5] In the "high-state" of black hole binaries, it is believed $R_{in} = R_{ISCO}$ (section 2.3.3 and 3.5.3)

[6] Such efficient acceleration takes place in, e.g., pulsars, supernova remnants, AGNs (blazers) in the universe. On the earth, in *synchrotron radiation facilities*, electrons are accelerated to radiate strong synchrotron lights which have many practical purposes. For instance, in Spring-8 (`http://www.spring8.or.jp/ja/`, electrons are accelerated up to ~8 GeV.

[7] X-rays and gamma-rays from blazers are explained by the SSC model such that X-rays are mostly due to synchrotron and gamma-rays are due to inverse-Compton.

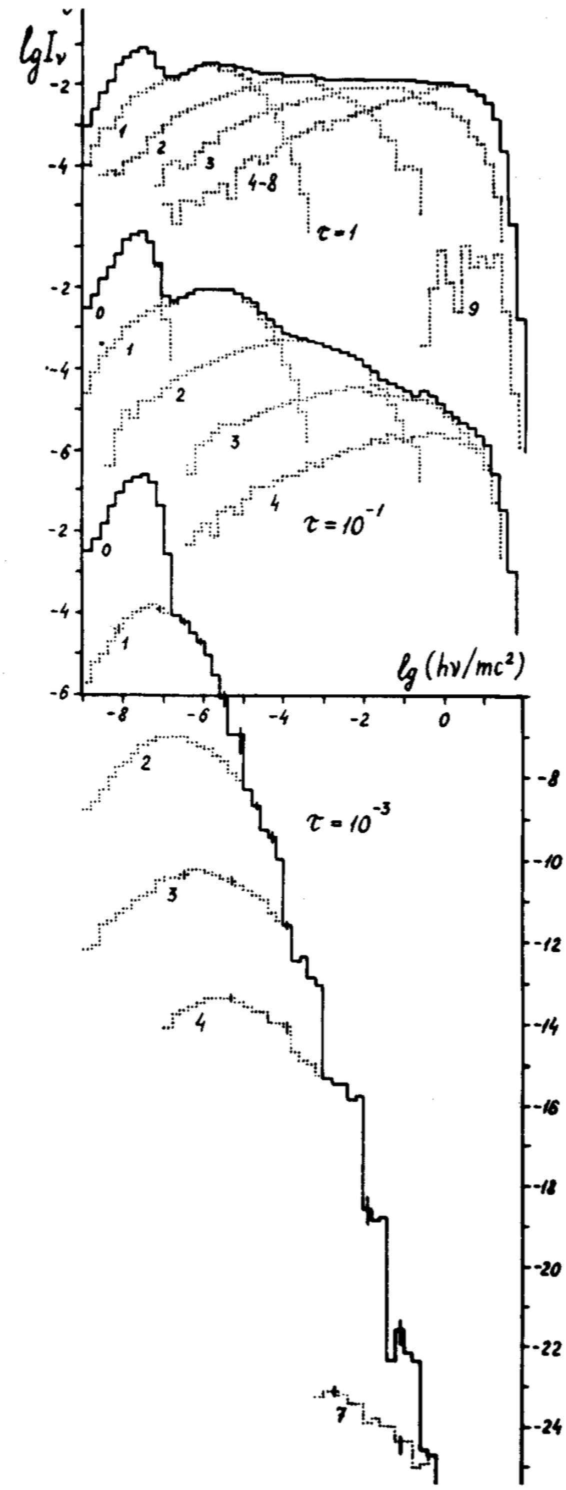

Figure 5.7: Repeated Comptonization from a cloud of thermal plasma for $\tau_{sct} = 1$, 0.1 and 0.001 (from top to bottom) to demonstrate that thermal Comptonization forms power-law spectra, and that the spectrum is flatter as the optical depth (Compton y-parameter) becomes larger. Taken from Pozdnyakov, Sobol and Syunyaev 1983, ASPR, v2, p.189.

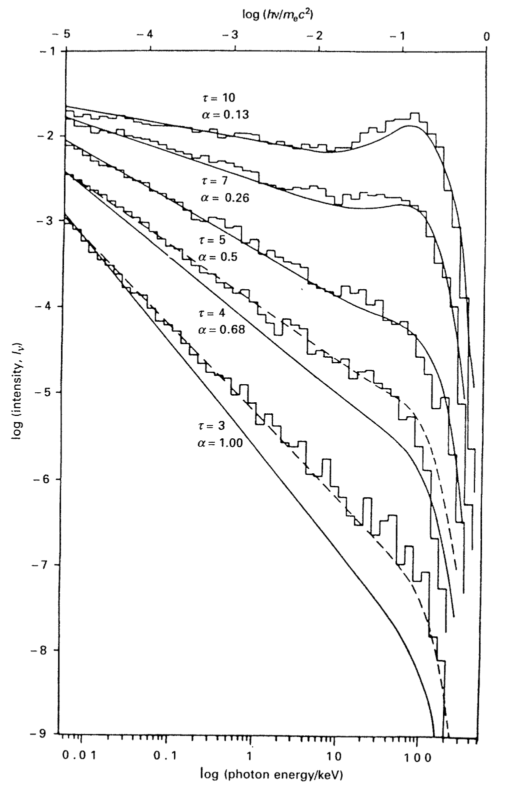

Figure 4.11. The Comptonisation of low frequency photons in a spherical plasma cloud having kT_e = 25 keV. The solid curves are analytic solutions of the Kompaneets equation (see Pozdnyakov *et al.* (1983)); the results of Monte Carlo simulations of the Compton scattering process are shown by the histograms and there is good agreement

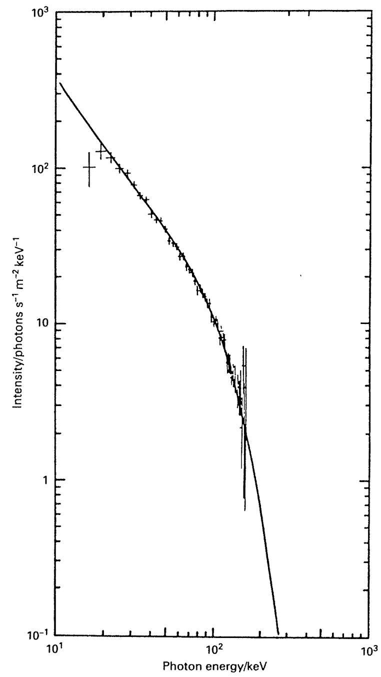

Figure 4.12. The hard X-ray spectrum of the Galactic X-ray source Cygnus X-1 observed in a balloon flight of the Max Planck Institute for Extraterrestrial Physics, on 20 September 1977 compared with the analytic solution of the Kompaneets equation with parameters τ_0 = 5, kT_e = 27 keV. (R. A. Sunyaev and L. G. Titarchuk (1980). *Astron. Astrophys.*, **86**, 121.)

Figure 5.8: (Left) Thermal bremsstrahlung model spectra with $kT_e = 25$ keV with $\tau_{sct} = 3, 4, 5, 7 and 10$. (Right) Cyg X-1 low-state energy spectrum fitted with a thermal bremsstrahlung spectrum with kT_e=27 keV and $\tau_{sct} = 5$. Both figures taken from Longair, "High Energy Astrophysics".

Since ν does not depend on γ nor ν_c,

$$\frac{d\gamma}{\gamma} \propto \left(\frac{\nu}{\nu_c}\right)^{-1} d\left(\frac{\nu}{\nu_c}\right).$$

Thus,

$$\begin{aligned} F(\nu) &= \int S(\nu/\nu_c)\gamma^{-p+1}\frac{d\gamma}{\gamma} \\ &\propto \int S(\nu/\nu_c)\nu_c^{-p/2+1/2}\left(\frac{\nu}{\nu_c}\right)^{-1} d\left(\frac{\nu}{\nu_c}\right) \\ &= \int S(\nu/\nu_c)\left(\frac{\nu_c}{\nu}\right)^{-p/2+1/2}\nu^{-p/2+1/2}\left(\frac{\nu}{\nu_c}\right)^{-1} d\left(\frac{\nu}{\nu_c}\right) \\ &= \nu^{-\frac{p-1}{2}}\int S(\nu/\nu_c)\left(\frac{\nu}{\nu_c}\right)^{\frac{p-3}{2}} d\left(\frac{\nu}{\nu_c}\right). \end{aligned} \tag{5.34}$$

When electron distribution (5.33) is over a large enough energy range, we may integrate from 0 to ∞, then the integral will take a constant value not depending on ν.

Now, we got the following important relationship; *when relativistic electron distribution is represented with a power-law* $\propto \gamma^{-p}$*, the expected synchrotron radiation and the inverse-Compton radiation have the power-law energy spectra,* $\propto \nu^{-s}$*, with the energy index*

$$s = \frac{p-1}{2}. \tag{5.35}$$

Note that we are *not* able to directly measure p of the *electron* energy distribution. When power-law energy spectra of *photons* are observed, we can measure s then estimate p using (5.35).

5.5.2 Synchrotron radiation

As we have seen in (2.13), cyclotron frequency of an electrons in the magnetic field B is

$$\nu = \frac{eB}{2\pi m_e c}. \tag{5.36}$$

Note that in the cyclotron motion, mono-energetic photons are emitted.

When the electron becomes relativistic, where the energy is $mc^2\gamma$, typical frequency of the synchrotron radiation is[8],

$$\nu_c = \frac{3\gamma^2 eB\sin\alpha}{2\pi m_e c}, \tag{5.37}$$

where α is the constant pitch-angle between magnetic field and the electron motion. Note that in synchrotron emission, not mono-energetic photons, but an energy spectrum of photons is observed (Figure 5.9 top). According to precise calculation, a single electron with the energy $mc^2\gamma$ emit synchrotron ration spectrum whose peak frequency is 0.29 ν_c (Figure 5.9, up).

[8] Definition is different for different text books or papers. We follow Katz's definition. Rybicki & Lightman adopts half of (5.37) as ν_c.

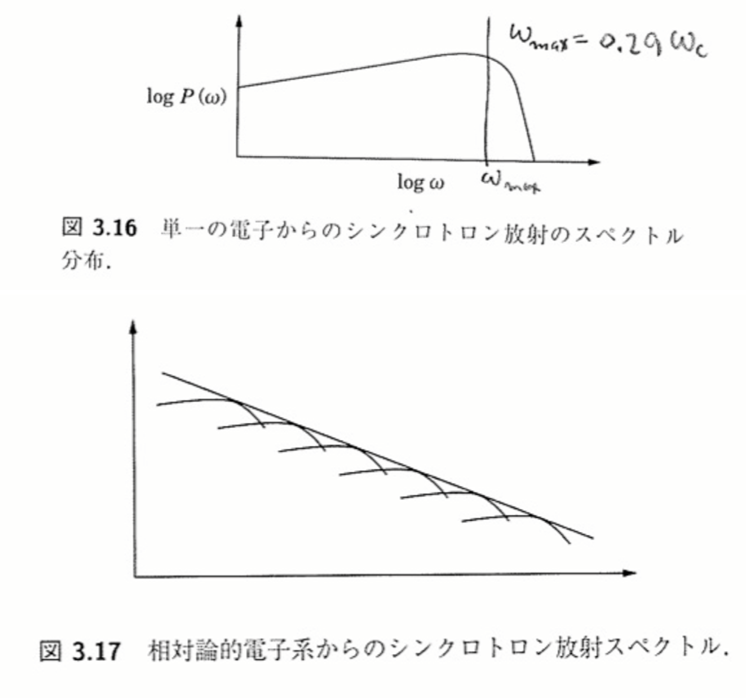

Figure 5.9: (Top) Synchrotron radiation spectrum from a single electron (above), where the peak is at $w_c = 0.29\nu_c$. (Bottom) Formation of a power-law spectrum by superposition of these spectra integrating over the power-law electron energy distribution (5.33). Taken from シリーズ現代の天文学 " 天体物理学の基礎 II".

If these spectra from elections following the power-law energy distribution (5.33) are superposed, power-law photon radiation spectrum is expected (Figure 5.9 bottom)。

Luminosity [erg/s] of the synchrotron radiation from a single electron is given as

$$P_{synch} = \frac{4}{3}\sigma_T c\beta^2\gamma^2 U_B, \tag{5.38}$$

where σ_T is Thomson cross-section, $U_B = B^2/8\pi$ is the magnetic energy density. This formula can be intuitively understood that *an electron having the cross-section σ_T [cm^2] is colliding with the magnetic field U_B [erg/cm^3] at the light velocity c [cm/s].*

5.5.3 Non-thermal (relativistic) inverse Compton emission

When the electron has the velocity v, and $\beta \equiv v/c, \gamma \equiv \left(1-\beta^2\right)^{-1/2}$, let's put the incident photon energy in the laboratory frame ν, and that in the electron rest-frame ν'. In the laboratory frame, put the angle between the electron direction and the incident photon as θ, then

$$\nu' = \nu\gamma(1-\beta\cos\theta). \tag{5.39}$$

We may assume $h\nu' \ll m_e c^2$ in the electron-rest frame, so that the this collision may be assumed as Thomson scattering, where the output photon frequency is ν'. In the electron rest-frame, if put the angle between the electron direction and output photon θ', the output photon frequency in the laboratory frame, ν'', is

$$\nu'' = \nu'\gamma(1 + \beta \cos\theta'). \tag{5.40}$$

Since θ and θ' are $\approx \pi/2$,

$$\nu'' \sim \gamma^2 \nu. \tag{5.41}$$

Now we got an important result that *a photon energy will be boosted by γ^2 times due to a single relativistic Comptonization.*

Luminosity [erg/s] of the relativistic Comptonization from a single electron is given as

$$P_{compt} = \frac{4}{3}\sigma_T c \beta^2 \gamma^2 U_{ph} \tag{5.42}$$

where σ_T is Thomson cross-section, U_{ph} is the photon energy density. This formula can be intuitively understood that *an electron having the cross-section σ_T [cm^2] is colliding with the photon field U_{ph} [erg/cm^3] at the light velocity c [cm/s].* This is similar to the interpretation of the synchrotron luminosity (5.38), where only U_B is replace with U_{ph}.

5.5.4 Synchrotron emission and inverse-compton emission from inter-stellar relativistic electrons

From (5.38) and (5.42), when low energy photons, whose energy density is U_{ph}, and magnetic field, whose energy density is U_B, co-exist in the relativistic electron distribution, ratio of the synchrotron radiation luminosity and the inverse-Compton radiation luminosity is given by

$$\frac{P_{synch}}{P_{compt}} = \frac{U_B}{U_{ph}}. \tag{5.43}$$

If we consider typical inter-stellar magnetic field $\sim 3\mu$Gauss, the magnetic energy density is

$$U_B \approx (3 \times 10^{-6})^2/(8\pi) \sim 3.6 \times 10^{-13}\ \ [\mathrm{erg/cm^3}] \sim 0.22\ [\mathrm{eV/cm^3}]. \tag{5.44}$$

On the other hand, the energy density of CMBR is $U_{ph} \approx 0.26$ eV (p.77), Namely, *when relativistic electrons exist in the inter-stellar space, their synchrotron radiation luminosity and the inverse-Compton luminosity, where soft-photons are supplied by the CMBR, are nearly equal.*

Appendix A

Bremsstrahlung

A.1 Preperation1: Variation of electromagnetic field and energy spectar

When electromagnetif fields vary, the electric field and magnetic field are orthogonal, and the Pointing vector,

$$S \equiv \frac{c}{4\pi}\left(\mathbf{E} \times \mathbf{B}\right) \tag{A.1}$$

show the energy flow in the direction of the electromagnetic wave. In the Gauss unit, $|E||B|$ or $|E|^2$ or $|B|^2$ have the unit of energy density [erg/cm^3], so the Pointing vector has the unit of energy flux, [erg/s/cm^2].

In electromagnetic wave, amplitudes of the electrci field and the magnetic field are the same, so energy flow of the electromagnetic wave per unit-time per unit-area in [erg/s/cm^2] is

$$\frac{dW}{dtdA} = \frac{c}{4\pi} E(t)^2. \tag{A.2}$$

If $E(t)$ varies like a "pulse", the total enerty in [erg/cm^2] is given by

$$\frac{dW}{dA} = \frac{c}{4\pi} \int_{-\infty}^{\infty} E(t)^2 dt. \tag{A.3}$$

Fourier transfor of $E(t)$ will be

$$\hat{E}(\omega) = \frac{1}{2\pi} \int_{-\infty}^{\infty} E(t) e^{i\omega t} dt, \tag{A.4}$$

and the following relation hold;

$$\int_{-\infty}^{\infty} E(t)^2 dt = 2\pi \int_{-\infty}^{\infty} |\hat{E}(\omega)|^2 d\omega. \tag{A.5}$$

Also, since $E(t)$ is real,

$$\hat{E}(-\omega) = \frac{1}{2\pi} \int_{-\infty}^{\infty} E(t) e^{-i\omega t} dt = \hat{E}^*(t). \tag{A.6}$$

Using these relations, (A.3) can be written as

$$\frac{dW}{dA} = c \int_0^\infty |\hat{E}(\omega)|^2 d\omega. \tag{A.7}$$

とかける。つまり、ひとつのパルスからの、単位振動数あたりのエネルギーフラックス [erg/cm^2/Hz] は、

$$\frac{dW}{dA d\omega} = c|\hat{E}(\omega)|^2 \tag{A.8}$$

となる。

フーリエ変換の性質より、周波数の幅 $\Delta\omega$ とパルスの持続時間 T の間に、$\Delta\omega \approx 1/T$ という関係があることに注意。たとえば、電子が単振動しているとき、エネルギースペクトルはその振動数の単色になる (サイクロトロン放射がその例; section 2.2.1)。一方、**電場の変化が非常に短いパルスによって引き起こされるとき、広い範囲のエネルギースペクトルが観測される** (シンクロトロン輻射がその例; 次節参照)。

A.2 準備 2:電気双極子放射 (electric dipole radiation)

ここでは非相対論的な場合だけを考える。$\mathbf{d} \equiv \sum_i q_i \mathbf{r}_i$ を電気双極子ベクトルとすると、それが加速度運動しているとき、方位ベクトル $\mathbf{n}$、距離 R の点に生じる電場は [1]、

$$\mathbf{E}_{rad} = \frac{\mathbf{n} \times (\mathbf{n} \times \ddot{\mathbf{d}})}{c^2 R}, |\mathbf{E}_{rad}| = \frac{|\ddot{\mathbf{d}}| \sin\theta}{c^2 R}, \tag{A.9}$$

θ は $\ddot{\mathbf{d}}$ と方位ベクトル $\mathbf{n}$ のなす角。導出は、Rybicki and Lightman などの教科書参照。次元が合っていることだけは確認しておくこと。$\ddot{\mathbf{d}}$ の方向には放射はされず、その垂直方向で放射強度が最大になる (下図参照)。

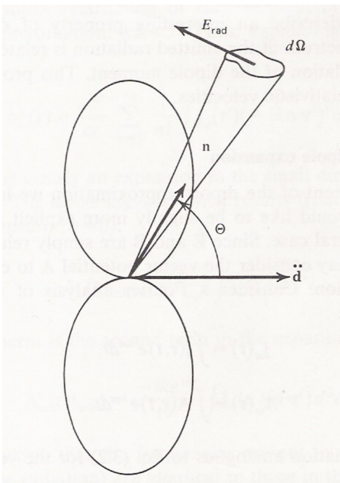

Rybicki & Lightman “Radiative and Processs in Astrophysics”, chapter 3 より。

(A.2)、(A.9) と、立体角 $d\Omega = dA/R^2$ を使って、電気双極子から単位立体角あたりに輻射されるエネルギー [erg/s/str] は、

$$\frac{dP}{d\Omega} = \frac{\ddot{\mathbf{d}}^2}{4\pi c^3} \sin^2\theta. \tag{A.10}$$

[1] 静電磁場は R^{-2} で距離とともに落ちていくが、輻射場は R^{-1} でしか減少しないことがポイント。これについては Rybicki & Lightman に直感的で美しい説明があるので参考にしてください。

立体角で積分して ($\int \sin^2\theta d\Omega = 2\pi \int_0^\pi \sin^3 d\theta = \frac{8\pi}{3}$)、電気双極子から放出されるパワー [erg/s] は、

$$P = \frac{2\ddot{\mathbf{d}}^2}{3c^3}. \tag{A.11}$$

電気双極子放射のエネルギースペクトルを考えるには、電場強度のフーリエ変換が必要。(A.9) より、

$$\hat{E}(\omega) = \frac{\sin\theta}{c^2 R}\frac{1}{2\pi}\int_{-\infty}^{\infty} \ddot{d}\, e^{i\omega t} dt. \tag{A.12}$$

電気双極子のフーリエ変換、

$$\hat{d}(\omega) = \frac{1}{2\pi}\int_{-\infty}^{\infty} d(t) e^{i\omega t} dt \tag{A.13}$$

を定義すると、

$$d(t) = \int_{-\infty}^{\infty} \hat{d}(\omega) e^{-i\omega t} d\omega, \tag{A.14}$$

$$\ddot{d}(t) = -\int_{-\infty}^{\infty} \omega^2 \hat{d}(\omega) e^{-i\omega t} d\omega \tag{A.15}$$

だから、(A.12) は、

$$\begin{aligned}
\hat{E}(\omega) &= -\frac{\sin\theta}{c^2 R}\frac{1}{2\pi}\int\int_{-\infty}^{\infty} \omega'^2 \hat{d}(\omega') e^{-i\omega' t} e^{i\omega t} dt d\omega'. \\
&= -\frac{\sin\theta}{c^2 R}\int_{-\infty}^{\infty} \omega'^2 \hat{d}(\omega') \delta\left((\omega' - \omega)t\right) dt \\
&= -\frac{\sin\theta}{c^2 R}\omega^2 \hat{d}(\omega).
\end{aligned} \tag{A.16}$$

(A.8) と (A.16) より、(A.11) と同様に立体角 $d\Omega = dA/R^2$ を使って、電気双極子から放射される単位振動数、単位立体角あたりのエネルギー [erg/Hz/str] は、

$$\frac{dW}{d\omega d\Omega} = \frac{1}{c^3}\omega^4 |\hat{d}(\omega)|^2 \sin^2\theta. \tag{A.17}$$

立体角で積分して、電気双極子放射の単位振動数あたりのエネルギー [erg/Hz] は、

$$\frac{dW}{d\omega} = \frac{8\pi}{3c^3}\omega^4 |\hat{d}(\omega)|^2. \tag{A.18}$$

A.3 制動放射のパワー

下図のように一つの電子 (電荷 $-e$) が一つの原子核 (電荷 $-Ze$) の近くを通り (インパクトパラメーター b)、クーロン力によって (ほんの少し) 曲げられる際の電気双極子輻射を、(A.18) に従って考える。

電子の速度ベクトルを $\mathbf{v}$ とすると、$\ddot{\mathbf{d}} = -e\dot{\mathbf{v}}$。(A.15) のフーリエ変換をとって、

$$\omega^2 \hat{d}(\omega) = -\frac{1}{2\pi}\int_{-\infty}^{\infty} \ddot{d}(t)\, e^{i\omega t} dt$$

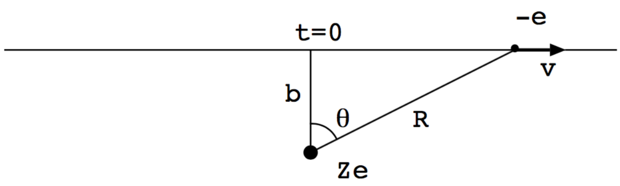

Figure A.1: An electron passing near a nuclei with the impact parameter b.

$$= \frac{e}{2\pi} \int_{-\infty}^{\infty} \dot{v}(t)\, e^{i\omega t} dt. \tag{A.19}$$

電子が原子核のクーロン場の影響を受ける時間スケールは、$\tau \equiv b/v$ なので、上式で $-\tau < t < \tau$ の時間範囲での積分が効く。もし $\omega\tau \gg 1$ ならば、exponential の項は振動するので、打ち消し合って積分はゼロになると近似してよい [2]。一方、$\omega\tau \ll 1$ のときは、exponential の項は 1 と近似して、垂直方向の運動方程式 $m\, dv/dt = Z \cos\theta e^2/R^2$ を用いて、

$$\begin{aligned} \omega^2 \hat{d}(\omega) &= \frac{e}{2\pi} \int_{-\infty}^{\infty} \frac{Ze^2 \cos\theta}{mR^2} dt \\ &= \frac{Ze^3}{2vb\pi m} \int_{-\pi/2}^{\pi/2} \cos\theta d\theta \\ &= \frac{Ze^3}{vb\pi m}. \end{aligned} \tag{A.20}$$

結局、(A.18) を用いて、速度 v を持つ一つの電子が一つの原子核の影響を受けて放出する制動輻射のエネルギー [erg/Hz] は (b の関数と考える)

$$\begin{aligned} \frac{dW(b)}{d\omega} &\approx \frac{8Z^2 e^6}{3\pi c^3 m^2 v^2 b^2} \quad (b \ll v/w) \\ &\approx 0 \qquad\qquad (b \gg v/w). \end{aligned} \tag{A.21}$$

(A.21) は、$b \to 0, v \to 0$ で発散するので、実際には現実的な b, v の下限値を設定しなくてはいけない。

電子密度 n_e [cm^{-3}], イオン密度 n_i [cm^{-3}] のプラズマ中で電子が一様な速さ v を持っていると過程して、単位体積、単位時間あたりに放射されるエネルギー [erg/s/cm^3/Hz] を考える。ひとつのイオンに対して、インパクトパラメーター b と $b + db$ の間を単位時間あたり通過する電子の数は、$2\pi b\, db\, v\, n_e$ [s^{-1}] であることを用いて、

$$\begin{aligned} \frac{dW(b)}{d\omega dV dt} &= n_e n_i 2\pi v \int_{b_{min}}^{\infty} \frac{dW(b)}{d\omega} b\, db \\ &\approx n_e n_i 2\pi v \int_{b_{min}}^{b_{max}} \frac{8Z^2 e^6}{3\pi c^3 m^2 v^2 b^2} b\, db \end{aligned}$$

[2] A.1 節の議論より、「パルス」の持続時間は $\sim \tau$ だから、電磁波は $\Delta\omega \sim 1/\tau$ の振動数の幅を持つ。電子が速く運動しているほど高周波の電磁波が放射される (電子がゆっくり運動しているときは高周波の電磁波は放出されない)。

$$
\begin{aligned}
&= \frac{16e^6}{3c^3m^2v} n_e n_i Z^2 \ln\left(\frac{b_{max}}{b_{min}}\right) \\
&= \frac{16\pi e^6}{3\sqrt{3}c^3m^2v} n_e n_i Z^2 \frac{\sqrt{3}}{\pi} \ln\left(\frac{b_{max}}{b_{min}}\right) \\
&= \frac{16\pi e^6}{3\sqrt{3}c^3m^2v} n_e n_i Z^2 g_{ff}(v,\omega). \qquad \text{(A.22)}
\end{aligned}
$$

ここで、$g_{ff}(v,w) = \frac{\sqrt{3}}{\pi}\ln\left(b_{max}/b_{min}\right)$ は、"Gaunt factor" と呼ばれ[3]、電子のエネルギーと制動放射で放射される振動数の関数であるが、大体 ~ 1 のオーダーと思って良い。

(A.22) の次元 [erg/s/Hz/cm^3] は確認しておくこと。単位時間、単位体積あたりから放射されるエネルギーが $n_e n_i$ に比例するので、**体積 V のプラズマから単位時間に放出される制動輻射のエネルギーは、$n_e n_i V$ に比例する**。$n_e n_i V$ を Emission Measure と呼ぶことがある [cm^{-3}]。

A.4 Energy spectra of thermal bremsstrahlung

(A.22) は電子が特定の速度 v を持つときの表式だが、これを実際の電子の速度分布について平均してやれば、制動輻射のエネルギースペクトルが得られる。電子分布が熱的 (Maxwell 分布) か、比熱的 (power-law) かによって、熱制動放射、非熱的制動放射になる。電子分布に応じて、前者は電子温度に対応したエネルギー $\sim kT$ にカットオフのあるスペクトルになり、後者は power-law になる。

電子が温度 T の Maxwell 分布をしているとき、速度が v と $v+dv$ の間にある確率 dP は、

$$dP \approx v^2 \exp\left(-\frac{mv^2}{2kT}\right) dv$$

だから、この重みで (A.22) を平均する。積分の下限、v_{min} は、振動数 ν の光を考えているとき、$h\nu = \frac{1}{2}mv_{min}^2$ という条件から決まる (もし $v < v_{min}$ ならエネルギー $h\nu$ の光子は発生しない)。

$$\frac{dW(T,\omega)}{dV\,dt\,d\omega} = \frac{\int_{v_{min}}^{\infty} \frac{dW(v,\omega)}{dV\,dt\,d\omega}\, v^2 \exp\left(-\frac{mv^2}{2kT}\right) dv}{\int_0^{\infty} v^2 \exp\left(-\frac{mv^2}{2kT}\right) dv}$$

$\int_0^\infty x^2\exp(-x^2)dx = \sqrt{\pi}/4$ だから、分母は $(2kT/m)^{3/2}\sqrt{\pi}/4$、分子には $\int_{v_{min}}^\infty v\exp(-mv^2/2kT)dv$ という積分が出てくるが、$\int_a^\infty x\exp(-x^2)dx = \frac{1}{2}\exp(-a^2)$ を用いて、これは $\frac{1}{2}(2kT/m)\exp(-h\nu/kT)$。よって、温度と周波数依存性は (Gaunt factor に弱く依存することを除けば)、$T^{-1/2}\exp(-h\nu/kT)$ になる。

結局、熱制動輻射のエネルギースペクトル [erg/s/cm^3/Hz] は、

$$
\begin{aligned}
\epsilon_\nu^{ff} \equiv \frac{dW}{dV\,dt\,d\nu} &= \frac{2^5\pi e^6}{3mc^3}\left(\frac{2\pi}{3km}\right)^{1/2} T^{-1/2}Z^2 n_e n_i e^{-h\nu/kT}\bar{g}_{ff}(T,\nu) \\
&= 6.8\times 10^{-38} T^{-1/2} Z^2 n_e n_i e^{-h\nu/kT} \bar{g}_{ff}(T,\nu) \quad \text{[CGS unit]}. \qquad \text{(A.23)}
\end{aligned}
$$

ここで、$\bar{g}_{ff}(T,\nu)$ は、電子の速度分布について平均した Gaunt factor で、温度、周波数に依存している。

[3] $\sqrt{3}/\pi$ がつくのが標準的な定義だそうだ。

Index